Statistical mechanics where Newton's third law is broken

Inaugural-Dissertation

zur Erlangung des Doktorgrades
der Mathematisch-Naturwissenschaftlichen Fakultät
der Heinrich-Heine-Universität Düsseldorf

vorgelegt von

Jörg Gerald Bartnick

aus Witten

Düsseldorf, November 2015

aus dem Institut für Theoretische Physik II: Weiche Materie
der Heinrich-Heine-Universität Düsseldorf

Gedruckt mit der Genehmigung der
Mathematisch-Naturwissenschaftlichen Fakultät der
Heinrich-Heine-Universität Düsseldorf

Referent: Prof. Dr. Hartmut Löwen
Koreferent: Priv.-Doz. Dr. Alexei Ivlev

Tag der mündlichen Prüfung: 14. Dezember 2015

PREFACE

This thesis was created at the department for *Theoretical Physics II: Soft Matter* at the *Heinrich Heine University Düsseldorf* from beginning of the year 2013 ot the end of the year 2015. The major results of this work have been published in scientific journals, or are submitted at the moment of writing this thesis. Here, I give a list of the publications or preprints, and provide the respective abstracts and references. The manuscripts were created in collaboration with other scientists, this section contains for each article a statement about the personal contribution.

List of published works

[1] Statistical mechanics where Newton's third law is broken
A. Ivlev, J. Bartnick, M. Heinen, C.-R. Du, V. Nosenko, H. Löwen, Phys. Rev. X 5, 011035 – Published 26 March 2015

Abstract:
There is a variety of situations in which Newton's third law is violated. Generally, the action-reaction symmetry can be broken for mesoscopic particles, when their effective interactions are mediated by a non-equilibrium environment. Here we investigate different classes of nonreciprocal interactions relevant to real experimental situations, and present their basic statistical mechanics analysis. We show that in mixtures of particles with such interactions, distinct species acquire distinct kinetic temperatures. In certain cases, the nonreciprocal systems are exactly characterized by a pseudo-Hamiltonian, i.e., being intrinsically non-equilibrium, they can nevertheless be described in terms of equilibrium statistical mechanics. Our results have profound implications, in particular demonstrating the possibility to generate extreme temperature gradients on the particle scale. We verify the principal theoretical predictions in experimental tests

performed with two-dimensional binary complex plasmas.

Statement of the author: This work was done in collaboration with scientists from the Max-Planck-Institute in Garching, the Donghua University in Shanghai and the German Aerospace Center in Weßling. While the experiments were carried out by Chengran Du and Vladimir Nosenko, I did the numerical simulations. The theory was developed by Alexei Ivlev in collaboration by Marco Heinen, Hartmut Löwen, and me. My contribution concerned particularly the rescaling argument for constant nonreciprocity.

[2] Structural correlations in binary colloidal mixtures with nonreciprocal interactions

J. Bartnick, M. Heinen, A. Ivlev, H. Löwen – *submitted*
arXiv:1510.01870

Abstract:
Nonreciprocal effective interaction forces can occur between mesoscopic particles in colloidal suspensions that are driven out of equilibrium. These forces violate Newton's third law *actio=reactio* on coarse-grained length and time scales. Here we explore the statistical mechanics of Brownian particles with nonreciprocal effective interactions. Our model system is a binary fluid mixture of spherically symmetric, diffusiophoretic microswimmers, and we focus on the time-averaged particle pair- and triplet-correlation functions. Based on the many-body Smoluchowski equation we develop a microscopic statistical theory for the particle correlations and test it by computer simulations. For model systems in two and three spatial dimensions, we show that nonreciprocity induces distinct nonequilibrium pair correlations. Our predictions can be tested in experiments with colloidal microswimmers.

Statement of the author: This project was developed together with Marco Heinen, Alexei Ivlev and Hartmut Löwen. The theory, the numerical solver and the Brownian dynamics simulation were my work, while a part of the numerical algorithm (the Fourier-transform on logarithmic grids for radial symmetries) was provided by Marco Heinen.

[3] Emerging activity in colloidal dispersions with wake-mediated interactions

J. Bartnick, A. Kaiser, A. Ivlev, H. Löwen – *submitted*
arXiv:1507.08962

Abstract:
When a planar bilayer of colloids is exposed to perpendicular flow, the wakes generated downstream from each particle mediate their effective interactions.

Most notably, the particle-wake interactions break the action-reaction symmetry for the colloids in different layers. Under quite general conditions we show that, if the interaction nonreciprocity exceeds a certain threshold, this creates an active dispersion of self-propelled particle clusters. The emerging activity promotes unusual melting scenarios and an enormous diffusivity in the dense fluid. Our results are obtained by computer simulation and analytical theory, and can be verified in experiments with colloidal dispersions and complex plasmas.

Statement of the author: This project was developed together with Andreas Kaiser, Alexei Ivlev and Hartmut Löwen. Here, I am responsible for the theory and the numerical simulations. The evaluation of the data and the development of the theory was strongly supported by my co-authors, in particular Andreas Kaiser.

Abstract

When the effective interactions between particles are mediated by some non-equilibrium environment, the *actio=reactio* symmetry from Newton's third law can be broken. Via theory and numerical simulations, this work studies the impact of such nonreciprocal pair interactions on the statistical mechanics. This is primarily done for binary mixtures in the context of colloidal dispersions and complex plasmas. The major results of this thesis are separated into three chapters.

Within the first part, nonreciprocal interactions in systems with Newtonian dynamics are considered. A nonreciprocity parameter is introduced as the fraction of nonreciprocal to reciprocal forces. Interactions where this parameter is independent from the inter-particle distance, will be referred to as interactions with constant nonreciprocity. For this case, it is shown that by renormalization a pseudo-Hamiltonian can be constructed and the principles of equilibrium statistical mechanics are applicable. One major result is the existence of a two-temperature steady-state, where the distinct species, i.e. the reciprocal sub-ensembles, acquire different kinetic temperatures. When the nonreciprocity parameter is a function of the distance, it is shown that there is a universal asymptotic temperature growth. Within numerical calculations, the impact of density is examined, while the theoretical results are confirmed by simulations and experiments.

In a subsequent chapter, a fully overdamped situation is inspected, where the temperature is imposed by a surrounding heat bath. A model is presented, where diffusiophoresis leads to effective nonreciprocal Yukawa-like pair-interactions. The impact of these nonreciprocal forces on the pair- and triplet correlations is studied in detail. A theory is presented, that allows to compute the pair distribution function based on the Smoluchowski equation and the Kirkwood approximation. It is shown, that for such situations nonreciprocal interactions lead to distinct pair-correlation functions. The theory is tested against Brownian dynamics simulations and shows a good agreement. The Kirkwood approximation for such systems is tested and shows good results.

The last part of the thesis studies wake-mediated interactions in the fully overdamped regime, under consideration of hydrodynamic interactions and thermal noise. It is shown, that nonreciprocal interactions can lead to active units, when the reciprocal part of the interaction vanishes. The onset of activity depends on the density of the system and can lead to unusual melting and freezing behavior. The activity and configuration of active units, as well as the freezing of many-body systems is predicted analytically. In a many-body simulation the particles show strong velocity alignment, which is enhanced by hydrodynamic interactions. For the case of finite temperature, the diffusion is drastically increased relative to case without wake-mediated interactions. Hydrodynamic interactions are shown to enhance the mobility of the fluid.

Zusammenfassung

Die Reziprozität von Paarwechselwirkungen wird durch Newtons drittes Gesetz beschrieben. Dieses Gesetz kann gebrochen werden, wenn effektive Kräfte in einem Nichtgleichgewichtssystem betrachtet werden. Im Rahmen dieser Dissertationsschrift wird der Einfluss von nichtreziproken Wechselwirkungen auf das Gebiet der statistischen Mechanik untersucht. Dies geschieht im Rahmen von Simulationen und theoretischen Beschreibungen für binäre Mischungen von Partikeln in kolloidalen Dispersionen oder komplexen Plasmen.

In einem ersten Teil, werden nichtrezipoke Wechselwirkungen in Systemen mit ungedämpfter oder schwach gedämpfter Dynamik untersucht. Der Quotient von nichtreziproken zu reziproken Kräften wird als „Nichtreziprozitätsparameter“ eingeführt. Wenn dieser Parameter unabhängig von dem Partikelabstand ist, sogenannte konstante Nichtreziprozität, kann durch eine Renormalisierung der Massen und Potentiale ein Pseudo-Hamilton-Operator eingeführt werden. Mit diesem Operator sind die Prinzipien von klassischer statistischer Mechanik aus dem Gleichgewicht anwendbar. Ein besonderes Ergebnis dieser Arbeit ist die Existenz eines Zwei-Temperatur-Gleichgewichts, bei dem sich für unterschiedliche Spezies im gleichen System verschiedene kinetische Temperaturen einstellen. Falls der Nichtreziprozitätsparameter von dem Abstand der Partikel abhängt, gibt es eine universelle Temperaturdivergenz. Die theoretischen Ergebnisse werden durch Simulationen und Experimente bestätigt.

In einem darauffolgenden Kapitel werden überdämpfte Systeme betrachtet, bei denen die Temperatur der Partikel durch ein umgebendes Wäremebad aufgeprägt wird. Es wird gezeigt, dass Diffusiophoresis zu Yukawa-ähnlichen nichtreziproken Paarwechselwirkungen führen kann. Der Einfluss von solchen nichtreziproken Wechselwirkungen auf die Paar- und Tripletkorrelationen wird durch Theorie und Computersimulation untersucht. Die vorgestellte Theorie erlaubt es, die Paarkorrelationen in guter Übereinstimmung mit Simulationsergebnissen vorherzusagen. Sie basiert auf der Smoluchowskigleichung und wird durch die Kirkwood-Approximation abgeschlossen. Die Kirkwoodtheorie wird unabhängig von der Theorie getestet und zeigt gute Übereinstimmungen, auch für nichtreziproke Wechselwirkungen.

Im letzten Teil dieser Arbeit wird der Einfluss von Wirbel-Vermittelten-Wechselwirkungen in überdämpften Systemen untersucht. Es wird gezeigt, dass sich aktive Einheiten bilden können, wenn der reziproke Teil der Wechselwirkung verschwindet. Der Aktivitätsübergang hängt dabei zum Einem von der Stärke der Nichtreziprozität ab, aber auch von der Dichte des Systems. Dieses Verhalten kann zu ungewöhnlichen Schmelzvorgängen bei Erhöhen der Dichte führen. Die Aktivität von einzelnen Paaren wird analytisch vorhergesagt, und für Vielteilchensysteme werden stabile Kristallregionen mit einer linearen Stabilitätsanalyse hergeleitet. In Simulationen werden die theoretischen Resultate bestätigt und man kann ein starkes Ausrichtungsverhalten der aktiven Teilchen erkennen. Für finite Temperaturen zeigt das System ein drastisch erhöhtes

Diffusionsverhalten. Der Einfluss von hydrodynamischen Wechselwirkungen verstärkt das Ausrichten und die Mobilität der Teilchen.

CONTENTS

Preface **i**
List of published works i
Abstract v
Zusammenfassung vii

1 Introduction **1**
1.1 Experimental systems 3
1.1.1 Colloidal Dispersions 3
1.1.2 Complex Plasmas 5
1.2 Theoretical basics 9
1.2.1 Undamped dynamics 10
1.2.2 Overdamped dynamics 11
1.3 Nonreciprocal forces 12
1.3.1 Hydrodynamic interaction 12
1.3.2 Wake interaction 15
1.3.3 Diffusiophoretic interaction 16

2 Many-body systems with nonreciprocal interactions **19**
2.1 Models for wake-mediated interactions 21
2.2 Constant nonreciprocity 21
2.2.1 Pseudo-Hamiltonian 22
2.3 General nonreciprocity 23
2.3.1 Pair collisions: Variation of energy and scattering functions . . 24
2.3.2 Asymptotic Universality 25
2.3.3 Effect of damping 27
2.4 Numerical simulations 27
2.5 Experimental test with complex plasma 33
2.6 Conclusion 39

3 Structural correlations in binary colloidal mixtures with nonreciprocal interactions 41
3.1 The Model . . . 42
3.2 Many-body theory for the pair correlation functions . . . 45
3.3 Numerical simulations . . . 47
3.4 Kirkwood approximation for nonreciprocal interactions . . . 50
3.5 Conclusions . . . 55

4 Emerging activity in bilayered dispersions with wake-mediated interactions 57
4.1 Model . . . 58
4.2 Stability analysis and self-organization . . . 60
4.2.1 Active and inactive doublets . . . 61
4.2.2 Active and inactive triplets . . . 64
4.2.3 Stability analysis for finite densities . . . 66
4.2.4 Diffusion of a doublet under thermal noise . . . 66
4.3 Numerical simulations . . . 68
4.3.1 Emerging states . . . 68
4.3.2 Characteristics of active fluids . . . 69
4.3.3 Finite Temperatures . . . 73
4.4 Conclusion . . . 79

5 Conclusion 81

Bibliography 84

CHAPTER 1

INTRODUCTION

The motion of all physical objects in our everyday life is subject to Newton's laws [4]. The third of these fundamental postulates states that for every force $\mathbf{F}_{AB}$ exerted by an object A on an object B, there is an opposing force $\mathbf{F}_{BA}$ on object A of equal magnitude

$$\mathbf{F}_{AB} = -\mathbf{F}_{BA} \,. \tag{1.1}$$

Newton's third law, Eq. (1.1), describes the reciprocity of pair interactions, which is often referred to as *actio = reactio*. It is generally employed for any analysis of many-body effects and forms the basics of modern statistical mechanics. Equation (1.1), is in particular true for fundamental microscopic forces between particles, but it is also valid for effective forces in equilibrium situations [5–9]. However, for effective forces, it is possible to break Newton's third law, if the system is out of equilibrium [10–13]. Multiple studies explored such situations in complex plasmas or colloidal dispersions. In both cases, mesoscopic particles are embedded in a surrounding fluid, where the particles are on much larger size range (typical diameters are between a few nanometers and a few micrometers) compared to the atoms or molecules of the fluid. Due to the different sizes, normally, the fluid is described by a mean-field approach, giving rise to effective forces between the particles. In complex plasmas [14–17] studies have shown that interactions between the micro-particles are nonreciprocal for many different kinds of interactions. For example so-called shadow interactions [17–19], occur when the presence of dust particle creates an anisotropy in its neighborhood in the plasma. If two particles are close together, this can lead to bombardment of plasma particles from a preferred direction, leading to an effective attraction which can be nonreciprocal. Also, interactions in complex plasmas can break the actio-reactio symmetry, if the charged particles are exposed to an external ion-flow. The resulting wake structures can be described by an effective charge downstream of their position, and the wake-mediated interactions [14–17, 20] are generally nonreciprocal. In colloidal

dispersions, forces can break the actio-reactio symmetry in the case of a solvent or depletant flow [11–13, 21], e.g. due to hydrodynamic interactions. Forces induced by non-equilibrium fluctuations [22, 23], e.g. when two solutes induce density fluctuations by reaction and diffusion, may also violate the action-reaction principle. Moreover, optical [22,24,25] or diffusiophoretic forces [26–28] generally violate Newton's third law. Naturally, the actio-reactio symmetry is also broken in predator-prey systems [29–31] or in the description of biological systems via effective forces, like human crowds in pedestrian dynamics [32, 33].

It is the aim of this thesis to explore the statistical mechanics in systems where the reciprocity of interactions can be broken. The focus is set on colloidal dispersions and complex plasmas, where uneven magnitudes of effective forces are known and studied in experiments. In this introduction, first both of these systems will be explained in more detail. Some basic approaches to statistical mechanics are introduced for the case of reciprocal interactions. Then, some typical situations where Newton's third law is broken are elaborated. In Chapter 2 the effect of nonreciprocal interactions on systems without or with weak damping are explored, and the existence of a two-temperature steady-state is shown. A characteristic nonreciprocity parameter is introduced and it is explained, how by renormalization arguments a pseudo-Hamiltonian can be constructed, for which the principles of equilibrium statistical mechanics are applicable. In Chapter 3, the effect of nonreciprocity in the case of overdamped systems is analyzed. By theory and simulations, it is shown that nonreciprocal interactions can lead to distinct pair-correlation functions. In Chapter 4, an example of an overdamped system is given, where nonreciprocal forces lead to the formation of active units. The activity gives rise to unusual melting scenarios, which is studied with Brownian dynamics simulations and theoretical descriptions.

1.1 Experimental systems

Colloidal dispersions and complex plasmas are ideal model-systems for the study of many-body physics and statistical mechanics. They fall in the class of soft matter systems, which is an active field of research. Topics like crystallization [34–41] and melting [42–44], liquid structure [28,45], self-organization [46], phase separation [47–53] or glass and gel formation [15, 54–57] are of current interest, e.g. in the development of new technologies and materials.

Colloidal dispersions and complex plasmas consist both of mesoscopic particles embedded in a surrounding fluid. This bears two major advantages: Unlike atoms in common liquids, particles are large enough that they are individually traceable. Additionally, the effective interactions between the particles can be tuned by accessible parameters, e. g. solvent properties or external fields. These systems immensely help to understand the processes that occur at the individual particle level. Since the effects are often generic, they serve as model system for atomistic processes. In this section, a short introduction to the field of complex plasmas and colloidal dispersions is given.

1.1.1 Colloidal Dispersions

Colloidal dispersions as commonly used for experiments, are solid particles dispersed in a liquid solvent [58]. Typically, the particles are of a size range between $1\,\mathrm{nm}$ and $1\,\mu\mathrm{m}$. There are many everyday examples for such systems, like paint, ink, blood or milk. They can be susceptible to external forces, e.g. paint is usually engineered such that it is highly viscous once distributed on the wall, but less viscous while painting [59].

For colloidal dispersions, there is normally a difference in the refractive index of the colloid and that of the solvent. This difference leads to spontaneously induced dipoles, which in turn lead to effective attractive forces. When the force between of a particle pair with distance $\mathbf{r}$ is reciprocal, it can be written as the gradient of a potential $\mathbf{F}(\mathbf{r}) = -\nabla V(\mathbf{r})$. For the interactions above, so-called non-retarded van der Waals interactions, the potential can be described as [60]

$$V_{\mathrm{vdW}} = -\frac{A_{\mathrm{H}}}{12}\left(\frac{\sigma^2}{r^2-\sigma^2} + \frac{\sigma^2}{r^2} + 2\ln\frac{r^2-\sigma^2}{\sigma^2}\right),$$

with the Hamaker constant A_{H} and colloid diameter σ. Usually $A_{\mathrm{H}} \propto (n_{particle} - n_{solvent})^2$, where $n_{particle}$ and $n_{solvent}$ are the refractive indices of the particle and the solvent, respectively. The strength of the van der Waals force can be reduced by index-matching. Since this force is purely attractive with a divergence at contact, colloids will coagulate if the dispersion is not stabilized.

One important stabilization method is electric charging of the colloids [44]. Due to dissociation of surface groups and absorption of charges, the colloids naturally acquire a charge Q. The sign or the magnitude of this charge is determined by e.g. the solvent's salt concentration or various material properties. For many organic solvents, the charge

is so small that it can be reasonably neglected. On the other hand, for solvents with high dielectric constants, e.g. water, the charging is strong. Assuming a constant surface charge density, the charge of a colloid scales with its surface area.

A charged colloid will attract oppositely charged ions. In the direct vicinity of the colloid a double layer forms, the so-called Stern layer. Usually, one differentiates between strongly coupled charges, and in a subsequent layer more mobile charges. For the mobile charges in the solution, a linearized screening theory is applicable. Under the assumption of linear Poisson-Boltzmann theory the Derjaguin-Landau-Verwey-Overbeek (DLVO) theory [61] is derived. The linearized Poisson-Boltzmann equation for the electric potential $\Phi(\mathbf{r})$ at a position $\mathbf{r}$ is:

$$\nabla^2\Phi(\mathbf{r}) = \frac{e^2}{\epsilon_0\epsilon_r}\sum_j [Z_j^2\rho_j^\infty]\ \beta\ \Phi(\mathbf{r})\ , \tag{1.2}$$

where ϵ_0 is the vacuum permittivity and ϵ_r the relative permittivity, and the charge number Z is the particle charge normalized by the electron charge e. The ion density at infinity is ρ^∞ and the inverse thermal energy $\beta = 1/k_\mathrm{B}T$. When working in spherical coordinates one finds, that $\Phi(r) = c\, e^{-r/\lambda}/r$, with a constant c and a screening length λ is a solution to this equation. Assuming total charge neutrality, the interaction between two charged colloids eventually reads:

$$V_\mathrm{Y}(r) = \begin{cases} \infty & \text{if } r < \sigma, \\ \epsilon_Y \frac{e^{-(r-\sigma)/\lambda_D}}{r/\sigma} & \text{if } r \geq \sigma, \end{cases}\ , \tag{1.3}$$

where $\lambda_D = (4\pi\lambda_B n_{ion})^{-1/2}$ is the Debye screening length and ϵ_Y the contact potential. The density of monovalent small ions is n_{ion} and the Bjerrum length $\lambda_B = e^2/\epsilon_r k_\mathrm{B}T$. For the contact potential

$$\epsilon_Y = \frac{Z^2}{(1+\sigma/2\lambda_D)^2}\frac{\lambda_B}{\sigma}k_\mathrm{B}T\ .$$

The linear Poisson Boltzmann theory breaks down at large charging values. However, for many applications it is sufficient to take linear screening theory and determine an effective charge [44].

Active particles

Nonreciprocal interactions in overdamped suspensions are shown to induce activity, i.e. a self-propulsion of particle clusters (see Chapter 4 or Refs. [27, 28]). Thus, it is appropriate to mention the field of so-called active particles, which is important for the area of colloidal dispersions [62]. Its study is initially motivated by effects in biological groups: Young desert locusts can form a huge marching army [63], and flocks of bird suddenly decide to land [64] without the existence of an leading alpha-bird. Such self-

organization or sudden state switches can also be observed for other animals such as fish [65], ants [66] or even human crowds [33, 67, 68].

Numerical studies show that such behavior might stem from simple local rules of interaction. The most famous example for an algorithm leading to effects like local swarming or global alignment is the Vicsek model [69]. There, individual animals, i.e. active entities, are modeled as particles with orientation rules. They are driven with a fixed absolute velocity, whereas the velocity direction is allowed to change depending on the local environment. With a fixed frequency, a particle's velocity direction is set to the average direction of velocity of the neighboring particles plus some noise. Then, depending on parameters as e.g. noise strength or density, there is a transition from random motion to directed global motion.

On the colloidal length scale, important representatives for active particles are bacteria, sperm, and also artificial microswimmers [62]. In the context of this thesis, an important class of artificial microswimmers are those, that propel by diffusiophoresis [70–73], which is a drift due to a chemical concentration gradient (see Section 1.3.3). The transport of colloidal particles can occur e.g. for asymmetrically coated particles.

1.1.2 Complex Plasmas

The term plasma was coined by Irving Langmuir in 1928 [74]. It describes a gas that is partially or fully ionized, i.e. it contains free charge carriers. Thus in a plasma, there are free ions and electrons, but usually also a neutral, uncharged component. Plasmas occur naturally, e.g. in the polar lights, lightnings, or space nebulæ [75]. For technical applications plasmas are used for example for light emission, as in common gas discharge lamps or in plasma TVs.

A plasma is typically distinguished from other gases by three important properties: *(i)* the Debye length (the plasma-analogue to λ_D in Eq. (1.3)) is small in comparison to the system size, *(ii)* the number of particles in a sphere with the radius of the Debye length (the plasma parameter) is large, *(iii)* the typical time between collisions is large compared to the period of the plasma oscillation. Typically, the charge ratio of positive and negative charges in a plasma is close to one (quasi-neutral). Also, the mass of the positively charged ions is much larger than the charge of the negatively charged electrons. Important for the classification of a plasma are the plasma density, whether or not it is in thermal equilibrium and the degree of ionization. All of the respective parameters can vary in a very broad range.

Commonly, in a plasma there are objects much larger than the size of the gas atoms. Typically this is known from space plasmas, e.g. in spokes of Saturn's rings [76]. However, also in laboratory systems, there can be micro-particles, or dust, in plasmas. This used to be considered an unwanted contamination. In 1994, several researchers reported the emergence of crystalline structures in dust particles in a plasma [77–79]. Since then, so-called *dusty plasmas*, or complex plasmas have received more attention [80]. These systems are used for industrial processing [81], but they also serve as a model system for

many-body problems [14, 17]. In this respect, similarly to colloidal dispersions, they are interesting, because they allow to observe the motion of particles at the individual-particle level.

Experiments in the field of complex plasmas usually use plasmas, created by low-temperature radio-frequency discharges. Seed electrons in a system are accelerated in a strong electric field. Upon collisions with neutral atoms or molecules, the highly accelerated electrons can remove another electron from its bound state. This leads to an avalanche effect and the ionization of the gas, which then enters the plasma state.

In laboratory complex plasmas, dust particles become charged due to interaction with the plasma environment. The particle charge Q influences the interaction between the particles themselves, with the plasma environment, and their response to external electric fields. The major mechanism behind particle charging is the balance of electron flux I_e and ion flux I_I on the particle surface. The time evolution of the charge is $\dot{Q} = I_i - I_e$. Typically the electron flux is much larger, because of the increased electron temperature. For the analysis of a stationary charge, one seeks the situation where the ion and electron fluxes are equal.

The orbital motion limited (OML) approximation [82] can describe the electron and ion fluxes under the approximation of a dilute plasma. It considers an isotropic situation, where the trajectories of ions and electrons in the vicinity of the particle are without collisions. The ion and electron currents on the particle surface [83] are the determined to be

$$I_i = 4\pi\sigma^2 n_i e \sqrt{\frac{k_\mathrm{B}T_i}{2\pi m_i}} \left(1 - \frac{e\phi_p}{k_\mathrm{B}T_i}\right)$$

and

$$I_e = 4\pi r_e^2 n_e e \sqrt{\frac{k_\mathrm{B}T_e}{2\pi m_e}} \exp\left(\frac{e\phi_p}{k_\mathrm{B}T_e}\right)$$

with the particle radius σ, the Boltzmann constant k_B, the particle floating potential ϕ_p , the electron charge e, and the number density n_e, n_i, the temperature T_i, T_e and the mass m_e, m_i for electrons and ions respectively. In the derivation, it was assumed that an ion has a single positive elementary charge. This fundamental theory also provides the basis for theories describing the charging in different situations, like when ion neutral collisions become important or the plasma is no longer isotropic [80].

Considering the charge of the dust particles as the major contribution to the interactions with each other and in respect to external fields, the interaction potential can be written as $V(r) = Q\varphi(r)$, where $\varphi(r)$ is the distribution of the electrostatic potential around a particle. Due to the charge of the particle, ions and electrons in the plasma will redistribute and shield the charge. Under the assumption, that the charge Q is independent of the inter-particle distance r, we consider the regime of linear response. Within this regime, where $e|\phi_s|/k_BT \lesssim 1$ electron and ion distributions can be linearized. Similarly to colloidal dispersions, we are using the linearized Poisson equation, Eq. (1.2).

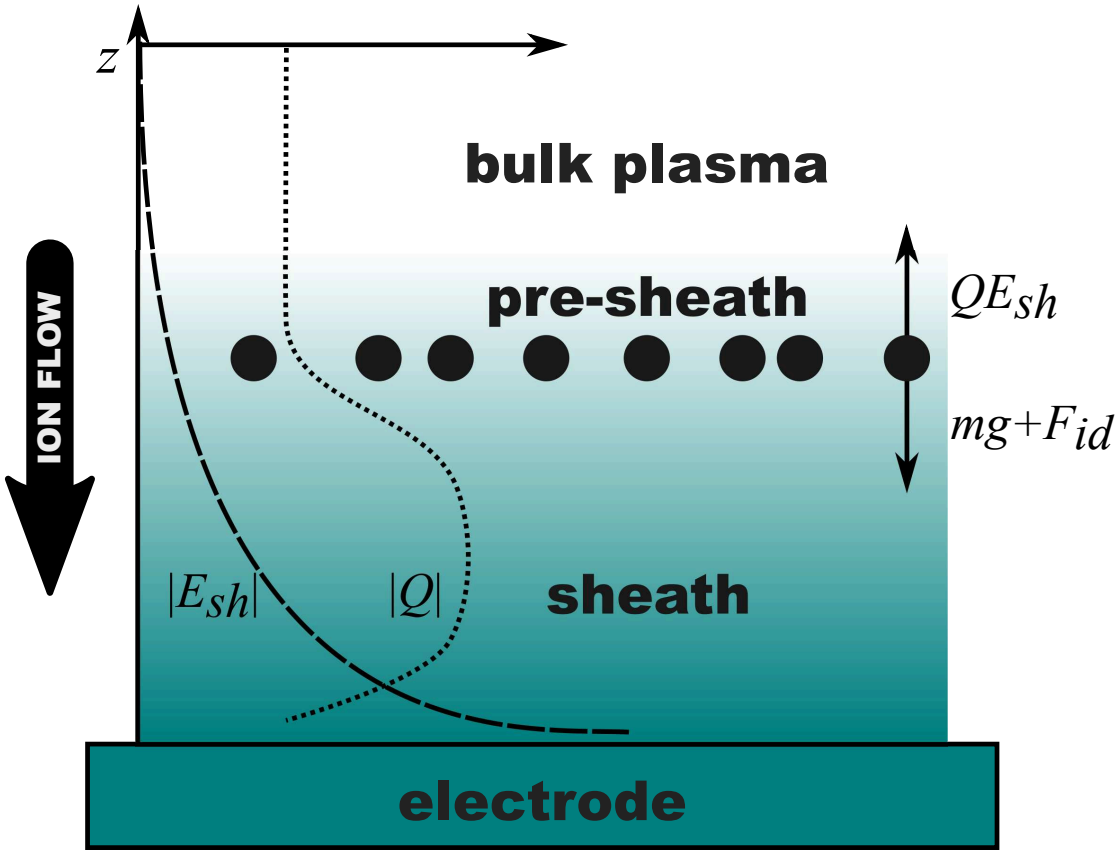

Figure 1.1: *Qualitative sketch of the force balances in the plasma sheath region. The absolute value of the potential $|E_{sh}|$ and the equilibrium particle charge $|Q|$ are given as dashed and dotted line, respectively. Particles levitate at that value z, where the electrostatic repulsion balances gravity and the ion drag force. (see Ref. [15])*

Then, with the boundary conditions $\varphi(\infty) = 0$ and $\varphi(a) = \varphi_s$ we determine the Yukawa potential

$$V(r) = \Gamma \frac{e^{-(r-\sigma)/\lambda_D}}{r/\sigma}$$

where Γ is the coupling parameter and the Debye length is $\lambda_{D_i} = \sqrt{k_B T_i / 4\pi e^2 n_i}$.

Sheath interaction

An important class of nonreciprocal interactions are the wake-mediated interactions (see Section 1.3.2), which are intensively studied in complex plasmas [14, 15, 20]. Plasma wakes naturally occur in the sheath region [81,84] sketched in Fig. 1.1. The sheath region is an important aspect in modern complex plasma experiments. These experiments are often carried out in a Gaseous Electronic Conference radio frequency-reference cell [85]. In this setup the electrode required for the plasma discharge is set at the

bottom of the experimental cell. The electrode is negatively charged, which generates a region of negative potential, attracting positively charged ions. Ions accumulate near the electrode and due to the resulting ion-flow, there is an ion drag on the particles. The ions shield the electro-negative potential of the electrode, and the dust particles levitate at the height, where the electric repulsion balances gravity and the ion drag force (see again Fig. 1.1). The dust particles are thus levitating on a plane with a perpendicular ion current. The particles act like lenses, and focus the ions downwards of the levitation plane [1, 14, 15, 17–19]. The important quantity in this respect is the thermal Mach Number M_T. It is defined as the ion flow velocity u_i divided by the ion thermal velocity v_T

$$M_T = \frac{u_i}{v_T} \, .$$

For Mach numbers larger than one, $M_T > 1$, the wakes are stronger than in the reverse case, where the anisotropic deviations of the particle potential are rather weak. In particular for a two-layer setup, these forces can become highly antisymmetric.

1.2 Theoretical basics

Before the study of nonreciprocal forces, here the focus is put on the description of dynamics in systems with classical reciprocal interactions in complex plasmas and colloidal dispersions. Clearly, the motion of particles in a system is governed by the inter-particle interaction and the particle's response to the environment. Generally, one starts derivations either from a individual particle approach or a probability density formalism. The individual particle approach presented here is the Langevin approach, for the probability density the Fokker-Planck formalism will be shortly introduced. For both cases however, the description of mesoscopic particles in a microscopic fluid usually involves a mean-field approach of the surrounding liquid. This is justified, since the atomistic motion of the surrounding fluid takes place on much shorter time- and length-scales than the particle motion.

The typical approach to include the fluid as a mean-field is via the assumption of a random force $\mathbf{L}_i(t)$, acting on the i-th particle at the time t. This is motivated by the many collisions of the fluid molecules with the particle surface. These collisions are undirected, i.e.

$$\langle \mathbf{L}_i(t) \rangle = \mathbf{0} \ ,$$

where the brackets represent the ensemble average. The correlation of the random force with itself is proportional to the damping rate of the liquid ν and the temperature T [86]

$$\langle \mathbf{L}_i(t) \ \mathbf{L}_j(t+\tau) \rangle = 2\nu k_{\mathrm{B}} T \delta_{ij} \delta(\tau) \ .$$

The Langevin equation is a stochastic equation, that bases on this model. In general, it does not differ much from the Newton's equation with a friction force that is proportional to the velocity. We write down the Langevin equation [87] as

$$\frac{\partial \mathbf{p}_i(t)}{\partial t} + \nu \mathbf{p}_i(t) = \mathbf{F}_i(t) + \mathbf{L}_i(t) \ , \tag{1.4}$$

where $\mathbf{p}_i(t) = m_i \ \mathbf{v}_i(t)$ is the momentum of the i-th particle with mass m_i and velocity $\mathbf{v}_i(t)$ and $\mathbf{F}_i$ the superposition of external $\mathbf{F}^{ext}$ and inter-particle forces $\mathbf{F}^{int}$.

Alternatively, one can approach the dynamics of a many body-system by a probability density. One writes the phase-space probability density $f^{(N)}(t, \mathbf{p}_1, \mathbf{r}_1, \ldots, \mathbf{p}_N, \mathbf{r}_N)$ for N particles with positions $\mathbf{r}_i$ and momenta $\mathbf{p}_i$. It describes the probability to find a system in a given state, with given positions and momenta of the particles. The Fokker-Planck formalism [88] describes the time evolution of this probability density. It is the equivalence of the Langevin Eq. (1.4) for the probability density. One writes the kinetic equation as

$$\frac{\partial f^{(N)}}{\partial t} + \sum_i \left(\mathbf{v}_i \cdot \frac{\partial f^{(N)}}{\partial \mathbf{r}_i} + \mathbf{F}_i \cdot \frac{\partial f^{(N)}}{\partial \mathbf{p}_i} \right) = \nu \sum_i \frac{\partial}{\partial \mathbf{p}_i} \cdot \left(\mathbf{p}_i f^{(N)} + m_i T \frac{\partial f^{(N)}}{\partial \mathbf{p}_i} \right) \ . \tag{1.5}$$

where m_i is the particle mass. The right hand side of Eq. (1.5) describes the collisions with the fluid, while the left hand side incorporates Newton's laws of motion. In the case of negligible fluid interaction, the right hand side of this equation vanishes. The following analysis considers the two extreme cases, where the dynamics are highly damped or undamped: Highly damped or overdamped dynamics are found mainly in colloidal dispersions, where the interaction with the fluid is essential. Undamped dynamics can be important in the case of complex plasmas, which often operate at very low densities and the motion is quasi undistributed Newtonian.

1.2.1 Undamped dynamics

If the damping rate ν is much smaller than the inverse of the timescale of the problem, it is a reasonable approximation to neglect the right hand side of Eq. (1.5). The phase space probability density $f^{(N)}$ includes the full information about the system. Often, this amount of information is unhandy or not even desired. Instead, the i-particle distribution $f^{(i)}$ is a preferred quantity. It is the partial integration over the remaining momenta and coordinates

$$f^{(i)} = \int \mathrm{d}\mathbf{p}_{i+1}\mathrm{d}\mathbf{r}_{i+1}\ldots\mathrm{d}\mathbf{p}_N\mathrm{d}\mathbf{r}_N f^{(N)} \,.$$

Of major importance are the first three i-particle distribution functions, i.e. $f^{(1)}$, $f^{(2)}$ and $f^{(3)}$. With these definitions and under the assumption of a large N, after multiple integrations in Eq. (1.5), an equation for the one-particle distribution function is derived

$$\frac{\partial f^{(1)}}{\partial t} + \mathbf{v}_1 \cdot \frac{\partial f^{(1)}}{\partial \mathbf{r}_1} = N \int \mathrm{d}\mathbf{p}_2\mathbf{r}_2 \, \frac{\partial V_{12}}{\partial \mathbf{r}_1} \cdot \frac{\partial f^{(2)}}{\partial \mathbf{p}_1} \,. \tag{1.6}$$

As long as no approximations are made concerning the kind of pair correlation, this equation is exact. It relates the one-particle distribution function $f^{(1)}$ to the two-particle distribution function $f^{(2)}$. A common approach to solve Eq. (1.6) is to replace the two particle distribution function in the so-called superposition approximation. There, the two-particle density is replaced by a product of two one-particle-distribution functions $f^{(2)}(\mathbf{r}_1, \mathbf{p}_1, \mathbf{r}_2, \mathbf{p}_2) \approx f^{(1)}(\mathbf{r}_1, \mathbf{p}_1)\, f^{(1)}(\mathbf{r}_2, \mathbf{p}_2)$. Then, the integral on the right hand side of Eq. (1.6) is reduced to the classical Boltzmann collision integral. In particular, this approach can be used for weakly coupled plasmas.

In denser systems, or systems with stronger interactions, this approximation is no longer valid. There, the two-particle distributions have to be taken into account. Developing a Bogoliubov-Born-Green-Kirkwood-Yvon (BBGKY) hierarchy is the standard method to predict higher-order particle distribution functions. As the one-particle distribution function $f^{(1)}$ is expressed as a function of the two-particle distribution, similarly,

one can express the two particle distribution as a function of the three-particle distribution function. Introducing relative coordinates $\mathbf{r} = \mathbf{r}_2 - \mathbf{r}_1$ and relative velocities $\mathbf{v} = \mathbf{v}_2 - \mathbf{v}_1$

$$\frac{\partial f^{(2)}}{\partial t} + \mathbf{v} \cdot \frac{\partial f^{(2)}}{\partial \mathbf{r}} - 2\frac{\partial V}{\partial \mathbf{r}} \cdot \frac{f^{(2)}}{\partial \mathbf{v}} = N \int \mathrm{d}\mathbf{p}_3 \mathrm{d}\mathbf{r}_3 \left(\frac{\partial V_{13}}{\partial \mathbf{r}_1} \cdot \frac{\partial f^{(3)}}{\partial \mathbf{r}_1} + \frac{\partial V_{23}}{\partial \mathbf{r}_2} \cdot \frac{\partial f^{(3)}}{\partial \mathbf{v}_2} \right) .$$

Under the assumption of spacial translational invariance, this gives a chain of equations each depending on the next higher $f^{(i)}$. Depending on the system parameters, this expansion usually is cut off at some point by some closure.

1.2.2 Overdamped dynamics

For colloids, the collision operator on the right hand side of Eq. (1.5) is very important. Concretely, the relevant time scales of a typical experiment are much larger than the inverse damping rate ν^{-1}. Then, the inertia term in the Langevin Eq. (1.4) loses importance and it is typically neglected. Equation 1.4 reduces to

$$\nu \mathbf{p}_i = \mathbf{F}_i + \mathbf{L}_i \, .$$

Since in overdamped dynamics, the inertia part is negligible, the n-particle distribution function is often written as a function of the positions only

$$\Psi(t, \mathbf{r}_1, \ldots, \mathbf{r}_N) = \int \mathrm{d}\mathbf{p}_1 \ldots \mathbf{p}_N \; f^{(N)}(t, \mathbf{p}_1, \mathbf{r}_1, \ldots, \mathbf{p}_N, \mathbf{r}_N) \, .$$

This approach allows, to derive the steady-state probability flux of the i-th particle $\mathbf{J}_i$ as

$$\mathbf{J}_i = \mu_0 \mathbf{F}_i \Psi - D_0 \frac{\partial \Psi}{\partial \mathbf{r}_i} \, ,$$

where μ_0 is the mobility coefficient and D_0 the free diffusion coefficient of a single particle. The two latter quantities are connected via the Einstein relation $D_0 = \mu_0 k_\mathrm{B} T$. By integration over the momenta in Eq. (1.5), all derivatives with respect to $\mathbf{p}_i$ become equal zero. With the probability flux, this immediately derives the Smoluchowski equation [89]

$$\frac{\partial \Psi}{\partial t} + \sum_i^N \frac{\partial \mathbf{J}_i}{\partial \mathbf{r}_i} = 0 \, . \tag{1.7}$$

The Smoluchowski equation is often used as a basic for further theories on colloidal dynamics. In Chapter 3 of this thesis, the theoretical derivation for two-particle distribution function also bases on this equation.

1.3 Nonreciprocal forces

In this section, some selected occurrences of interactions that break the actio-reactio symmetry shall be introduced. As mentioned earlier, this is done with the focus on complex plasmas and colloidal dispersions, of which some basic properties and theoretical descriptions were outlined above. Nonreciprocal forces are nonconservative, which can be illustrated by a simple example: Let the force of particle A on particle B be $\mathbf{F}_{AB} = 0$, but for the force of particle B on particle A: $\mathbf{F}_{BA} \neq 0$. Then, the "work" of bringing these two particles together, drastically depends on the path chosen. It is highly important, how much the A or B particle is moved, with respect to the other one.

Even worse, nonreciprocal forces are not only nonconservative, but also energy conservation is not valid. One might stipulate a situation where Eq. (1.1) would be reversed, such that for two particles A and B the forces are equal $\mathbf{F}_{AB} = \mathbf{F}_{BA}$. Due to the mere presence of both of the two particles, in an undamped situation they would accelerate infinitely. This breaking of energy conservation would allow to build a perpetual motion machine, which is of course unphysical.

However, nonreciprocal effective forces, occur naturally in many nonequilibrium situations. Most intuitively, this is the case for biological predator-prey systems [29, 30], where e.g. a lion chases a gazelle [90]. More "physical" systems were mentioned earlier in this chapter: In particular, wake-mediated interactions in complex plasmas, and also hydrodynamic or diffusiophoretic interactions in colloidal dispersions. Even though, nonreciprocal interactions represent an important general class of interactions, they have so far received little attention. In this section, the scientific discourse on the three mentioned situations is introduced, where the actio-reactio symmetry is broken. Typically, this is done in the context of some of binary mixtures, where the particles can be separated in two reciprocal sub-ensembles. While the generalization to more species is in principle straight forward, it may drastically complicate calculations. In this thesis, all results are presented for two species systems.

1.3.1 Hydrodynamic interaction

Hydrodynamic interactions are nonreciprocal and play a major role in colloidal dispersions. They are of particular importance, if the environment moves with respect to the particles, e.g. by an external flow. Thus they naturally occur in many systems, but are often ignored, since their long-ranged nature encumbers simulations. Neglecting hydrodynamic interactions is justified, if the suspension is strongly interacting, but the volume fraction of the particles is low. The intuition behind hydrodynamic interactions is straight forward: When a particle moves through a fluid it induces a flow field, and when a particle is placed in moving fluid, it will respond to that motion. Now, when N particles are dispersed in a fluid, they will induce a flow field, and respond to it. In that sense, the velocity of a particle does not only depend on the forces it is exposed to, but

also on the motion of the other particles. In a simplified picture, under the assumption of immediate and linear fluid response and neglecting rotations, one writes [91],

$$\mathbf{v}_i = \sum_j \boldsymbol{L}_{ij}(\{\mathbf{r}\})\, \mathbf{F}_j \ ,$$

where the coefficients $\boldsymbol{L}_{ij}$ are the 3×3 mobility-matrices. Ideally, one would directly solve the Navier-Stokes equations for the fluid flow. However, this is not simple: Hydrodynamic interactions depend on all particle positions and have drastically different near and far field behavior. For low concentrations and large distances, a multipole-like expansion for particle pairs can be carried out. In this picture, the self interactions is $\boldsymbol{L}_{ii} = \boldsymbol{I}/\gamma$, where γ is the particle friction and $\boldsymbol{I}$ the unit matrix. For the pair-interaction between particle i and j one has $\boldsymbol{L}_{ij} = \boldsymbol{L}_{RP}(\mathbf{r}_i - \mathbf{r}_j)$, where $\boldsymbol{L}_{RP}$ is the Rotne-Prager tensor [92]:

$$\boldsymbol{L}_{RP}(\mathbf{r}) = \frac{1}{\gamma}\left[\frac{3}{4}\frac{R_\mathrm{h}}{r}(I + \hat{\mathbf{r}}\hat{\mathbf{r}}) + \frac{1}{2}\frac{R_\mathrm{h}^3}{r^3}(I - 3\hat{\mathbf{r}}\hat{\mathbf{r}})\right] \ ,$$

where R_H is the hydrodynamic radius of the particles, $r = |\mathbf{r}|$, $\hat{\mathbf{r}} = \mathbf{r}/r$ and $\mathbf{rr}$ denotes a dyadic product. Another frequently used approximation for hydrodynamic interactions corresponds to the monopole part of the Rotne-Prager tensor. The so-called Oseen tensor $\boldsymbol{L}_O(\mathbf{r})$ [92] decays with $1/r$ and is the dominant part of the long-range interactions. For the pair interactions between the particles i and j one has $\boldsymbol{L}_{ij} = \boldsymbol{L}_O(\mathbf{r}_i - \mathbf{r}_j)$, with

$$\boldsymbol{L}_O(\mathbf{r}) = \frac{3R_\mathrm{h}}{4\gamma r}(\boldsymbol{I} + \hat{\mathbf{r}}\hat{\mathbf{r}}) \ . \tag{1.8}$$

Hydrodynamic interactions can lead to effective nonreciprocal interparticle forces. Within the Oseen regime $|\mathbf{r}| \gg R_\mathrm{h}$, this can lead to the extreme case of nonreciprocity, where $\mathbf{F}_{AB} = \mathbf{F}_{BA}$. Consider a bilayer setup in an external flow, as depicted in Fig. 1.2 (see Ref. [93] for an actual experiment). The motion of the particles in the system is confined in the two parallel layers. The solvent flows in perpendicular direction with velocity $\mathbf{v}_0$, and induces hydrodynamic interactions between the particles. Then, the Stokes solution for a single sphere at the origin is

$$\mathbf{u}(\mathbf{r}) = \mathbf{v}_0 - \frac{3R_\mathrm{h}}{4\,|\mathbf{r}|}\left(\mathbf{v}_0 + \frac{1}{\mathbf{r}^2}(\mathbf{v}_0\mathbf{r})\mathbf{r}\right) \ .$$

The total flow field $\mathbf{v}(\mathbf{r})$ of many of spheres is a linear superposition, such that $\mathbf{v}(\mathbf{r}) = \sum_{i=1}^{N} \mathbf{u}(\mathbf{r} - \mathbf{r}_i)$. In this picture, the effective forces between a particle in the upper layer A and a particle in the lower layer B are

$$\mathbf{F}_{AB}(h, v_0, r) = \mathbf{F}_{BA}(h, v_0, r) = -\frac{9\pi\eta R_\mathrm{h}^2 v_0 h}{2(r^2 + h^2)^{3/2}}\ \mathbf{r} \ , \tag{1.9}$$

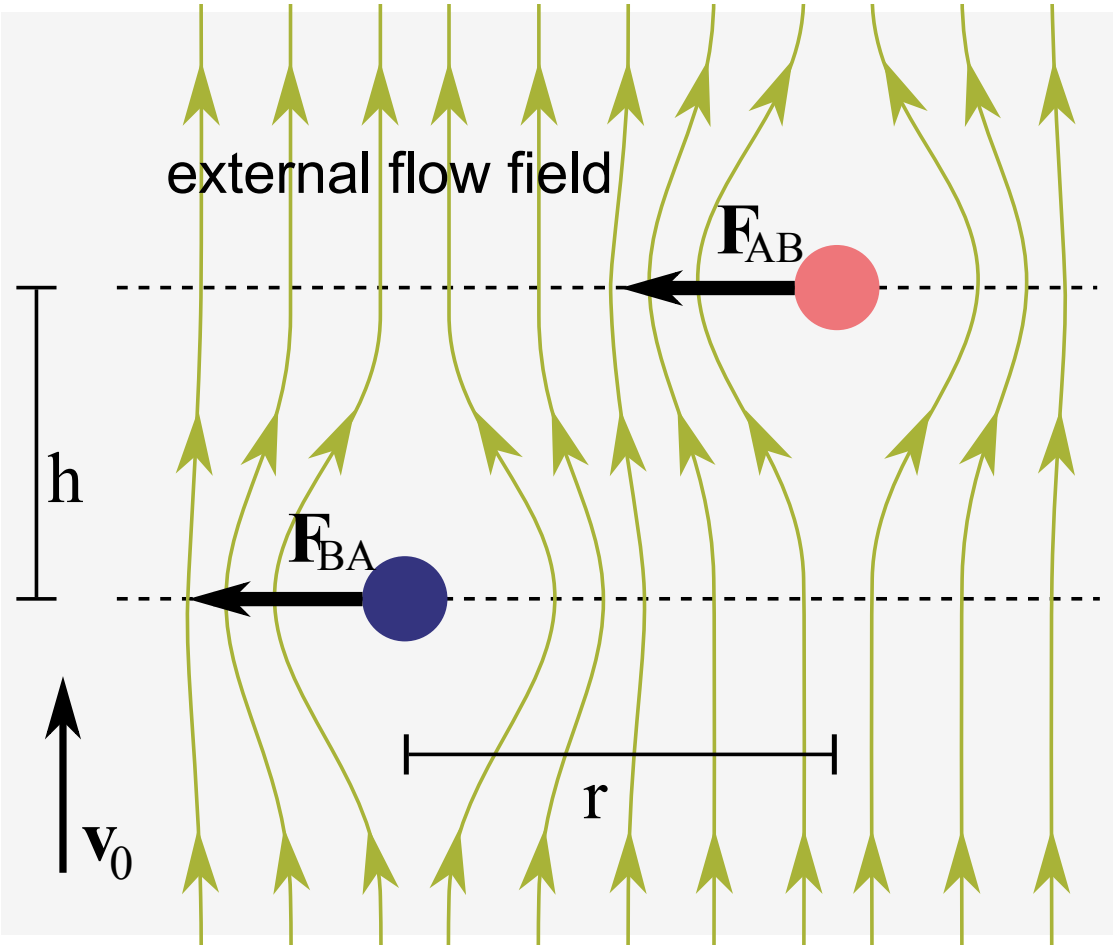

Figure 1.2: *The effective forces between two colloidal particles are nonreciprocal, when the interactions are mediated by an external flow. In this example, two colloidal particles are confined in two layers at different heights of distance h. Hydrodynamic interactions lead to the extreme case of nonreciprocity, where the effective forces are of equal strength and direction.*

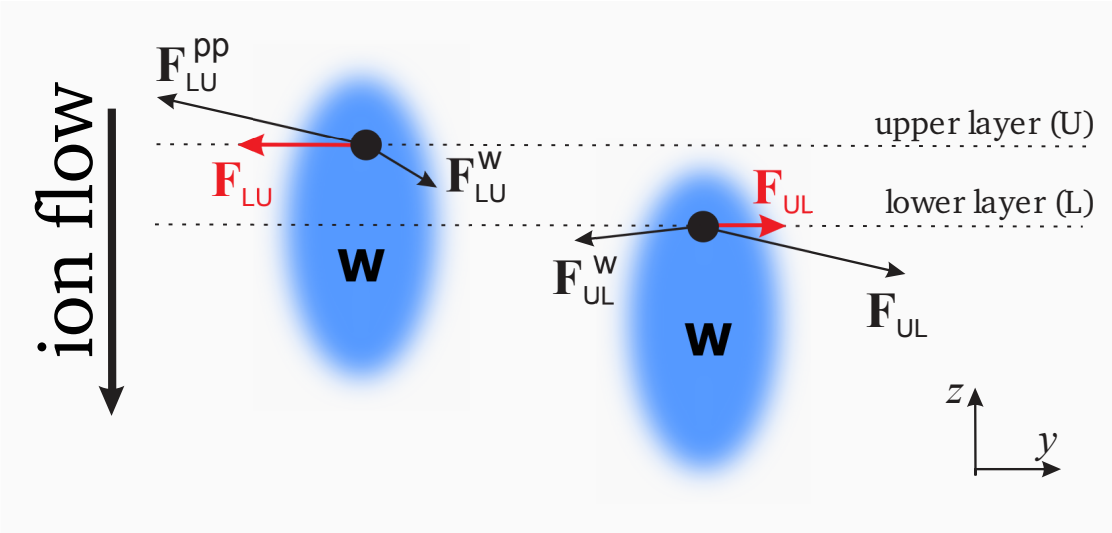

Figure 1.3: *The total force exerted on the upper-layer (U) particle from the lower-layer (L) particle is the sum of the repulsive force* $\mathbf{F}^{\mathrm{p}}_{\mathrm{LU}}$ *of direct interparticle interaction and the attractive force* $\mathbf{F}^{\mathrm{w}}_{\mathrm{LU}}$ *from the wake of the lower particle (and similar for the total force on the lower particle). While the direct forces are reciprocal,* $\mathbf{F}^{\mathrm{p}}_{\mathrm{LU}} = -\mathbf{F}^{\mathrm{p}}_{\mathrm{UL}}$*, the wake forces are not,* $\mathbf{F}^{\mathrm{w}}_{\mathrm{LU}} \neq -\mathbf{F}^{\mathrm{w}}_{\mathrm{UL}}$*; since the forces decrease with the distance, we have* $|\mathbf{F}^{\mathrm{w}}_{\mathrm{LU}}| < |\mathbf{F}^{\mathrm{w}}_{\mathrm{UL}}|$ *and therefore* $|\mathbf{F}_{\mathrm{LU}}| > |\mathbf{F}_{\mathrm{UL}}|$*. (Figure and caption from Ref. [1])*

where η is the fluid viscosity, $v_0 = |\mathbf{v}_0|$, h the height difference between the layers and r the distance between the particles projected on the layer. For the interaction in the same particle species, the flow-induced forces vanish. Additionally, one would expect some kind of reciprocal interaction between the particles, e.g. charge interaction. Then, the relative magnitude of the nonreciprocity could be tuned by the external flow velocity.

1.3.2 Wake interaction

In a complex plasma, a charged particle will induce a wake, if placed in an ion flow. In particular, this is the case for particles levitating in the sheath region [15]. The negatively charged electrode attracts positively charged ions. The induced flow field is disturbed by the particles, which act as a lens to focus the ions downstream of the particle. This wake formation is a well-known and well studied phenomenon (see Section 1.1.2). In a good approximation, one can consider every wake as a positive point-charge.

The levitation height of particles in the sheath region depends dominantly on the balance of electrostatic repulsion, ion drag force and gravitation. Consider an experiment with a bidisperse mixture in a complex plasma, i.e. two species of particles with distinct diameters. Due to the different associated masses, the two particle species will levitate at a different heights of distance h. This generates a bilayered set-up as depicted in Fig. 1.3. Assuming that the distance between the particle and the wake is δ, every particle at

position $\mathbf{r}_i$ can be associated with a wake at position $\mathbf{r}_i - \delta\ \mathbf{e}_z$, where $\mathbf{e}_z$ is the unit vector in flow direction. Then, the interparticle forces are the superposition of particle-particle forces $\mathbf{F}^p$ and particle-wake forces $\mathbf{F}^w$. While the particle-particle forces are reciprocal, the particle-wake forces are not. The height difference between the wake of an upper layer particle U and a particle in the lower layer L is $h - \delta$. For the reverse case, the height difference between a lower layer particle's wake and an upper layer particle is $h + \delta$. Following this simple geometric argument, the superposition of the effective pair forces violates Newton's third law.

1.3.3 Diffusiophoretic interaction

Gradients in concentration of a solute in colloidal dispersions can lead to net motion of particles [94–97]. This motion along a concentration gradients $\nabla c(\mathbf{r})$ is called diffusiophoresis and typically connected to an equation of motion like

$$\mathbf{v}(\mathbf{r}) = \mu\ \nabla c(\mathbf{r})\ , \tag{1.10}$$

which states that the velocity $\mathbf{v}$ of a particle is proportional to the concentration gradient of the solute with a surface mobility μ [98]. The concentration gradients in the system can be created by catalytic activity, e.g. of some object placed in the solvent. Let the surface of that object emit some chemical with a surface activity s. Particular interesting effects happen, when the catalyst is on the surface of the colloid itself. In the case of asymmetric coating, this can lead to self-propulsion [70, 72, 98–101]. For the simpler case, where the catalytic activity takes place on the surface homogeneously, the colloid generates an isotropic concentration field around the particle [27]. Concretely, the concentration field is obtained by solving the diffusion equation in the steady state:

$$\nabla^2 c(\mathbf{r}) = 0 \qquad \text{and} \qquad -D\ \frac{\partial c(r)}{\partial r}\bigg|_{r=\sigma} = s\ ,$$

where ∇^2 is the Laplacian, r the distance to the particle, σ is the radius of the colloid and D the effective diffusion coefficient of the solute. This results in a concentration field around the particle as

$$c(r) = \frac{s\ \sigma^2}{D\ r}\ . \tag{1.11}$$

From Eq. (1.10) it can be seen, that this is quite similar to an effective potential of a particle.

Soto and Golestanian proposed a model, where in a binary mixture the two species have different surface mobilities μ_A, μ_B and different surface activities s_A, s_B [27]. The effective forces exerted by particle of type α on a particle of type β is then $\mathbf{F}_{\alpha\beta} \propto \mu_\beta\ s_\alpha$. Then, the quantities μ_A, μ_B, s_A and s_B can be tuned by surface chemistry. In general, one has $\mathbf{F}_{AB} \neq \mathbf{F}_{BA}$, i.e. for these effective interactions Newton's third law is broken. This model was studied in detail [27, 28]; for particular choices it is shown to form

self-assembled active molecules. Also, one can achieve assemblies of particles that show oscillatory motion, similar to bacteria. A model based on this is explained in detail in Chapter 3.

CHAPTER 2

MANY-BODY SYSTEMS WITH NONRECIPROCAL INTERACTIONS

As described in the very beginning of this thesis, one of the fundamental postulates in physics is Newton's third law *actio=reactio*, laying the foundations of classical mechanics. This law, which states that the pair interactions between particles are reciprocal, holds not only for the fundamental microscopic forces, but also for *equilibrium* effective forces on classical particles, obtained by integrating out microscopic degrees of freedom [5–9]. However, the action-reaction symmetry for particles can be broken when their interaction is mediated by some *non-equilibrium environment*: This occurs, for instance, when the environment moves with respect to the particles, or when a system of particles is composed of different species and their interaction with the environment is out of equilibrium (of course, Newton's third law holds for the complete "particles plus environment" system). Recently there have been numerous studies of nonreciprocal interactions on the mesoscopic length-scale. Examples include forces induced by non-equilibrium fluctuations [22, 23], optical [24, 25] and diffusiophoretic [26, 27] forces, effective interactions between colloidal particles under solvent or depletant flow [11–13, 21], shadow [17–19] and wake-mediated [14, 15, 20] interactions between microparticles in a flowing plasma, etc. A very different case of nonreciprocal interactions are "social forces" [32, 33] governing, e.g., pedestrian dynamics.

A natural violation of Newton's third law in non-equilibrium environments can be easily illustrated. One example for nonreciprocal interactions occurs in the context of catalytically driven colloids (microswimmers) [27]. Typically, a single colloidal particle which produces or consumes chemicals on its surface, being embedded in a solution with a gradient in the chemical concentration, is propelled along the gradient – this

This chapter was published in a very similar form under the title "Statistical Mechanics where Newton's Third Law is Broken" by Alexei Ivlev, Jörg Bartnick, Marco Heinen, Chengran Du, Vladimir Nosenko and Hartmut Löwen, Phys. Rev. X 5, 011035 – Published 26 March 2015, see Reference [1].

non-equilibrium transport phenomenon is termed as diffusiophoresis. Since each particle generates an inhomogeneous concentration profile in its vicinity, the action-reaction symmetry in a binary mixture of microswimmers (with different mobilities and surface activities) is broken. The magnitude of the nonreciprocity can be tuned by varying the relative disparity of the activities or/and mobilities. The other very different system where the action-reaction symmetry is broken are quasi-two-dimensional (2D) binary complex plasmas [15,16]. These are binary mixtures of charged microparticles, levitating in a plasma over a flat horizontal electrode at slightly different heights. The horizontal interactions between the microparticles are nonreciprocal, because they are mediated by the plasma wakes – the perturbations below each particle, generated in a plasma streaming towards the electrode. The magnitude of the nonreciprocity is controlled by varying the difference of the levitation heights for the two species.

Nonreciprocal forces are in principle non-Hamiltonian (i.e., they cannot be derived from a classical many-body Hamiltonian), so the standard Boltzmann description of classical equilibrium statistical mechanics breaks down. Hence, it is a priori unclear whether concepts like temperature and thermodynamic phases can be used to describe them. Apart from a few considerations in the context of the multi-scale coarse graining [7, 102], the classical statistical mechanics of systems with nonreciprocal interactions – despite their fundamental importance – remains widely unexplored.

In this chapter we present the statistical foundations of systems with nonreciprocal interparticle interactions. To describe various classes of interactions relevant to real experimental situations, we consider a generic model where the action-reaction symmetry is broken for the pair interaction between two sub-ensembles. The asymmetry is characterized by the nonreciprocity parameter Δ, which is the ratio of the nonreciprocal to reciprocal forces. We show that for the "constant" nonreciprocity, when Δ is independent of the interparticle distance r, one can construct a (pseudo) Hamiltonian with renormalized masses and interactions. Hence, being intrinsically non-equilibrium, such systems can nevertheless be described in terms of equilibrium statistical mechanics and exhibit detailed balance with distinct temperatures for different sub-ensembles (the temperature ratio is determined by Δ). For a general case, when Δ is a function of r, the system is no longer conservative – it follows a universal asymptotic behavior with the temperatures growing with time as $\propto t^{2/3}$. The temperature ratio in this case is determined by an *effective* constant nonreciprocity which is uniquely defined for a given interaction. The temperatures reach a steady state when the damping due to surrounding medium is taken into account, while their ratio remains practically unchanged. One of the remarkable implications of our results is the occurrence of extreme temperature gradients, generated in mixtures of particles at the ultimate scale of interparticle distance.

To verify the principal theoretical predictions, we have also performed experimental tests with quasi-2D binary complex plasmas. The interactions of particles of one sort with the wakes generated by particles of the other sort results in a very general mechanism of the action-reaction symmetry breaking due to the presence of a flow (as explained in detail in the caption of Fig. 1.3. This makes 2D complex plasmas perfectly suited for studying generic properties of many-body systems with nonreciprocal interactions.

2.1 Models for wake-mediated interactions

All available self-consistent models for the interaction between microparticles in 2D complex plasmas are based on the solution of the kinetic equation for ions moving in the electrostatic field of the sheath, while electrons are described by the Boltzmann distribution [103]. Different approximations used for the ion collision operator (describing the interaction with neutral gas) merely reflect different experimental regimes (in terms of the rf discharge power and pressure) when the particular model is applicable. Note that the wake generated by a given particle is practically unaffected by the field of the neighbors, because the characteristic lateral range of the ion-particle interaction (providing the main contribution to the formation of wake, the Coulomb radius) is typically 1-2 orders of magnitude shorter than the interparticle distance [103].

In order to illustrate the essential features of the wake-mediated interaction, we consider a simple "Yukawa/point-wake model" [20, 104]. In this model, the wake is treated as a positive, point-like effective charge q located at the distance δ below each negatively charged particle (of charge $-Q$). So, the total interaction between two particles is a simple superposition of the particle-particle and particle-wake interactions, both described by the (spherically-symmetric) Yukawa potentials with effective screening length λ.

For a binary 2D system of particles, it is convenient to introduce the horizontal (radial) distance r and the vertical distance z. The total potential governing the interparticle interactions is $\varphi_Q(r,z) - \varphi_q(r,z)$, where the particle-particle and particle-wake terms are $\varphi_Q(r,z) = (Q^2/R_Q)e^{-R_Q/\lambda}$ and $\varphi_q(r,z) = (qQ/R_q)e^{-R_q/\lambda}$, respectively, $R_Q = \sqrt{r^2+z^2}$ is the interparticle distance, and $R_q = \sqrt{r^2+(z+\delta)^2}$ is the distance to the neighboring wake. For the layers separated by the height difference H, we readily obtain the potentials of the reciprocal and nonreciprocal forces,

$$\begin{aligned} \varphi_{\rm r}(r) &= \varphi_Q(r,H) - \frac{1}{2}\left[\varphi_q(r,H) + \varphi_q(r,-H)\right], \\ \varphi_{\rm n}(r) &= \frac{1}{2}\left[\varphi_q(r,H) - \varphi_q(r,-H)\right]. \end{aligned}$$

The interaction is reciprocal for particles levitating in the same layer. For the interlayer interactions, when the height difference is much smaller than the interparticle distance (within each layer), the nonreciprocity parameter scales linearly with H, as $\Delta(r) \propto (q/Q)H\delta/r^2$.

2.2 Constant nonreciprocity

In the introduction we mentioned several prominent examples of nonreciprocity, including the situations when different particles interact differently with the surrounding non-equilibrium environment [17, 27], or when the action-reaction symmetry is broken in the presence of a flow [13, 15] (while the particles themselves may be identical). In

what follows, for the sake of convenience we generally attribute particles to "different species" when their pair interaction is nonreciprocal.

To describe the variety of nonreciprocal forces we employ the following generic model: We consider a binary mixture of species A and B, where the spatial dependence of the pair-interaction force is proportional to the derivative of the function $\varphi(r)$. The interaction is reciprocal for the AA and BB pairs, whereas between the species A and B the action-reaction symmetry is broken. The measure of the asymmetry is the *nonreciprocity parameter* $\Delta(\geq 0)$.

It is noteworthy that the only assumption made about the general form of isotropic nonreciprocal interactions is that non-pairwise additive many-body forces between different species are negligible (which is always justified to describe, e.g., complex plasmas and dilute colloids [15]). Apart form that, no further assumption is imposed on the model, i.e., the parameter Δ completely characterizes any isotropic type of pairwise nonreciprocal forces.

First, we consider the case when Δ is independent of the interparticle distance ("constant") – this represents, e.g., binary colloidal dispersions with the dominating diffusiophoretic interactions [26, 27] or complex plasmas with the shadow interactions [17–19]. We present the force $\mathbf{F}_{ij}$ exerted *by the particle i on the particle j* as follows:

$$\mathbf{F}_{ij} = -\frac{\partial\varphi(r_{ij})}{\partial\mathbf{r}_j} \times \begin{cases} 1-\Delta & \text{for } ij \in AB; \\ 1+\Delta & \text{for } ij \in BA; \\ 1 & \text{for } ij \in AA \text{ or } BB, \end{cases} \tag{2.1}$$

where $r_{ij} = |\mathbf{r}_i - \mathbf{r}_j|$ and each particle can be of the sort A or B. In order to distinguish the effect of nonreciprocity $\varphi(r)$ must be the same for the AB and BA pairs, while for other pairs it may be different.

2.2.1 Pseudo-Hamiltonian

By writing the Newtonian equations of motion of individual particles interacting via the force (2.1), we notice that the interaction symmetry is restored if the particle masses and interactions are renormalized as follows:

$$\tilde{m}_i = m_i \times \begin{cases} (1+\Delta)^{-1} & \text{for } i \in A; \\ (1-\Delta)^{-1} & \text{for } i \in B, \end{cases} \tag{2.2}$$

$$\tilde{\varphi}(r_{ij}) = \varphi(r_{ij}) \times \begin{cases} (1+\Delta)^{-1} & \text{for } ij \in AA; \\ (1-\Delta)^{-1} & \text{for } ij \in BB; \\ 1 & \text{for } ij \in AB \text{ or } BA. \end{cases} \tag{2.3}$$

Hence, a binary system of N particles with nonreciprocal interactions of the form of Eq. (2.1) is described by a *pseudo-Hamiltonian* with the masses (2.2) and interactions (2.3). In particular, this implies the pseudo-momentum and energy conservation,

$$\begin{aligned} \sum_i^N \tilde{m}_i \mathbf{v}_i &= \text{const}, \\ \sum_i^N \frac{1}{2}\tilde{m}_i v_i^2 + \sum_{i<j}^N \tilde{\varphi}(r_{ij}) &= \text{const}, \end{aligned}$$

and allows us to employ the methods of equilibriums statistical mechanics to describe such systems. For instance, from equipartition, $\frac{1}{2}\tilde{m}_A\langle v_A^2\rangle = \frac{1}{2}\tilde{m}_B\langle v_B^2\rangle \equiv \frac{1}{2}Dk_{\mathrm{B}}\tilde{T}$ (where $\tilde{T}$ is the pseudo-temperature and D is the dimensionality), it immediately follows that in detailed balance $T_A = (1+\Delta)\tilde{T}$ and $T_B = (1-\Delta)\tilde{T}$, i.e.,

$$\frac{T_A}{T_B} = \frac{1+\Delta}{1-\Delta}. \tag{2.4}$$

We conclude that mixtures of particles with nonreciprocal interactions, being intrinsically non-equilibrium, can nevertheless reach a remarkable state of *detailed dynamic equilibrium*, where the species have different temperatures T_A and T_B. Note that the equilibrium is only possible for $\Delta < 1$, otherwise the forces $\mathbf{F}_{AB}$ and $\mathbf{F}_{BA}$ are pointed in the same direction [see Eq. (2.1)] and the system cannot be stable.

2.3 General nonreciprocity

Now we shall study a general case, when the interactions between the species A and B are determined by the forces $\mathbf{F}_{AB,BA}(r) = \mp\mathbf{F}_{\mathrm{r}}(r) + \mathbf{F}_{\mathrm{n}}(r)$. The reciprocal, $\mathbf{F}_{\mathrm{r}}(r)$, and nonreciprocal, $\mathbf{F}_{\mathrm{n}}(r)$, components are arbitrary functions of the interparticle distance, they can always be presented as $\mathbf{F}_{\mathrm{r,n}}(r) = (\mathbf{r}/r)F_{\mathrm{r,n}}(r)$, where $F_{\mathrm{r,n}} = -d\varphi_{\mathrm{r,n}}/dr$. As we show below, the dynamic equilibrium is no longer possible in this case, and analytical results can only be obtained in certain limiting regimes.

To facilitate the analysis, we shall distinguish between the weakly- and strongly-coupled systems: The former regime represents the situation when binary collisions between particles play the dominant role ("dilute" systems), while in the latter regime simultaneous interactions with many neighbors are crucial ("dense" systems). The transition between the regimes is determined by the coupling parameter Γ, which is the ratio of the mean energy of the (reciprocal) pair interaction to the particle thermal energy (i.e., $\Gamma \propto T^{-1}$).

2.3.1 Pair collisions: Variation of energy and scattering functions

Let us first study weakly-coupled ($\Gamma \ll 1$) systems whose dynamics is governed by binary interparticle collisions (numerical analysis of strongly-correlated systems is presented in Sec. 2.4). It is instructive to write the equations of motion for a pair of particles A and B in terms of the relative coordinate $\mathbf{r} = \mathbf{r}_A - \mathbf{r}_B$ and the center-of-mass coordinate $\mathbf{R} = (m_A\mathbf{r}_A + m_B\mathbf{r}_B)/M$,

$$M\ddot{\mathbf{R}} = 2\mathbf{F}_{\rm n}(r), \tag{2.5}$$

$$\mu\ddot{\mathbf{r}} = \mathbf{F}_{\rm r}(r) + \frac{m_B - m_A}{m_A + m_B}\mathbf{F}_{\rm n}(r), \tag{2.6}$$

where $\mu = m_A m_B/(m_A + m_B)$ and $M = m_A + m_B$ are the reduced and total masses, respectively. Using Eqs. (2.5) and (2.6), we calculate the variation of the kinetic energy after a collision, $\delta E_{A,B}$, which is expressed via the relative velocity $\mathbf{v} = \dot{\mathbf{r}}$, the center-of-mass velocity $\mathbf{V} = \dot{\mathbf{R}}$, and the scattering angle χ for the relative motion. We define the relative velocity, $\mathbf{v} = \dot{\mathbf{r}}$, the center-of-mass velocity, $\mathbf{V} = \dot{\mathbf{R}}$, and their values after a collision, $\mathbf{v}' = \mathbf{v} + \delta\mathbf{v}$ and $\mathbf{V}' = \mathbf{V} + \delta\mathbf{V}$. From Eq. (6) we infer that the relative motion is conservative, i.e., the absolute value of the relative velocity remains unchanged after a collision, $|\mathbf{v} + \delta\mathbf{v}| = |\mathbf{v}|$. Equation (5) governs the variation of the center-of-mass velocity, $\delta\mathbf{V}$, which is determined by the relative motion via $\mathbf{F}_{\rm n}(r)$. By employing the relation $\mathbf{v}_{A,B} = \mathbf{V} \pm (\mu/m_{A,B})\mathbf{v}$, we obtain the variation of the kinetic energy $E_{A,B}$ after a collision,

$$\delta E_{A,B} = m_{A,B}\left[\mathbf{V}\cdot\delta\mathbf{V} + \frac{1}{2}(\delta\mathbf{V})^2\right] \pm\mu\left(\mathbf{V}\cdot\delta\mathbf{v} + \mathbf{v}\cdot\delta\mathbf{V} + \delta\mathbf{V}\cdot\delta\mathbf{v}\right).$$

Since the relative motion is conservative, from Eq. (5) we conclude that $\delta\mathbf{V}$ is parallel to $\delta\mathbf{v}$, i.e., $\delta\mathbf{V}\cdot\delta\mathbf{v} = \delta V\delta v$. For 2D collisions, let us introduce the angle θ between $\mathbf{V}$ and $\mathbf{v}$, and the scattering angle χ between $\mathbf{v}'$ and $\mathbf{v}$ (Fig. 2.1). Then we have $\mathbf{V}\cdot\delta\mathbf{V} = V\delta V\sin(\theta - \frac{1}{2}\chi)$, $\mathbf{V}\cdot\delta\mathbf{v} = V\delta v\sin(\theta - \frac{1}{2}\chi)$, and $\mathbf{v}\cdot\delta\mathbf{V} = -v\delta V\sin\frac{1}{2}\chi$ [105, 106]. For 3D systems the corresponding expressions are easily derived using the cosine rule of spherical trigonometry.

In order to calculate the magnitudes of the velocity variations and the scattering angle, we consider the approximation of small-angle scattering, $\chi \ll 1$. Using Eqs. (5) and (6), for a given impact parameter ρ we get the following expressions [105]:

$$\delta V(\rho) = \frac{4}{Mv}f_{\rm n}(\rho),$$

$$\chi(\rho) = \frac{\delta v}{v} = \frac{2}{\mu v^2}\left[f_{\rm r}(\rho) + \frac{m_B - m_A}{m_A + m_B}f_{\rm n}(\rho)\right],$$

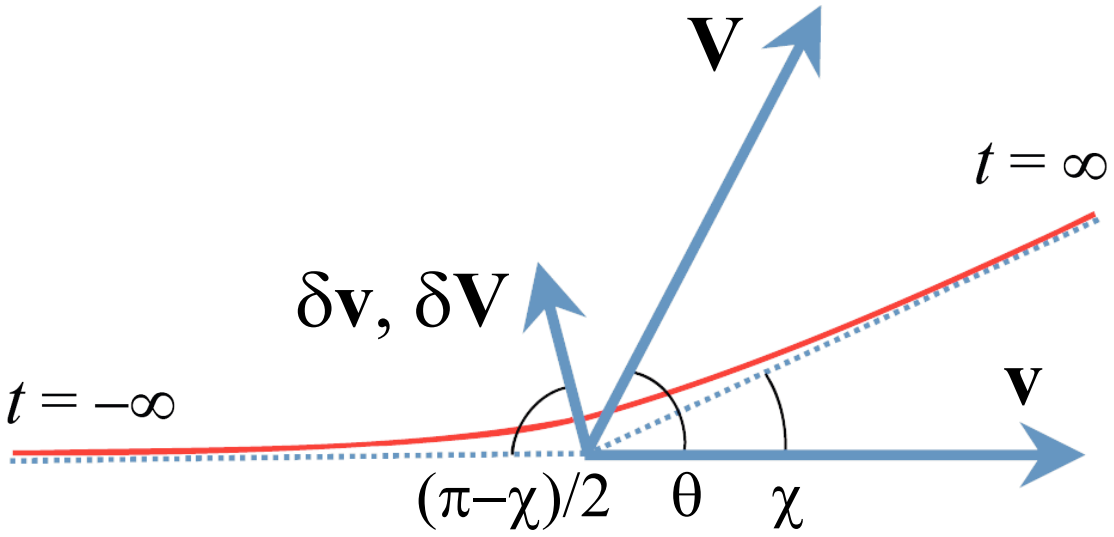

Figure 2.1: *Sketch illustrating pair collisions in 2D systems. Shown are the variations of the center-of-mass velocity* **V** *and the relative velocity* **v** *as well as the scattering angle* χ*, plotted in polar coordinates.*

determined by the scattering functions (α =r,n),

$$f_\alpha(\rho) = \rho \int_\rho^\infty dr \frac{F_\alpha(r)}{\sqrt{r^2-\rho^2}}. \tag{2.7}$$

General equations describing the asymptotic evolution of the mean kinetic temperatures of species A and B are obtained by multiplying $\delta E_{A,B}$ with the collision frequency between the species and averaging it over the Maxwellian velocity distributions [106]. The collision cross section is represented by the integral over the impact parameter [105], $\int d\rho$ for 2D systems or $\int d\rho\, 2\pi\rho$ for 3D systems. Note that after the integration over θ all terms in the above expression for $\delta E_{A,B}$ yield contributions $\sim \chi^2$.

2.3.2 Asymptotic Universality

In the approximation of *small-angle scattering* [105], $\chi \ll 1$, which significantly simplifies the analysis and is valid for sufficiently high kinetic energies (provided the pair interaction is not of the hard-sphere-like type), one can derive general equations describing the asymptotic evolution of the kinetic temperatures $T_{A,B}$. To obtain a closed-form solution, we assume that the elastic energy exchange in collisions provides efficient Maxwellization of the distribution functions (which can be verified by molecular

dynamics simulations discussed below). This yields the following equations for 2D systems:

$$\dot{T}_{A,B} = \pm\frac{1\pm\Delta_{\text{eff}}}{1+\epsilon}\frac{\sqrt{2\pi}n_{B,A}I_{\text{rr}}}{m_A m_B\left(\frac{T_A}{m_A}+\frac{T_B}{m_B}\right)^{3/2}} \left[(1+\Delta_{\text{eff}})T_B-(1-\Delta_{\text{eff}})T_A+\frac{\epsilon}{1\pm\Delta_{\text{eff}}}(T_B-T_A)\right], \quad (2.8)$$

where n_α is the areal number density (for simplicity, below we assume $n_A = n_B = n$). The equations depend on the *effective nonreciprocity* Δ_{eff} and the *interaction disparity* ϵ,

$$\begin{aligned}\Delta_{\text{eff}} &= I_{\text{nn}}/I_{\text{rn}},\\ \epsilon &= I_{\text{rr}}I_{\text{nn}}/I_{\text{rn}}^2-1,\end{aligned} \quad (2.9)$$

the integrals $I_{\alpha\beta} = \int_0^\infty d\rho\, f_\alpha f_\beta$ are expressed via the scattering functions $f_\alpha(\rho)$ [see Eq. (2.7) in Appendix 2.3.1; it is assumed that the integrals converge]. We point out that Δ_{eff} and ϵ are numbers uniquely defined for given functions $\varphi_{\text{r,n}}(r)$; from the Cauchy inequality it follows that $\epsilon \geq 0$.

For 3D systems the r.h.s. of Eq. (2.8) should be multiplied by the additional factor 8/3, and the integrals become $I_{\alpha\beta} = \int_0^\infty d\rho\, \rho f_\alpha f_\beta$. Note that for a reciprocal Coulomb interaction, I_{rr} is proportional to the so-called Coulomb logarithm (see e.g., [106, 107]) and $\Delta_{\text{eff}} = 0$; Eq. (2.8) is then reduced to the classical equation for the temperature relaxation in a plasma [106].

For the constant nonreciprocity [i.e., when $F_{\text{n}}(r)/F_{\text{r}}(r) = \Delta$ is independent of r] we get $\Delta_{\text{eff}} = \Delta$ and $\epsilon = 0$. In this case, Eq. (2.8) has an equilibrium solution given by Eq. (2.4). Otherwise, we have $\epsilon > 0$ and an equilibrium is no longer possible – the temperatures grow with time, approaching the asymptotic solution,

$$t\to\infty: \quad T_A(t) = \tau T_B(t) = ct^{2/3}, \quad (2.10)$$

where $c \propto (\epsilon n I_{\text{rr}})^{2/3}$. The asymptotic temperature ratio,

$$\tau = \sqrt{\frac{(1+\Delta_{\text{eff}})^2+\epsilon}{(1-\Delta_{\text{eff}})^2+\epsilon}}, \quad (2.11)$$

is a constant which tends to the equilibrium value (2.4) for $\epsilon \to 0$.

Thus, the disparity ϵ is the measure of "deviation" from pseudo-Hamiltonian systems, where $\epsilon = 0$ and different species reach the detailed dynamic equilibrium with distinct temperatures. For $\epsilon > 0$ this remarkable balance is broken and a system acquires the energy, so the temperatures continuously grow. Nevertheless, in the next section we show that even an infinitesimally small damping causes the temperatures to saturate, and then systems with sufficiently small ϵ behave as "nearly equilibrium".

2.3.3 Effect of damping

Dynamics of individual particles can be damped due to friction against the surrounding medium. To take this into account, one has to add the dissipation term $-2\nu_{A,B}(T_{A,B}-T_\mathrm{b})$ to the r.h.s. of Eq. (2.8), where ν_α is the respective damping rate in the friction force $-m_\alpha\nu_\alpha\mathbf{v}_\alpha$ and T_b is the background temperature determined by the medium [15, 108].

In complex plasmas the damping is usually very weak, i.e., the damping rate is much smaller than the rate of momentum/energy exchange due to interparticle interactions [15]. Let us use Eq. (2.8) to understand the effect of damping in this regime. For the constant nonreciprocity we derive the following equilibrium temperatures: $T_{A,B} = T_\mathrm{b}/(1 \mp \Delta)$ plus small terms proportional to the ratio of $\nu_{A,B}$ to the energy exchange rate. Thus, to the first approximation the damping does not affect the equilibrium temperature ratio (2.4). In a general case, $T_{A,B}$ are no longer growing with time but reach a steady state, since the growth term in Eq. (2.8) decreases with temperature. The resulting steady-state temperature ratio, τ_ν, can be easily derived assuming that $T_{A,B}$ are much larger than T_b. For similar particles, this requires the strong inequality $\nu \ll \epsilon\Delta_\mathrm{eff} n I_\mathrm{rr}/\sqrt{mT_\mathrm{b}^3}$ to be satisfied, which always holds for experiments with 2D complex plasmas discussed below [1]. Then we obtain the following equation for τ_ν:

$$\tilde{\nu}[(1-\Delta_\mathrm{eff})^2+\epsilon]\tau_\nu^2 - (\tilde{\nu}-1)(1-\Delta_\mathrm{eff}^2+\epsilon)\tau_\nu = (1+\Delta_\mathrm{eff})^2+\epsilon, \tag{2.12}$$

where $\tilde{\nu} = \nu_A/\nu_B$. For $\tilde{\nu} = 1$ we get $\tau_\nu = \tau$, i.e., the steady-state temperature ratio is not affected by friction. Generally, τ_ν exhibits a weak dependence on $\tilde{\nu}$: e.g., for the Hertzian interactions (see next section) the deviation between τ_ν and τ is within $\simeq 1\%$ in the range $0.8 \le \tilde{\nu} \le 1.3$.

In colloidal dispersions, where the dynamics is fully damped, the temperatures of both species tend to T_b. This, however, does not imply elimination of nonreciprocity effects: One can easily show that the Brownian dynamics of particles with nonreciprocal interactions (2.1) is exactly equivalent to the dynamics with conservative interactions (2.3) and different thermostat temperatures, equal to $T_\mathrm{b}/(1 \pm \Delta)$ for the A, B species. Therefore, nonreciprocal interactions are expected to have profound effects, e.g., on the dynamic correlations of colloids.

2.4 Numerical simulations

To complement the analytical results and understand the behavior in the strongly-coupled ($\Gamma \gg 1$) regime, we carried out a molecular dynamics simulation of a 2D binary, equimolar mixture of soft spheres. We implemented the velocity Verlet algorithm [109] with an adaptive time step. The simulation box with periodic boundary conditions contained

[1] For the Yukawa potential $\varphi_\mathrm{r}(r) = (Q^2/r)e^{-r/\lambda}$ we get $I_\mathrm{rr} \sim Q^4/\lambda$; so the r.h.s. of the inequality is proportional to the squared coupling parameter $\Gamma = Q^2\sqrt{n}/T_\mathrm{b}$, which is $\sim 10^2 - 10^3$ for typical 2D experiments [15].

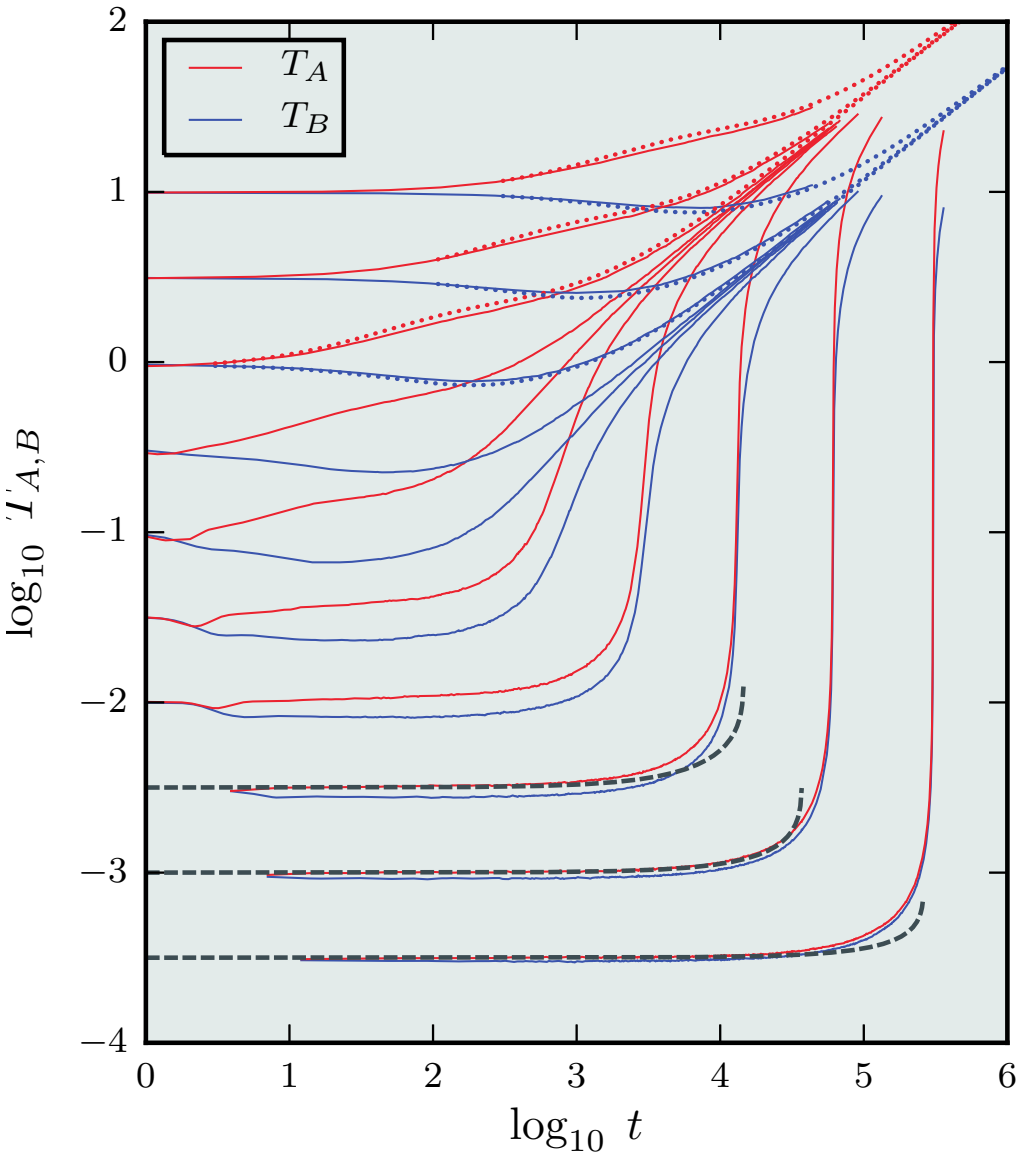

Figure 2.2: *Growth of the mean kinetic energy in a 2D binary system (no damping). Particles interact via the nonreciprocal Hertzian forces. Shown are the time dependence of the temperatures T_A and T_B. The solid lines show the development obtained from the simulations for the areal fraction $\phi = \pi r_0^2 n = 0.3$ and different initial temperatures T_0. All curves approach the universal asymptotes $\propto t^{2/3}$ described by Eqs. (2.10) and (2.11). The doted lines represent the solution of Eq. (2.8) for $T_0 \gtrsim 1$. The early development at $T_0 \ll 1$ is fitted by the explosive solution (2.14), shown by the dashed lines. The temperatures are normalized by φ_0, time is in units of $\sqrt{mr_0^2/\varphi_0}$.*

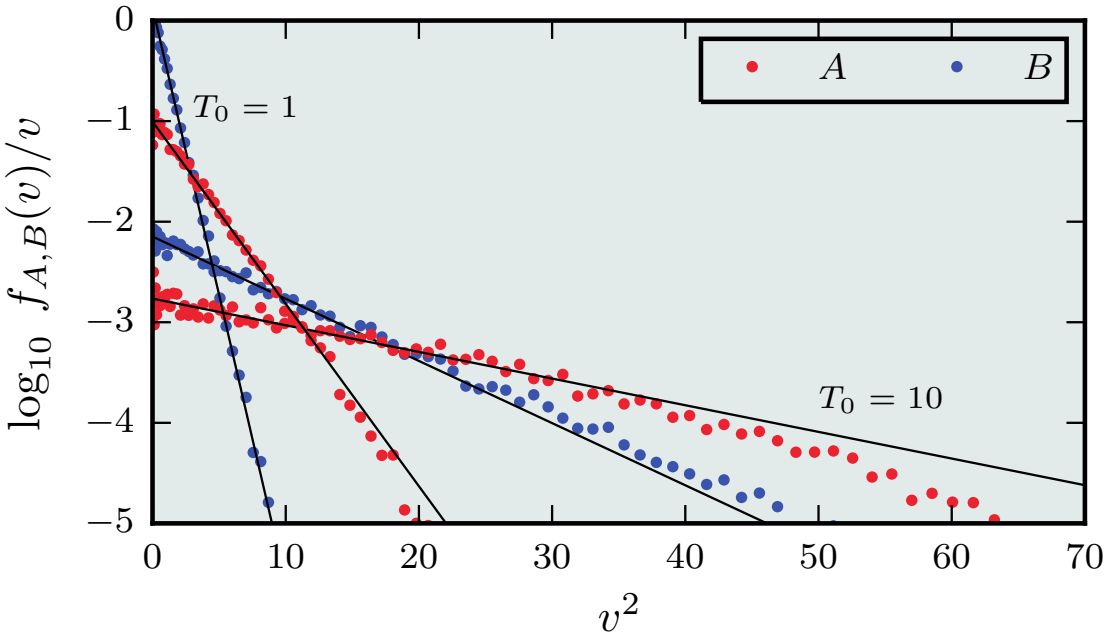

Figure 2.3: *The velocity distributions $f_{A,B}(v)$ at $t \simeq 700$ for $T_0 = 1$ and 10. At high temperatures, weak collisions cannot provide efficient Maxwellization of the velocity distribution.*

$2 \times 20,000$ particles with equal masses. To ensure precise numerical calculations at low and high temperatures, we chose the Hertzian interactions [110, 111]. The reciprocal and nonreciprocal parts of the Hertzian potential are given by

$$\begin{aligned} \varphi_{\rm r}(r) &= \frac{1}{2}\varphi_0(\max\{0, 1 - r/r_0\})^2, \\ \varphi_{\rm n}(r) &= \frac{1}{3}\varphi_0(\max\{0, 1 - r/r_0\})^3, \end{aligned}$$

where φ_0 is the interaction energy scale and r_0 is the interaction range. At $t = 0$ the particles were arranged into two interpenetrating square lattices with the initial temperature $T_A = T_B = T_0$ (therefore, at early simulation time a certain fraction of T_0 was converted into the interaction energy).

The numerical results are summarized in Figs. 2.2 – 2.5, where the temperature evolution is presented in the dimensionless form (using parameters of the Hertzian potential).

In Fig. 2.2 we plot the dependencies $T_{A,B}(t)$ for different T_0. By substituting $F_{\rm r,n}(r) = -d\varphi_{\rm r,n}/dr$ for the Hertzian potential in Eq. (2.7) and utilizing Eq. (2.9), we obtain $\Delta_{\rm eff} = 0.57$ and $\epsilon = 0.082$, so Eq. (2.11) yields the asymptotic temperature ratio $\tau = 3.1$. One can see that for all T_0 the numerical curves approach the expected universal asymptotes described by Eqs. (2.10) and (2.11). Note that the early development at sufficiently low temperatures (i.e., when $\Gamma_0 \propto T_0^{-1}$ is sufficiently large) exhibits a sharp

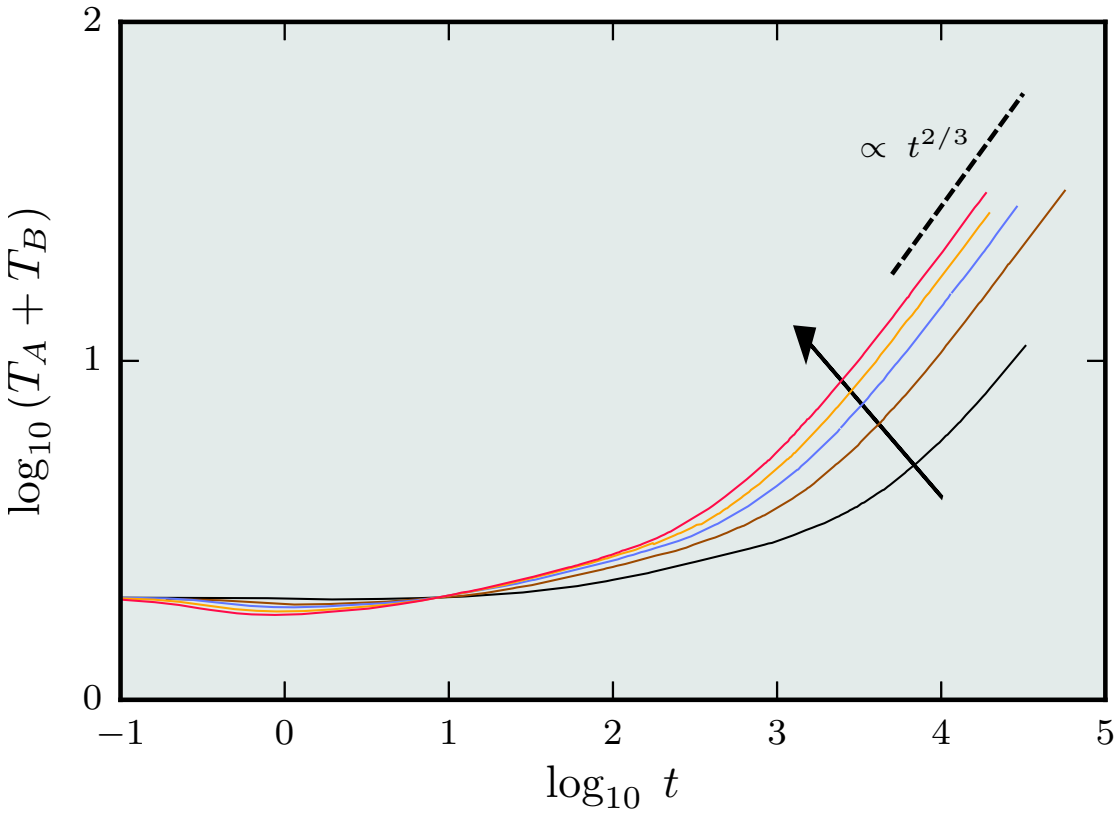

Figure 2.4: *Time dependence of the total kinetic energy (no damping). The development obtained from the simulations for $T_0 = 1$ and different ϕ (0.1, 0.3, 0.5, 0.7, 0.9, increasing along the arrow) is shown. The inset demonstrates the $\propto n^{2/3}$ density scaling of the asymptotic temperature growth. The temperature and time units are the same as in Fig. 2.2.*

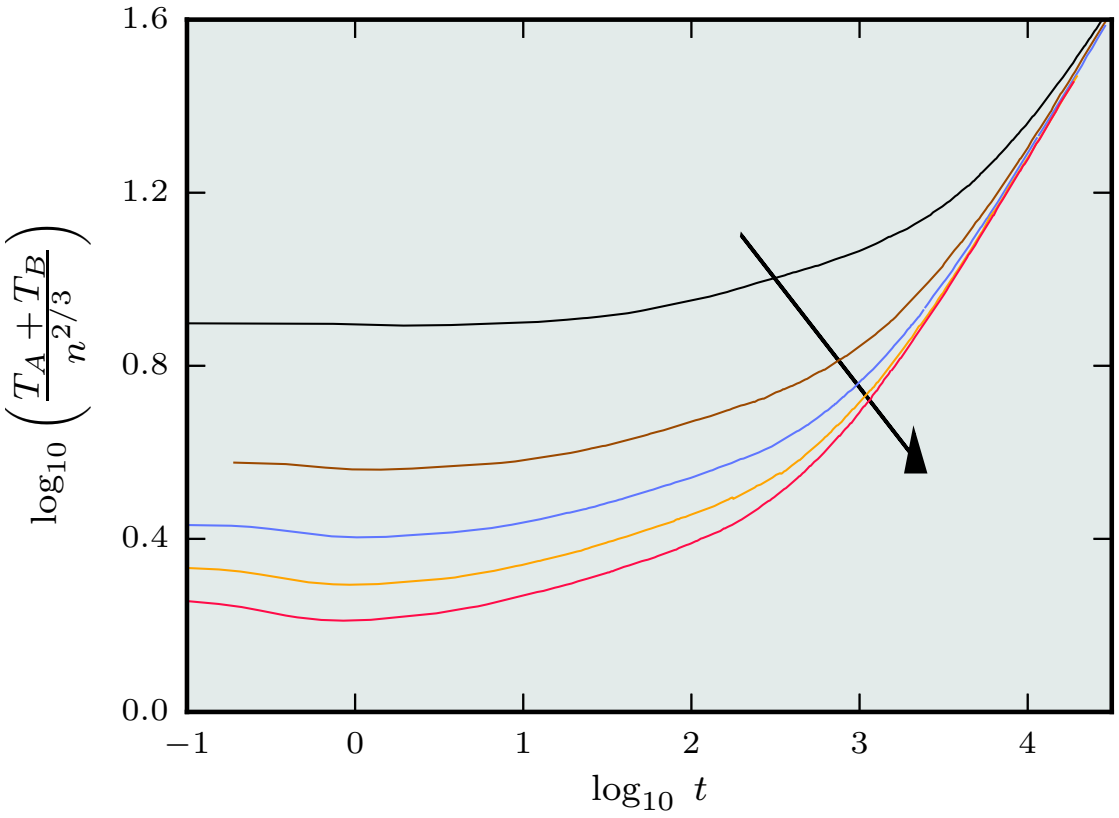

Figure 2.5: *Time dependence of the total kinetic energy (no damping) demonstrating the $\propto n^{2/3}$ density scaling of the asymptotic temperature growth. As in Fig. 2.4, the data is obtained from the simulations for $T_0 = 1$ and different ϕ (0.1, 0.3, 0.5, 0.7, 0.9, increasing along the arrow). The temperature and time units are the same as in Fig. 2.2.*

dependence on T_0 – we observe the formation of a plateau which broadens dramatically with decreasing T_0. On the other hand, for $T_0 \gtrsim 1$ the numerical results are very well reproduced by the solution of Eq. (2.8), as expected. A small ($< 10\%$) deviation observed in this case is due to the fact that weak collisions cannot provide efficient Maxwellization of the velocity distribution for the "hotter" species A (see Fig. 2.3).

In Fig. 2.4 we show how the temperature evolution depends on the density n. Here, the total kinetic energy $T_A(t) + T_B(t)$ calculated for different values of the areal fraction $\phi = \pi r_0^2 n$ is plotted. In contrast to the sharp dependence on T_0 seen in Fig. 2.2, the increase of n is accompanied by an approximately proportional shortening of the plateau (a small dip in the early development is due to partial conversion of the initial kinetic energy into the interaction energy). Fig. 2.5 demonstrates the predicted $\propto n^{2/3}$ scaling for the asymptotic temperature growth.

In order to explain the observed behavior at low temperatures, we point out that the approximation of small-angle scattering is not applicable in this strong-coupling regime and, hence, Eq. (2.8) is no longer valid. Strong correlations make the analysis rather complicated in this case, but one can implement a simple phenomenological model to understand the essential features. We postulate that at sufficiently low temperatures the energy growth caused by nonreciprocal interactions can be balanced by nonlinearity, forming a "dynamic potential well" where the system can reside for a long time. Qualitatively, one can then expect the development around the initial temperature to be governed by the activation processes, and introduce the effective Arrhenius rate characterizing these processes. Assuming the dimensionless temperature T (normalized by the effective depth of the well) to be small, we employ the following model equation:

$$\dot{T} = C \exp(-T^{-\gamma}), \tag{2.13}$$

where C is a constant (possible power-law factors can be neglected for $T \ll 1$) and γ is an exponent determined by the particular form the potential well. Substituting $T^{-\gamma} \simeq T_0^{-\gamma} - \gamma T_0^{-\gamma-1}(T - T_0)$ in Eq. (2.13) yields the explosive solution,

$$T(t) = T_0 - \frac{T_0^{\gamma+1}}{\gamma} \ln\left[1 - \frac{C\gamma}{T_0^{\gamma+1}} \exp(-T_0^{-\gamma})t\right], \tag{2.14}$$

with the explosion time $t_{\rm ex} = (T_0^{\gamma+1}/C\gamma)\exp(T_0^{-\gamma})$. In Fig. 2.2 we demonstrate that at the lowest temperatures the explosive solution provides quite a reasonable two-parametric fit (with $C = 4 \times 10^{-5}$ and $\gamma = 0.305$) to the numerical results. In the end we observe a natural crossover of $T_{A,B}(t)$ to the solution of Eq. (2.8).

When a weak damping is included in the simulations, the temperatures reach a steady state with the ratio given by Eq. (2.12), as described above. Interestingly, at low temperatures the system can be dynamically "arrested" due to friction and the asymptotic stage is never reached. A simple analysis of Eq. (2.13) with the dissipation term shows that the arrest occurs when $\nu t_{\rm ex} \gtrsim 1$, which is also confirmed by the simulations.

2.5 Experimental test with complex plasma

The principal predictions of the theory have been verified in experimental tests performed with weakly damped 2D binary complex plasmas. Such systems are obtained in radio-frequency (rf) plasma discharge chambers [112–115] sketched in Fig. 2.6. Microparticles injected in a plasma acquire equilibrium negative charges due to absorption of the surrounding electrons and ions [14]. This enables particle levitation above a flat horizontal rf electrode, where gravity is balanced by an inhomogeneous electrostatic force – the latter is exerted by a steady vertical electric field ("sheath field") generated in this region. The combination of the two forces provides a stiff vertical confinement for particles, inhibiting their vertical motion. The weak-damping regime is ensured by performing the experiments at low gas pressures.

By injecting two sorts of monodisperse microparticles it was possible to obtain a quasi-2D mixture. The particles formed two horizontal layers levitated at *slightly different* heights, so that no vertical pairs were formed. Unlike earlier experiments with binary complex plasmas [113], we utilized particles with specially chosen combinations of sizes and material densities. The experiments were performed using a low-pressure capacitively coupled plasma discharge [112–115]. The microparticles injected into the plasma acquire negative charges Q and can be levitated in the sheath above the horizontal rf electrode, due to steady vertical electric field generated in this region. In order to create a "quasi-monolayer" binary mixture, we selected a particular combination of two sorts of monodisperse microparticles whose material densities $\rho_{A,B}$ and sizes $a_{A,B}$ satisfy the relation $\rho_A a_A^2 \simeq \rho_B a_B^2$; the latter is based on the assumption that $Q_{A,B} \propto a_{A,B}$ and the gravity is fully compensated by the electric force (i.e., the contribution of the drag force due to flowing ions [103] is neglected). As the result, the particles of different sorts formed two horizontal layers levitated at slightly different heights. By tuning the rf discharge power $P_{\rm rf}$ it was possible to effectively vary the strength of the vertical confinement [116] and, hence, the height difference H.

A high-resolution video camera Photron FASTCAM 1024 PCI was mounted above the chamber, capturing a top view with a size of 14×14 mm^2. In addition, a side-view video camera was used to measure the vertical distance between the layers. The recording rate for the top-view camera was set at 60 frames per second (to assure correct particle velocity measurements, in accordance with recommendations of Refs. [117, 118]), the obtained video was analyzed to find the positions of all particles in every frame. The pixel intensity distribution of each particle image was fitted by a 2D Gaussian, its center gave the particle position with subpixel resolution. The particles were traced from frame to frame and their horizontal velocities were calculated from their positions in two consecutive frames.

For the experimental test presented here, the plasma was generated in argon at a pressure of 0.68 Pa. The upper and lower layers were composed, respectively, of melamine-formaldehyde spherical particles of diameter 9.19 ± 0.09 μm and density $\simeq 1.51$ g/cm^3, and polystyrene particles of diameter 11.36 ± 0.12 μm and density $\simeq 1.05$ g/cm^3. The mean interparticle distance in each layer was about $\simeq 0.9$ mm. The

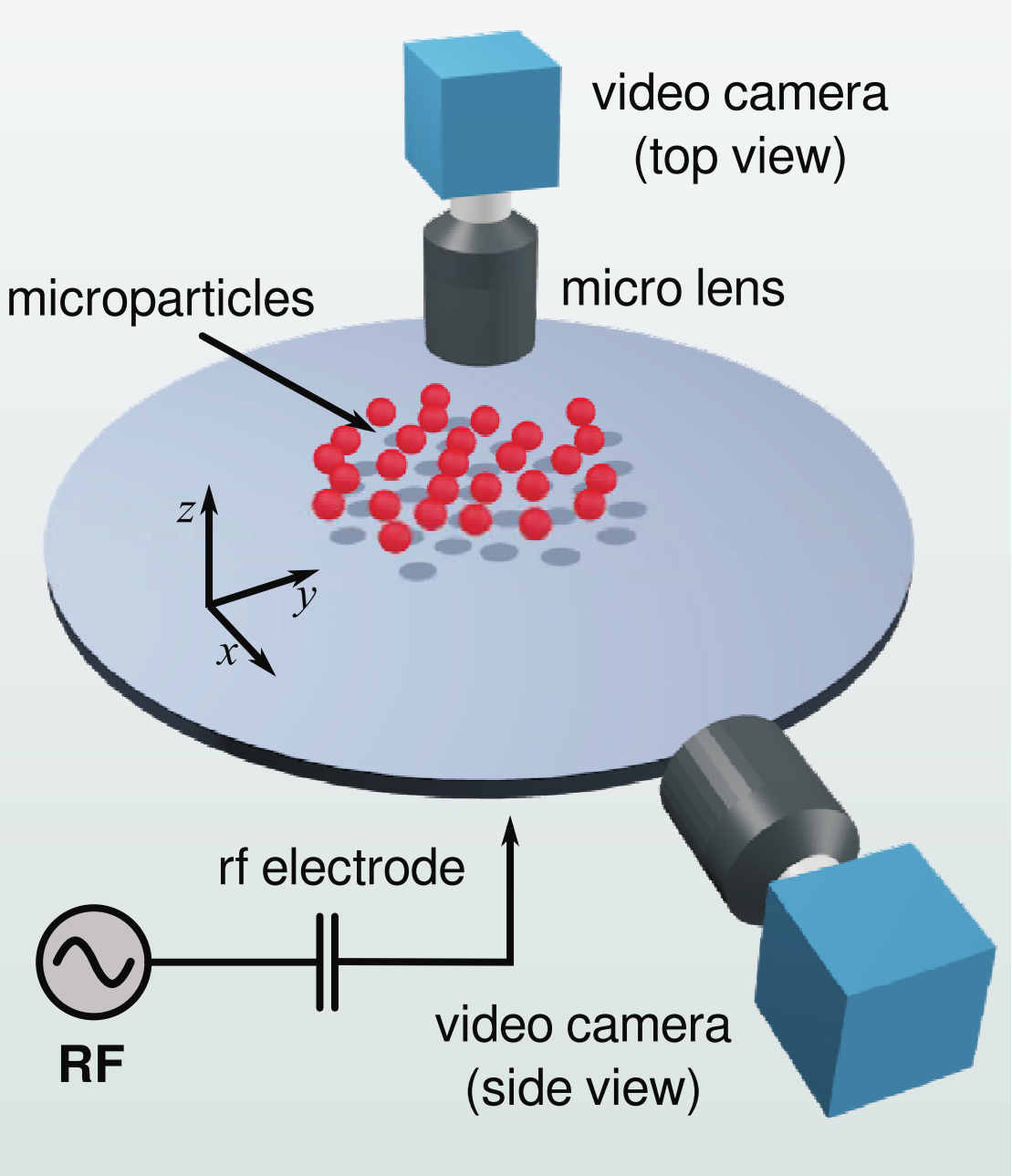

Figure 2.6: *Scheme of the experimental test and the mechanism of nonreciprocal wake-mediated interactions. Sketch showing the experimental setup. Microparticles levitate above a flat horizontal rf electrode. Two sorts of monodisperse particles form two horizontal monolayers at slightly different levitation heights. The layers are observed with the top-view and side-view video cameras, providing complete information about the position of individual particles.*

damping rates for the two species, determined by the free-molecular (Epstein) regime of interaction with neutral gas [103], were $\simeq 0.96$ s^{-1} and $\simeq 1.2$ s^{-1}, respectively. These values are $\sim 30 - 100$ times smaller than the characteristic Einstein frequency of microparticles.

Figure 2.7 shows the top-view and side-view images of the layers obtained with the respective video cameras. The height difference H between the layers was varied, from quite small values (when the layers practically merged) to a significant fraction of the horizontal interparticle distance, by tuning the rf power $P_{\rm rf}$ which effectively controls the sheath field [116].

The sheath field also drives a strong vertical plasma flow, and each microparticle acts as a lens causing the flowing ions to focus downstream from it. This results in the formation of plasma wakes "attached" to particles [14–16, 20, 119–121]. Figure 2.6c (see also figure caption) demonstrates how the wakes exert attractive forces and break the action-reaction symmetry for particles levitating in different layers [15, 20].

Figs. 2.8 and 2.9 show that the mean kinetic energy (temperature) of the horizontal motion was noticeably higher for particles in the upper layer, and the temperature difference between the layers increased with H. From Fig. 1.3 we infer that the wake-mediated interactions of particles levitating at different heights are such that nonreciprocity for the upper layer is positive, and for the lower layer it is negative. Since Δ is an increasing function of H ($\Delta \propto H$ for a small height difference), the theory predicts that (i) the upper layer should have a higher temperature than the lower one, and (ii) the temperature ratio $T_{\rm U}/T_{\rm L} = (1+\Delta)/(1-\Delta)$ should increase with H. We see that the both predictions are fully confirmed by the observations.

We point out that while the resolution of the side-view camera used for the experiment was not sufficient to accurately measure the vertical velocities, it showed that the particle motion was almost entirely horizontal. This observation indicates that mechanisms of the individual-particle heating associated with charge fluctuations (which result in the enhancement of the vertical motion, see, e.g., [122–124]) played a minor role in the experiments.

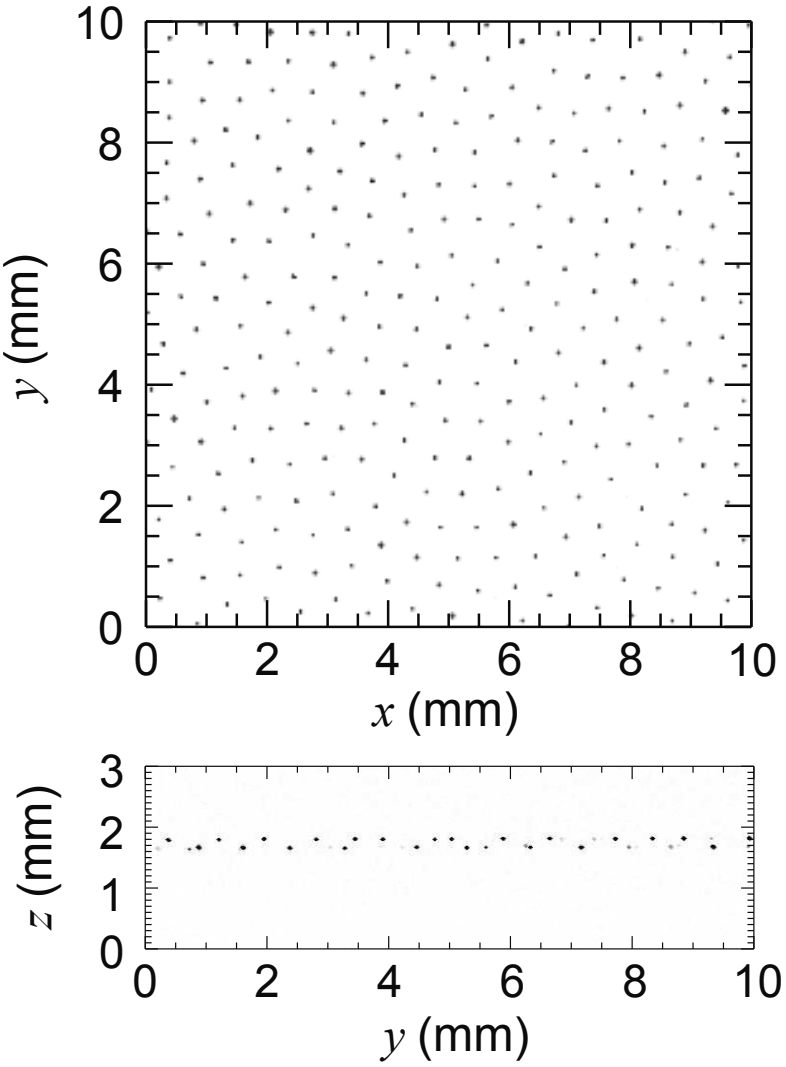

Figure 2.7: *Scheme of the experimental test and the mechanism of nonreciprocal wake-mediated interactions. Top and side views of a binary mixture forming the two layers. The respective images are obtained by illuminating the particles with thin horizontal and vertical laser sheets.*

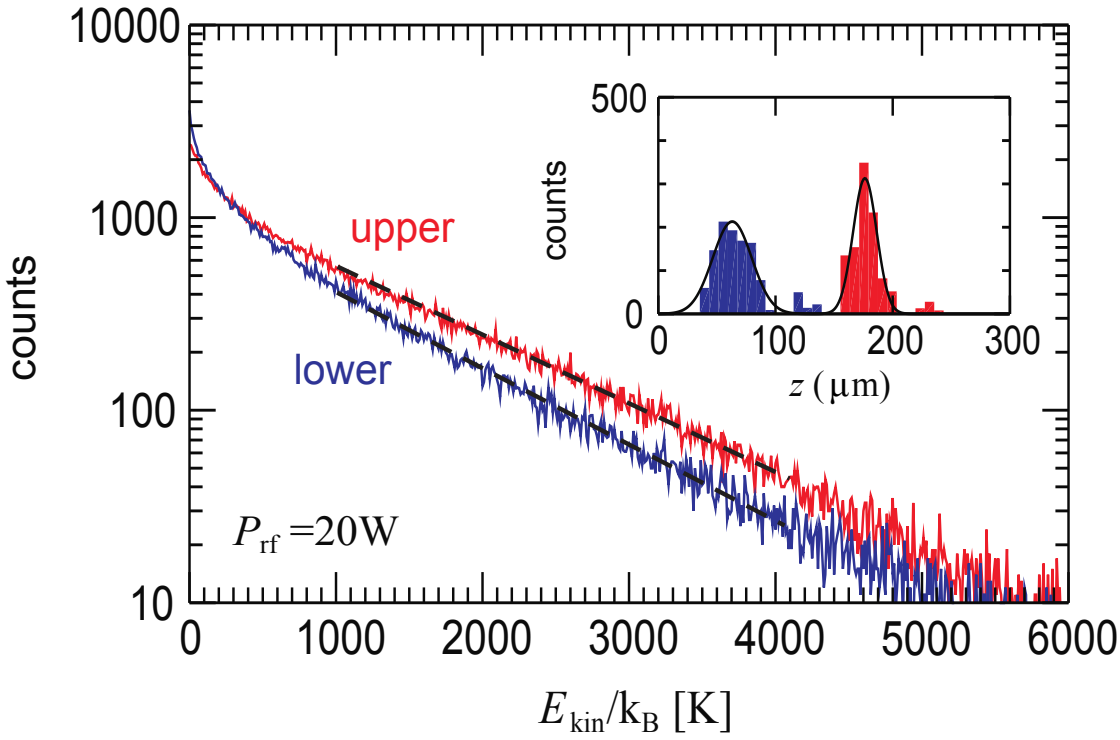

Figure 2.8: *Kinetic energy distribution for microparticles in monolayers. Shown are the energy distributions measured for two different values of the rf discharge power P_{rf}, which controls the height difference H between the upper and lower layers. The insets depict the height histogram for particles in the layers, the solid lines are Gaussian fits. $P_{\mathrm{rf}} = 20$ W, $H \simeq 110$ μm, the temperatures of the upper and lower layers are estimated as $T_{\mathrm{U}} \simeq 1250$ K and $T_{\mathrm{L}} \simeq 1100$ K, respectively (from Maxwellian fit, shown by the dashed lines)*

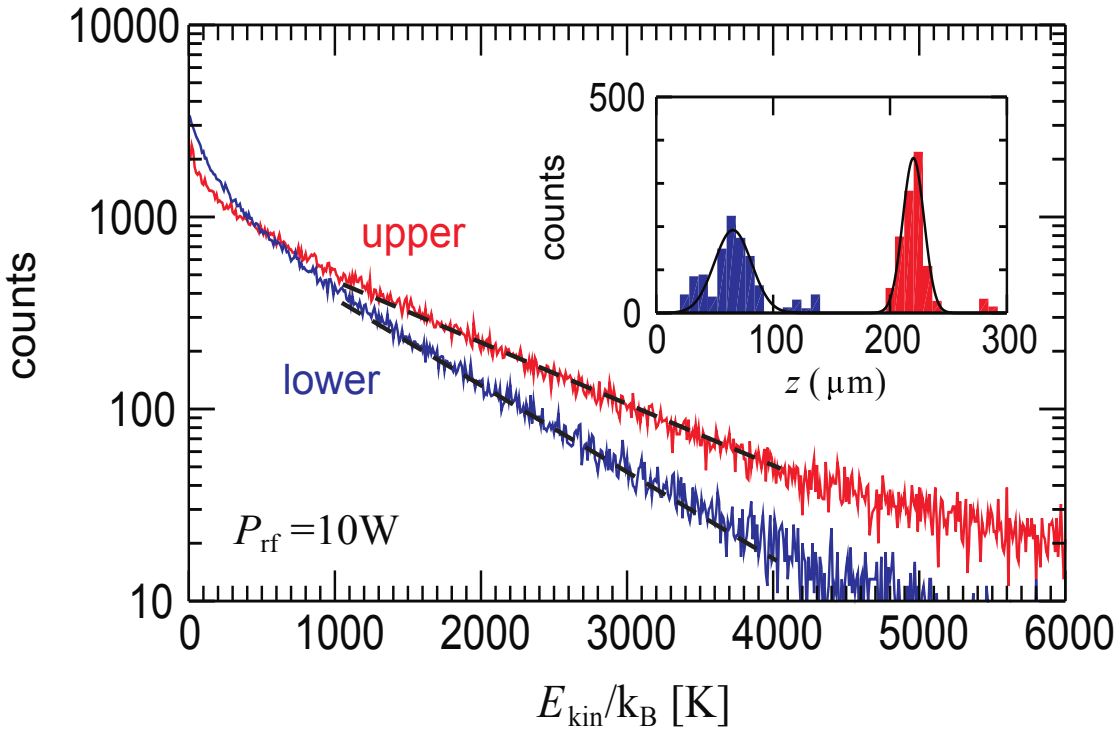

Figure 2.9: *Kinetic energy distribution for microparticles in monolayers, similar to Fig. 2.8. Shown are the energy distributions measured for two different values of the rf discharge power P_{rf}, which controls the height difference H between the upper and lower layers. The insets depict the height histogram for particles in the layers, the solid lines are Gaussian fits. $P_{\mathrm{rf}} = 10$ W, $H \simeq 150$ μm, the temperatures of the upper and lower layers are estimated as $T_{\mathrm{U}} \simeq 1350$ K and $T_{\mathrm{L}} \simeq 1000$ K, respectively (from Maxwellian fit, shown by the dashed lines).*

2.6 Conclusion

The presented results provide a basic classification of many-body systems with nonreciprocal interactions. We investigated different nonreciprocity classes in 2D and 3D systems which are relevant to a plethora of real situations. For instance, the shadow [17, 18] or diffusiophoretic [26, 27] interactions have a constant nonreciprocity and can dominate the kinetics of 3D systems, while the forces induced by the flow of the surrounding plasma [15, 121] or solvent/depletant [13, 21] are generally characterized by a variable nonreciprocity and govern the action-reaction symmetry breaking in 2D systems.

Irrespective of the particular nonreciprocity class, all such systems are expected to reveal remarkable behavior. In the weak-damping regime typical – but not limited – to complex plasmas (e.g., nonreciprocal optical forces [24, 25] can operate in different systems and do not imply any damping), the reciprocal sub-ensembles reach distinct steady-state temperatures, with the ratio uniquely determined by the effective nonreciprocity. In the opposite fully damped regime typical to colloidal dispersions, the Brownian particle dynamics of the coupled sub-ensembles can be equivalently described with the thermostats having distinct temperatures.

We have verified our theoretical predictions by performing experimental tests with weakly damped 2D binary complex plasmas, and expect that similar tests can be also carried out with 3D clouds under microgravity conditions. Furthermore, colloidal dispersions open up a variety of options to probe the effect of nonreciprocal interactions in the strong-damping regime, in particular by analyzing the dynamic correlations. In this respect, binary suspensions of catalytic colloids are very attractive model systems for which the strength of nonreciprocity can be tuned [27]. Another interesting analogy could be found in the purely kinetic clustering transition occurring with one-component microswimmers, which was recently discovered experimentally [125–127] for catalytically-driven particles (see also Refs. [128, 129]). It is intriguing to check whether the cluster coexisting with a gas of microswimmers acts formally as a second species, at an effective temperature different from that of the surrounding phase. We believe that all these problems constitute promising research topics for the future.

CHAPTER 3

STRUCTURAL CORRELATIONS IN BINARY COLLOIDAL MIXTURES WITH NONRECIPROCAL INTERACTIONS

In the previous chapter, we introduced the nonreciprocity parameter Δ and analyzed the kinetic energy for systems with Newtownian Dynamics and nonreciprocal interactions. Here, we analyze structural correlations for mesoscopic Brownian particles in colloidal suspensions, with typical particle diameters between a few nanometers and a few micrometers. These exert forces on each other that depend on the microscopic position and velocity variables of many molecules in the suspending solvent. On coarse-grained length and time scales where the solvent microstructure and dynamics are not resolved, the solvent molecule's degrees of freedom can be 'integrated out' and one is left with colloidal particles that interact via *effective* forces. These effective forces depend on the thermodynamic state of the solvent. The tunability of the effective interactions between colloidal particles makes colloidal suspensions ideal model systems for studying classical many-body behavior such as crystallization [34–37], melting [42–44], phase separation [47–50] as well as glass and gel formation [15, 54–56]. In thermodynamic equilibrium, the effective interactions fulfill Newton's third law *actio=reactio*. That is: the effective force generated by a particle and acting on a second particle is equal in magnitude and opposite in direction, when compared to the force generated by the second particle, acting on the first particle [5, 6, 9].

However, the *actio=reactio* principle can be broken in a nonequilibrium situation. Nonreciprocity occurs in a multitude of systems. Naming a few examples only, non-

At the time of writing this thesis, this chapter is submitted in a very similar form by Jörg Bartnick, Marco Heinen, Alexei V. Ivlev and Hartmut Löwen, see Reference [2].

reciprocity can arise from nonequilibrium fluctuations [22, 23] and also in case of diffusiophoretic forces [27, 28], optical forces [24, 25], out-of-equilibrium depletion interactions [11, 13, 21], hydrodynamic interactions [130], and 'social forces' in pedestrian dynamics modeling [32, 33]. Nonreciprocal effective interactions are typically superimposed by the classical reciprocal interactions, stemming from electric charges or dipole moments on the particles, van der Waals interactions, excluded volume, or other types of direct interactions.

Despite their importance, the many-body statistics of particles with nonreciprocal interactions have not been studied so far in the context of colloidal suspensions. This stands in stark contrast to the topic of complex (dusty) plasmas [15], where nonreciprocal interactions are a familiar feature of anisotropic trailing space-charges in the downstream direction behind charged mesoscopic particles in a flowing plasma. The phenomenon is known as the plasma wake. Consequences of nonreciprocity have been explored in various studies concerning complex plasmas [104, 116, 131–135]. The most prominent difference between colloidal suspensions and complex plasmas is that the dynamics of colloidal particles in high-density viscous solvent is completely overdamped while the dust-grain dynamics in complex plasmas typically contain a large inertial contribution.

The binary colloidal model system that we study in this chapter is governed by pairwise additive nonreciprocal forces and erratic Brownian forces. Like in Chapter 2, we characterize the strength of nonreciprocity by a scalar parameter Δ which is the ratio of the nonreciprocal to reciprocal forces. We focus on the time-averaged pair- and triplet-correlation functions for particle positions, developing a microscopic statistical theory based on the many-body-Smoluchowski equation and the Kirkwood superposition approximation as a closure. The theory is successfully tested against our Brownian dynamics computer simulations. As a result, we find that nonreciprocity induces distinct nonequilibrium pair correlations, and we also analyze the triplet correlations and the impact of the Kirkwood superposition approximation.

3.1 The Model

Our model system is a generalized variant of a diffusiophoretic microswimmer suspension that has been studied by Soto and Golestanian [27]. Consider an equimolar Brownian suspension containing two different types, A and B, of spherically symmetric, catalytic microswimmers. We denote the time-depended position of swimmer i of type α by the row vector $\boldsymbol{r}_i^\alpha(t)$. The suspension contains $2N$ swimmer particles, and we define the super vector

$$\mathbf{R}(t) = \big(\mathbf{r}_1^A(t), \ldots, \mathbf{r}_N^A(t), \mathbf{r}_1^B(t), \ldots, \mathbf{r}_N^B(t)\big)$$

as short-hand notation for the positions of all swimmer particles. Throughout this chapter, upper indices containing Greek or capital Roman letters are species indices that should not be confused with exponents.

Let each swimmer particle of type A act as a source of strength s_A, for a chemical substance $\mathcal{A}$ that consists of small molecules. Likewise, let each swimmer of type B be a source of strength s_B for a low molecular weight chemical substance $\mathcal{B}$. The molecules of substances $\mathcal{A}$ and $\mathcal{B}$ undergo diffusive motion in the solvent phase, characterized by the Stokes-Einstein-Sutherland translational diffusion coefficients $D_\mathcal{A}$ and $D_\mathcal{B}$, respectively. Evaporation or chemical decomposition into inert products causes molecules of types $\mathcal{A}$ and $\mathcal{B}$ to disappear at constant rates $\nu_\mathcal{A}$ and $\nu_\mathcal{B}$, respectively [136, 137]. The explicitly position- and time-dependent concentration fields of the two chemical substances, $c_\mathcal{A}(\mathbf{r}, t)$ and $c_\mathcal{B}(\mathbf{r}, t)$, depend in general also on $\mathbf{R}(\tau)$ at all times $\tau < t$. However, we assume that the diffusion coefficients $D_\mathcal{A}$ and $D_\mathcal{B}$ are large enough to allow for a separation of time scales: At a coarse-grained time scale, each individual swimmer particle traverses a distance that is much smaller than the average distance to the nearest neighboring swimmer and the swimmer configuration $\mathbf{R}$ is therefore practically unchanged. At the same time scale, the fast diffusion of $\mathcal{A}$- and $\mathcal{B}$-type molecules has already led to steady-state concentration fields $c_\mathcal{A}(\mathbf{r}, t)$ and $c_\mathcal{B}(\mathbf{r}, t)$ that depend only on the instantaneous swimmer positions $\mathbf{R}(t)$, but not on the history $\mathbf{R}(\tau)$ [138]. Restricting our study to time scales that are longer than the mentioned coarse-grained time scale, and neglecting all direct correlations between the two chemical substances' molecules, the concentration fields are governed by the instantaneous diffusion equations

$$\nu_\mathcal{A} c_\mathcal{A}(\mathbf{r}, t) - D_\mathcal{A} \nabla^2 c_\mathcal{A}(\mathbf{r}, t) = s_A \sum_{i=1}^{N} \delta(\mathbf{r} - \boldsymbol{r}_i^A(t)) \tag{3.1}$$

and

$$\nu_\mathcal{B} c_\mathcal{B}(\mathbf{r}, t) - D_\mathcal{B} \nabla^2 c_\mathcal{B}(\mathbf{r}, t) = s_B \sum_{i=1}^{N} \delta(\mathbf{r} - \boldsymbol{r}_i^B(t)), \tag{3.2}$$

where ∇^2 is the Laplace operator with respect to the field point $\mathbf{r}$ and $\delta(\mathbf{r})$ is the Dirac delta function. For the sake of simplicity we approximate the swimmers as point-like objects, as reflected by the point sources on the right-hand sides of Eqs. (3.1) and (3.2). This point-particle approximation is justified if the typical distances between swimmer particles are much larger than the particle diameters, which is the case for the systems that we have studied (see Fig. 3.1 and the relating text in Sec. 3.2).

Solving the linear screened Poisson equations (3.1) and (3.2) by standard Green's function methods gives the result

$$c_\mathcal{A}(\mathbf{r}, t) = \frac{s_A}{D_\mathcal{A}} \sum_{j=1}^{N} G\left(\sqrt{\frac{D_\mathcal{A}}{\nu_\mathcal{A}}}, |\mathbf{r} - \mathbf{r}_j^A(t)|\right) \tag{3.3}$$

and an analogous expression for $c_\mathcal{B}(\mathbf{r}, t)$ which is obtained after the interchange of indices $\mathcal{A} \to \mathcal{B}$ and $A \to B$. In Eq. (3.3), $G(\lambda, r) = \exp(-r/\lambda)/(4\pi r)$ is the isotropic Green's function in terms of the norm $r = |\mathbf{r}|$ of vector $\mathbf{r}$, satisfying the equation $(\nabla^2 - \lambda^{-2})G(\lambda, r) = -\delta(\mathbf{r})$ with an exponential screening length λ. Nonzero values of

$\nu_{\mathcal{A}}$ and $\nu_{\mathcal{B}}$ correspond to finite values for λ, which sets our model apart from unscreened chemotatic models with zero evaporation rate and $\lambda \to \infty$ [139].

We continue by picking an arbitrary tagged particle i of species A, and splitting the sum in Eq. (3.3) into a self-part ($i = j$) and a complementary distinct part ($i \neq j$). The self-part gives the concentration field

$$c^{s}_{\mathcal{A},i}(\mathbf{r},t) = \frac{s_A}{D_{\mathcal{A}}} G\left(\sqrt{\frac{D_{\mathcal{A}}}{\nu_{\mathcal{A}}}}, |\mathbf{r} - \mathbf{r}^A_i(t)|\right) \tag{3.4}$$

of chemical $\mathcal{A}$, which is created by the tagged particle around itself, and which is isotropic around $\mathbf{r} = \mathbf{r}^A_i$. The anisotropic distinct part

$$c^{d}_{\mathcal{A},i}(\mathbf{r},t) = \frac{s_A}{D_{\mathcal{A}}} \sum_{\substack{j=1 \\ j\neq i}}^{N} G\left(\sqrt{\frac{D_{\mathcal{A}}}{\nu_{\mathcal{A}}}}, |\mathbf{r} - \mathbf{r}^A_j(t)|\right) \tag{3.5}$$

is created by the remaining particles of species A and, obviously, $c_{\mathcal{A}}(\mathbf{r},t) = c^{s}_{\mathcal{A},i}(\mathbf{r},t) + c^{d}_{\mathcal{A},i}(\mathbf{r},t)$. Once again, Eqs. (3.4) and (3.5) can be repeated analogously for the chemical species $\mathcal{B}$ and a tagged particle of species B, by interchange of indices $\mathcal{A} \to \mathcal{B}$ and $A \to B$.

Diffusiophoretic particles tend to swim in the direction parallel or opposite to a chemical substance's concentration gradient [26, 29, 94, 140]. Assuming concentration- and configuration-independent mobility coefficients $\mu_{A\mathcal{A}}$, $\mu_{A\mathcal{B}}$, $\mu_{B\mathcal{A}}$ and $\mu_{B\mathcal{B}}$, with dimension Force $\times$ Length^4, we define the total diffusiophoretic forces

$$\mathbf{F}^A_i(\mathbf{R}) = -\mu_{A\mathcal{A}} \nabla c^{d}_{\mathcal{A},i}(\mathbf{r})\big|_{\mathbf{r}=\mathbf{r}^A_i} - \mu_{A\mathcal{B}} \nabla c_{\mathcal{B}}(\mathbf{r})\big|_{\mathbf{r}=\mathbf{r}^A_i} \tag{3.6}$$

and

$$\mathbf{F}^B_j(\mathbf{R}) = -\mu_{B\mathcal{A}} \nabla c_{\mathcal{A}}(\mathbf{r})\big|_{\mathbf{r}=\mathbf{r}^B_j} - \mu_{B\mathcal{B}} \nabla c^{d}_{\mathcal{B},j}(\mathbf{r})\big|_{\mathbf{r}=\mathbf{r}^B_j} \tag{3.7}$$

acting on particle i of species A, and on particle j of species B, respectively. In Eqs. (3.6) and (3.7) we drop the instantaneous time-dependence for clarity. Note that the diffusiophoretic force on a particle is not affected by the isotropic self-part of the concentration field around the respective particle, but only by the distinct part of the concentration fields, created by all other particles. This is analogous to the forces among a set of point-like electric charges, *e.g.* electrons: The Lorentz force on a single electron depends on the positions and velocities of all other electric charges, but it is not affected by the field that the tagged particle creates itself.

Our model shares many properties with a system of electric point charges that interact via pairwise additive screened Coulomb forces, like charged particles moving in an electrolyte, with electric fields calculated in the Debye-Hückel approximation. Combining Eqs. (3.3) and (3.5)-(3.7) We can interpret the individual summands that contribute to $\mathbf{F}^A_i(\mathbf{R})$ and $\mathbf{F}^B_j(\mathbf{R})$ as pairwise additive forces $\mathbf{F}^{\alpha\beta}(\mathbf{r}^\beta_j - \mathbf{r}^\alpha_i)$, exerted by particle i of

species α on particle j of species β. However, a peculiarity of the binary diffusiophoretic swimmer mixture that sets it qualitatively apart from the ensemble of electric point charges is the action-reaction symmetry breaking: An inequality

$$\mathbf{F}^{AB}(\mathbf{r}_j^B - \mathbf{r}_i^A) \neq -\mathbf{F}^{BA}(\mathbf{r}_i^A - \mathbf{r}_j^B) \tag{3.8}$$

occurs in the general case and, like in the simpler model of Ref. [27], a symmetry breaking $\mu_{A\mathcal{B}} s_B / D_{\mathcal{B}} \neq \mu_{B\mathcal{A}} s_A / D_{\mathcal{A}}$ among products of transport coefficients and production rates is generally sufficient to cause the symmetry breaking in Eq. (3.8). As in Chapter 2, we introduce a scalar nonreciprocity parameter $\Delta(r)$ by the defining equation

$$\Delta(r) \left[\mathbf{F}^{AB}(r) + \mathbf{F}^{BA}(r)\right] = \mathbf{F}^{BA}(r) - \mathbf{F}^{AB}(r). \tag{3.9}$$

In the reciprocal case, where $\mathbf{F}^{AB}(r) = \mathbf{F}^{BA}(r)$, this parameter vanishes and we have $\Delta = 0$.

In the following we neglect hydrodynamic interactions, which can be justified if the suspension is highly dilute but still strongly interacting. For our analysis to be valid, the hydrodynamic diameters of the particles have to be much smaller than the shortest typical particle distances in the suspension. Particles with sufficiently strong, repulsive Yukawa-like interactions virtually never come into close contact, and the characteristic length scale that dominates the correlation functions of such particles in d-dimensional space is $\rho^{-1/d}$, where ρ is the particle number density [141, 142]. Suspensions of such particles can exhibit strong structural correlations, even if they are highly dilute from a hydrodynamic point of view.

The Brownian particle dynamics, on time scales that exceed the momentum relaxation time, are described by the overdamped Langevin equation [91]

$$\xi^\alpha \, \dot{\mathbf{r}}_i^\alpha = \mathbf{F}_i^\alpha(\mathbf{R}, t) + \mathbf{f}_i^\alpha(t) \tag{3.10}$$

with a friction coefficient ξ^α, Boltzmann's constant k_B, absolute temperature T, and a random force $\mathbf{f}_i^\alpha(t)$ with zero mean, $\langle \mathbf{f}_i^\alpha(t) \rangle = 0$, and variance $\langle \mathbf{f}_i^\alpha(t) \mathbf{f}_j^\beta(\tau) \rangle = 2k_\mathrm{B} T \xi^\alpha \delta_{ij} \delta_{\alpha\beta} \delta(t-\tau) \mathbb{1}$. Here, δ_{ij} is the Kronecker symbol, $\mathbb{1}$ the unit matrix and the brackets $\langle \ldots \rangle$ represent an average with respect to the time t.

3.2 Many-body theory for the pair correlation functions

On the coarse-grained time scale at which the Langevin equation is valid, an overdamped complex liquid is fully described by the many-body distribution function $\mathbf{p}$. Often times one is interested in more accessible quantities like the pair distribution functions

$g^{\alpha\beta}(\mathbf{r},\mathbf{r}')$, which, for the equimolar suspensions studied here, can be defined in the limit $N\to\infty$ in terms of the following $(2N-2)$-fold integrals over $\mathbf{p}$:

$$\begin{aligned}
\frac{\rho^2 g^{AA}(\mathbf{r},\mathbf{r}')}{N(N-1)} &= \left\langle \int d\mathbf{r}_3^A \cdots \int d\mathbf{r}_N^A \int d\mathbf{r}_1^B \cdots \int d\mathbf{r}_N^B \Psi(\mathbf{R},t) \right\rangle, \\
\frac{\rho^2 g^{AB}(\mathbf{r},\mathbf{r}')}{N^2} &= \left\langle \int d\mathbf{r}_2^A \cdots \int d\mathbf{r}_N^A \int d\mathbf{r}_2^B \cdots \int d\mathbf{r}_N^B \Psi(\mathbf{R},t) \right\rangle, \\
\frac{\rho^2 g^{BB}(\mathbf{r},\mathbf{r}')}{N(N-1)} &= \left\langle \int d\mathbf{r}_1^A \cdots \int d\mathbf{r}_N^A \int d\mathbf{r}_3^B \cdots \int d\mathbf{r}_N^B \Psi(\mathbf{R},t) \right\rangle,
\end{aligned}$$

with $\rho = 2N/V$ where V is the suspension volume in case of three-dimensional (3D) systems, or the suspension area in case of two-dimensional (2D) systems. Alternatively, $g^{\alpha\beta}(\mathbf{r})$ can be written as

$$g^{\alpha\beta}(\mathbf{r}) = \frac{V}{N^2}\left\langle \sum_{i=1}^{N}\sum_{\substack{j=1\\ j\neq i\vee\alpha\neq\beta}}^{N} \delta\left(\mathbf{r}-\mathbf{r}_i^\alpha(t)+\mathbf{r}_j^\beta(t)\right)\right\rangle. \tag{3.11}$$

For an isotropic and homogeneous system $g^{\alpha\beta}(r)$ is a function of particle distance only. The triplet distribution function $g_3^{\alpha\beta\gamma}(\mathbf{r},\mathbf{r}',\mathbf{r}'')$, which is a $(2N-3)$-fold integral over $\mathbf{p}$, is analogously defined [143].

We start our analysis of particle correlations with the Smoluchowski equation

$$\frac{\partial\Psi}{\partial t} = \sum_{\alpha=A,B}\frac{1}{\xi^\alpha}\sum_{i=1}^{N}\nabla_i^\alpha\cdot\left(k_\mathrm{B}T\,\nabla_i^\alpha\Psi - \mathbf{F}_i^\alpha\,\Psi\right), \tag{3.12}$$

which is stochastically equivalent to Eq. (3.10), and where ∇_i^α is the Nabla operator that differentiates with respect to the particle position $\boldsymbol{r}_i^\alpha$ and the time- and configuration dependence of Ψ has been dropped for clarity. Using a $(2N-2)$-fold integration, we transform Eq. (3.12) into an equation for the pair distribution function [144]. This equation, however, does not only depend on the pair correlations, but also on the triplet correlations which, in turn, depend on the quadruplet correlations and so on. We truncate this Bogoliubov–Born–Green–Kirkwood–Yvon (BBGKY) hierarchy [15] using the Kirkwood-superposition approximation [145]

$$g_3^{\alpha\beta\gamma}(\mathbf{r},\mathbf{r}',\mathbf{r}'') \approx g^{\alpha\beta}(\mathbf{r},\mathbf{r}')\,g^{\alpha\gamma}(\mathbf{r},\mathbf{r}'')\,g^{\beta\gamma}(\mathbf{r}',\mathbf{r}''). \tag{3.13}$$

In our derivation we use the fact that $g^{AB}(r) = g^{BA}(r)$, which is apparent from Eq. (3.11). The final set of coupled integro-differential equations for $g^{AA}(r)$, $g^{AB}(r)$ and $g^{BB}(r)$ reads

$$\left(\frac{k_\mathrm{B}T}{\xi^\alpha} + \frac{k_\mathrm{B}T}{\xi^\beta}\right) \nabla^2 \, g^{\alpha\beta} = - \sum_{\substack{(\alpha',\beta')= \\ (\alpha,\beta),\ (\beta,\alpha)}} \frac{1}{\xi^{\alpha'}} \nabla \cdot \Bigg[\mathbf{F}^{\alpha'\beta'} \, g^{\alpha\beta} + \frac{\rho}{2} \, g^{\alpha\beta} \sum_{\gamma=A,B} \mathbf{F}^{\alpha'\gamma} \left(g^{\alpha'\gamma} * g^{\beta'\gamma} \right) \Bigg] , \tag{3.14}$$

where $g^{\alpha\beta} \equiv g^{\alpha\beta}(r)$ and $F^{\alpha\beta} \equiv F^{\alpha\beta}(r)$. In Eq. (3.14), $(f * g)(r)$ denotes the d-dimensional convolution of two isotropic functions $f(r)$ and $g(r)$, defined as

$$(f * g)(r) \equiv \int d^d \boldsymbol{r}' f(r') g(|\mathbf{r} - \mathbf{r}'|).$$

Eq. (3.14) cannot be solved analytically for nonzero density or non-vanishing force. We therefore solve it numerically, using fixpoint iteration algorithms [142]. With a double integration, we eliminate the Laplace operator and the divergence. We solve the convolutions in Fourier space, making use of the FFTLog algorithm for the d-dimensional Hankel transform [146, 147].

3.3 Numerical simulations

To test the accuracy of the approximate theory, we perform Brownian dynamics simulations for two and three dimensions. We use the forces derived in Eqs. (3.6) and (3.7), for both the 2D and the 3D case. The former corresponds to swimmer particles that are confined to move in a 2D plane, while the surrounding solvent is fully three-dimensional. In our model system, the chemical substances $\mathcal{A}$ and $\mathcal{B}$ are free to diffusive throughout the 3D solvent, irrespective of whether or not the swimmer particles are confined to a 2D plane. We express our simulation parameters in terms of the thermal energy $k_\mathrm{B}T$, the density ρ and the friction coefficient, choosing $\xi^A = \xi^B$. For the sake of symmetry and in order to better isolate the effects of nonreciprocity, we consider a system where $\mathbf{F}^{AA} = \mathbf{F}^{BB}$. We limit our study to the case of a r-independent parameter Δ, which is the case in our model system if $D_\mathcal{A}/\nu_\mathcal{A} = D_\mathcal{B}/\nu_\mathcal{B}$. As in our discussion of the Green's function method in Sec. 3.1, we have $\lambda = \sqrt{D_\mathcal{A}/\nu_\mathcal{A}}$, which is now a unique exponential

screening length for the concentration profiles of both chemical species $\mathcal{A}$ and $\mathcal{B}$. We quantify the strength of the interactions by a constant Γ, satisfying the equations

$$\frac{\mu_{A\mathcal{A}}\, s_A}{4\pi k_\mathrm{B} T D_\mathcal{A}} = \frac{\Gamma}{\rho^{1/d}} \qquad \frac{\mu_{A\mathcal{B}}\, s_B}{4\pi k_\mathrm{B} T D_\mathcal{B}} = \frac{(1+\Delta)\,\Gamma}{\rho^{1/d}},$$
$$\frac{\mu_{B\mathcal{A}}\, s_A}{4\pi k_\mathrm{B} T D_\mathcal{A}} = \frac{(1-\Delta)\,\Gamma}{\rho^{1/d}} \qquad \text{and} \qquad \frac{\mu_{B\mathcal{B}}\, s_B}{4\pi k_\mathrm{B} T D_\mathcal{B}} = \frac{\Gamma}{\rho^{1/d}}.$$

A potential energy in the usual sense cannot be defined in the general case $\Delta \neq 0$. However, for the special case of reciprocal interactions ($\Delta = 0$), the interactions above can be described by a pairwise additive potential energy $V(r) = \Gamma k_\mathrm{B} T \rho^{-1/d} \exp(-r/\lambda)/r$. Using a simple forward time-step algorithm [148], we solve the Langevin Eq. (3.10) for $2 \times 20,000$ particles in a 2D quadratic or 3D cubic simulation box with periodic boundary conditions. The forces are set equal to zero, when the distance between two particles exceeds $5/\rho^{1/d}$. The particles are initialized at random positions throughout the system, and the setup is given time to relax. We monitor the average forces $\langle|\mathbf{F}_i^\alpha(\mathbf{R},t)|\rangle$ and measure that for all of our simulations this value first reduces, and eventually reaches a time-independent steady state. Then, we calculate the pair and triplet correlations by averaging over multiple snapshots at different times. Figure 3.1 shows a comparison of the pair distribution functions obtained from the theory and the BD simulations for 2D and 3D in the reciprocal and the nonreciprocal case. For the reciprocal case, $\Delta = 0$, where $g^{AA}(r) = g^{AB}(r) = g^{BB}(r)$, the theory predicts the simulation results for $g^{\alpha\beta}(r)$ with high precision. In case of nonreciprocal forces, $\Delta = 0.5$, the deviations between theory and simulation results are larger, but the theory maintains a rather good accuracy level and it continues to capture all qualitative features of the simulation. Note also, that all functions $g^{\alpha\beta}(r)$ exhibit a pronounced 'correlation hole' at small values of r, because the repulsive particles almost never come into close contact. This provides an *a posteriori* justification of our point-particle assumption in Sec. 3.1: Particles that are significantly smaller in diameter than the correlation hole have a negligible likelihood of direct contact, and can therefore be approximated as point-like.

Without showing all results here, we have observed both in our simulations and our theory results, and for 2D as well as for 3D systems, that the principal peak value, $g^{AA}(r^{AA}_{max})$, of the function $g^{AA}(r)$ can assume a smaller or larger value than the principal peak $g^{AB}(r^{AB}_{max})$. The peak-height ordering depends on the parameters $(\Gamma, \lambda, \Delta)$ of the nonreciprocal interactions and on the density ρ. In our simulation and theory results we observe that the principal peak height of function $g^{BB}(r)$ is always less than the peak heights of both functions $g^{AB}(r)$ and $g^{AA}(r)$. For an intuitive understanding of the less pronounced peak in $g^{BB}(r)$, let us introduce effective radii $r^{\alpha\beta}_\mathrm{eff}$ via the condition that $|\mathbf{F}^{\alpha\beta}(r^{\alpha\beta}_\mathrm{eff})| = k_\mathrm{B}T/\lambda$. In Fig. 3.2 we show a snapshot from a 2D system with nonreciprocal interactions twice, using different effective radii for the plotted disks that are centered around the particle positions r_i^A (blue) and r_i^B (red): In the top panel of the figure, the effective radius of the red, B-type disks is r^{BA}_eff, and in the bottom panel, the effective radius of the blue, A-type disks is r^{AB}_eff, which is less than r^{BA}_eff. The same

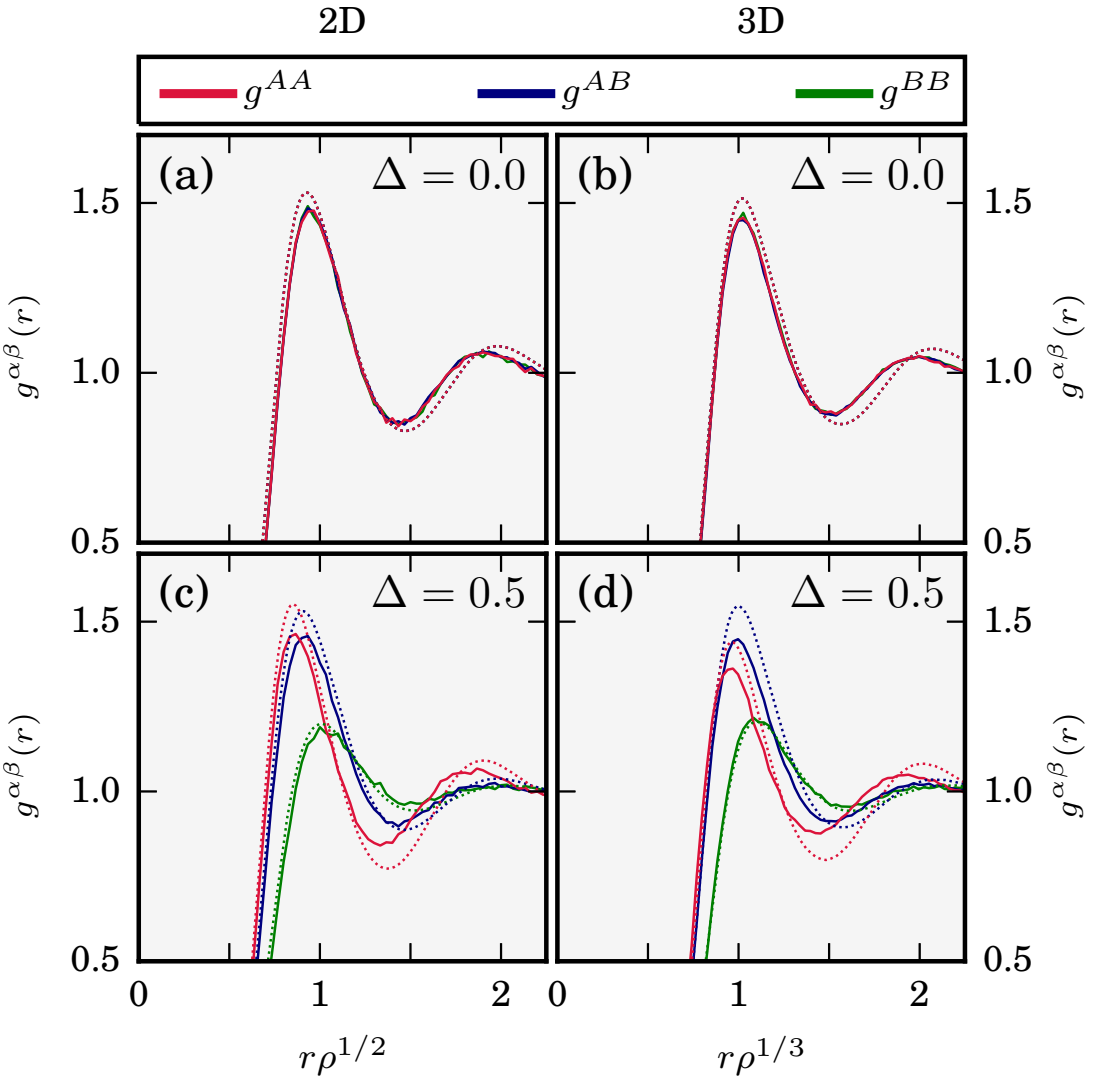

Figure 3.1: *Pair distribution functions $g^{\alpha\beta}(r)$ from computer simulation (solid) and theory (dotted). Panels on the left (a, c) are for $d = 2$ spatial dimensions, and panels on the right (b, d) are for $d = 3$. The upper panels (a,b) correspond to the reciprocal case $\Delta = 0.0$. A nonreciprocal case with $\Delta = 0.5$ is shown in the bottom panels (c, d). The remaining parameters of the simulation are $\lambda\rho^{1/d} = 1/4$ and (a) $\Gamma = 100/3$, (b) $\Gamma = 200/3$, (c) $\Gamma = 25$ and (d) $\Gamma = 50$. The plot does not show the region $g(r) < 0.5$, where we observe a very good agreement between theory and simulation.*

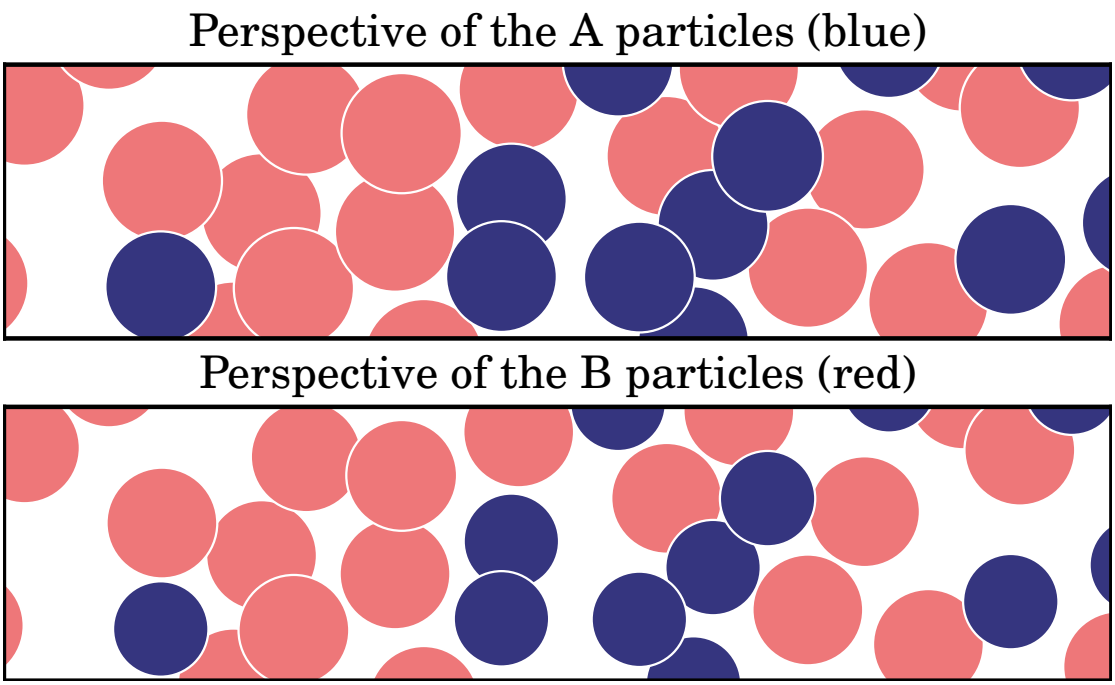

Figure 3.2: *Typical snapshot for a $2D$-simulation with $\Delta = 0.5$ and $\Gamma = 25$. The system exhibits different effective densities for A and B particles. The radii of the plotted disks are proportional to the effective radii $r_{\mathrm{eff}}^{\alpha\beta}$.*

effective radius, $r_{\mathrm{eff}}^{AA} = r_{\mathrm{eff}}^{BB}$, is used for the blue disks in the upper panel and for the red disks in the lower panel. Clearly, the system is effectively more crowded for the A-type particles than for the B-type particles, which explains the weaker principal peak in $g^{BB}(r)$.

3.4 Kirkwood approximation for nonreciprocal interactions

The approximation that allows us to solve the many-body Smoluchowski equation numerically is the Kirkwood superposition in Eq. (3.13). In case of thermodynamic equilibrium, it is known how this approximation breaks down at high density [149–151]. In the following, we test the Kirkwood superposition approximation in case of the nonequilibrium steady state of Brownian suspensions with nonreciprocal interactions, by comparison to our highly accurate computer simulation data.

One way to visualize a projection of the triplet correlation function $g_3^{\alpha\beta\gamma}(\mathbf{r}, \mathbf{r}', \mathbf{r}'')$ is via the bond angle distribution function $g_3(\theta, r_1, r_2)$ [151]. This function characterizes triplets that have one inter-particle distance smaller than r_1 and another inter-particle distance smaller than r_2, by the bond angle θ between the two straight lines that connect the particle centers (see Fig. 3.3). The function $g_3(\theta, r_1, r_2)$ is normalized such that

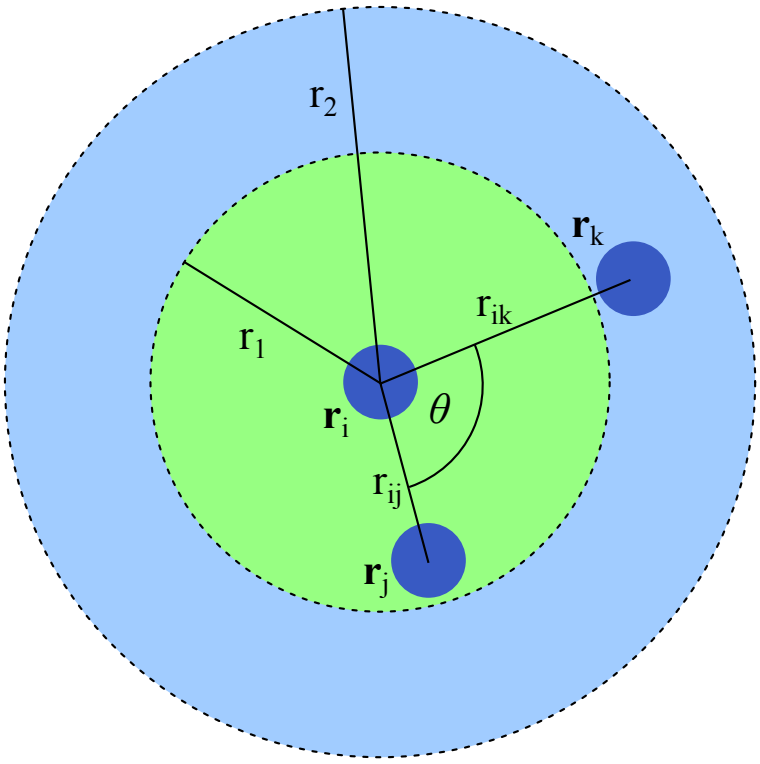

Figure 3.3: *The bond angle distribution function $g_3(\theta, r_1, r_2)$ characterizes triplets of particles with the inter-particle distances $r_{ij} < r_1$ and $r_{ik} < r_2$ by the bond angle theta θ.*

the integral over all bond angles yields unity. Often, r_1 and r_2 are chosen as the first minimum of the pair distribution function. However, this is not uniquely defined for a binary mixture. To avoid this ambiguity, we choose the parameters as the first minimum of a corresponding $g^{AA}(r)$ for a simulation with $\Delta = 0$, which we call R, and which should not be confused with the norm of the super vector $\mathbf{R}$. For 2D and strong particle interactions, pronounced peaks around values of θ that are integer multiples of 60° indicate triangular short-range order of the liquid [151].

Assuming Kirkwood superposition we can approximate the bond angle distribution function trough a combination of pair distribution functions. We define the unnormalized Kirkwood-approximation $G_{3,K}^{\alpha\beta\gamma}(\theta, r_1, r_2)$ for the bond angle distribution function in 2D as

$$G_{3,K}^{\alpha\beta\gamma}(\theta, r_1, r_2) \equiv \int_0^{r_1}\int_0^{r_2} dr dr'\; r\; r' g^{\alpha\beta}(r) g^{\alpha\gamma}(r') \times g^{\beta\gamma}(\sqrt{r^2 + r'^2 - 2rr'\cos\theta})$$

and similarly in 3D as

$$G_{3,K}^{\alpha\beta\gamma}(\theta, r_1, r_2) \equiv \sin\theta \int_0^{r_1}\int_0^{r_2} dr dr'\; r^2\; r'^2 g^{\alpha\beta}(r) g^{\alpha\gamma}(r') \times g^{\beta\gamma}(\sqrt{r^2 + r'^2 - 2rr'\cos\theta}).$$

Applying normalization we arrive at the Kirkwood approximation of the bond angle distribution function,

$$g_{3,K}^{\alpha\beta\gamma}(\theta, r_1, r_2) = \frac{G_{3,K}^{\alpha\beta\gamma}(\theta, r_1, r_2)}{\int_0^{\pi} d\theta\; G_{3,K}^{\alpha\beta\gamma}(\theta, r_1, r_2)}. \tag{3.15}$$

In Figs. 3.4 and 3.5 we plot the functions $g_3^{\alpha\beta\gamma}(\theta, R, R)$ and $g_{3,K}^{\alpha\beta\gamma}(\theta, R, R)$, both extracted from our simulations. As in Fig. 3.1, we show data for the 2D and 3D case, both for reciprocal and nonreciprocal interactions. All simulated systems are clearly in the liquid state, as signaled by the very gentle principal peak at a bond angle θ just below $\pi/3$. Low values of the bond angle distribution functions at small values of θ correspond once again to a correlation hole: It is very unlikely for a pair of repulsive particles to occupy the same space. In the 3D case, large bond angles are also untypical. The probability of finding a particle at a given angle scales with the solid angle in $3D$, which is proportional to $\sin\theta$. For 2D systems, the bond angle distribution functions at angles larger than $\pi/2$ are almost constant.

We find that the Kirkwood approximation is very accurate for the studied systems with reciprocal interactions, and somewhat less accurate in case of systems with nonreciprocal interactions. As expected, the discrepancies between $g_{3,K}^{\alpha\beta\gamma}(\theta, R, R)$ and $g_3^{\alpha\beta\gamma}(\theta, R, R)$ are strongest for those systems where the pair distribution functions from the many-body

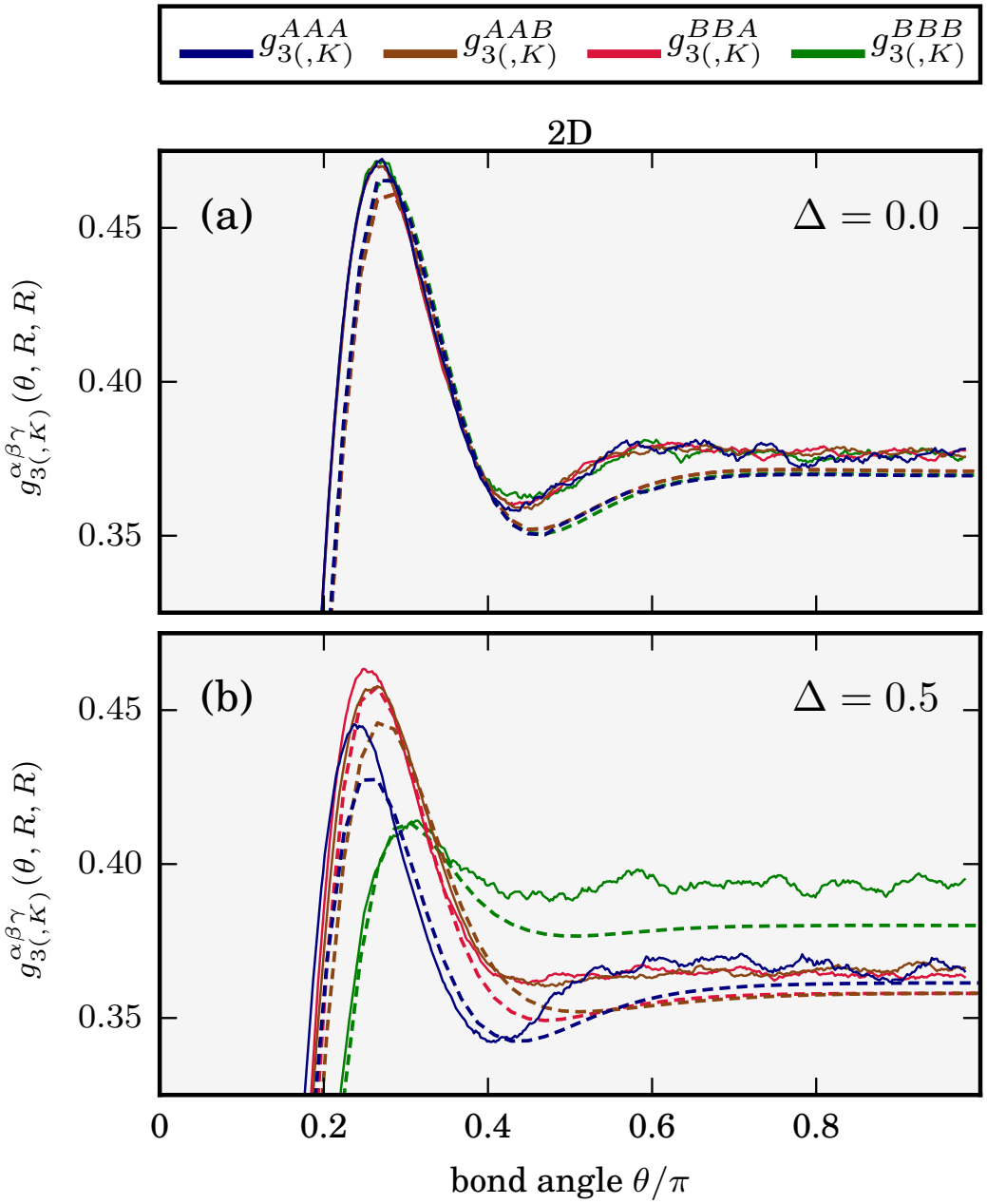

Figure 3.4: *2D bond angle distribution function $g_3^{\alpha\beta\gamma}(\theta, R, R)$ computed directly from our computer simulation (solid curves) and Kirkwood approximations, $g_{3,K}^{\alpha\beta\gamma}(\theta, R, R)$, of the bond angle distribution functions (dashed curves). The functions $g_{3,K}^{\alpha\beta\gamma}(\theta, R, R)$ are computed on basis of Eq.* (3.15)*, using the pair correlation functions $g^{\alpha\beta}(r)$ from the simulations as input. Simulation parameters are the same as for Fig. 3.1.*

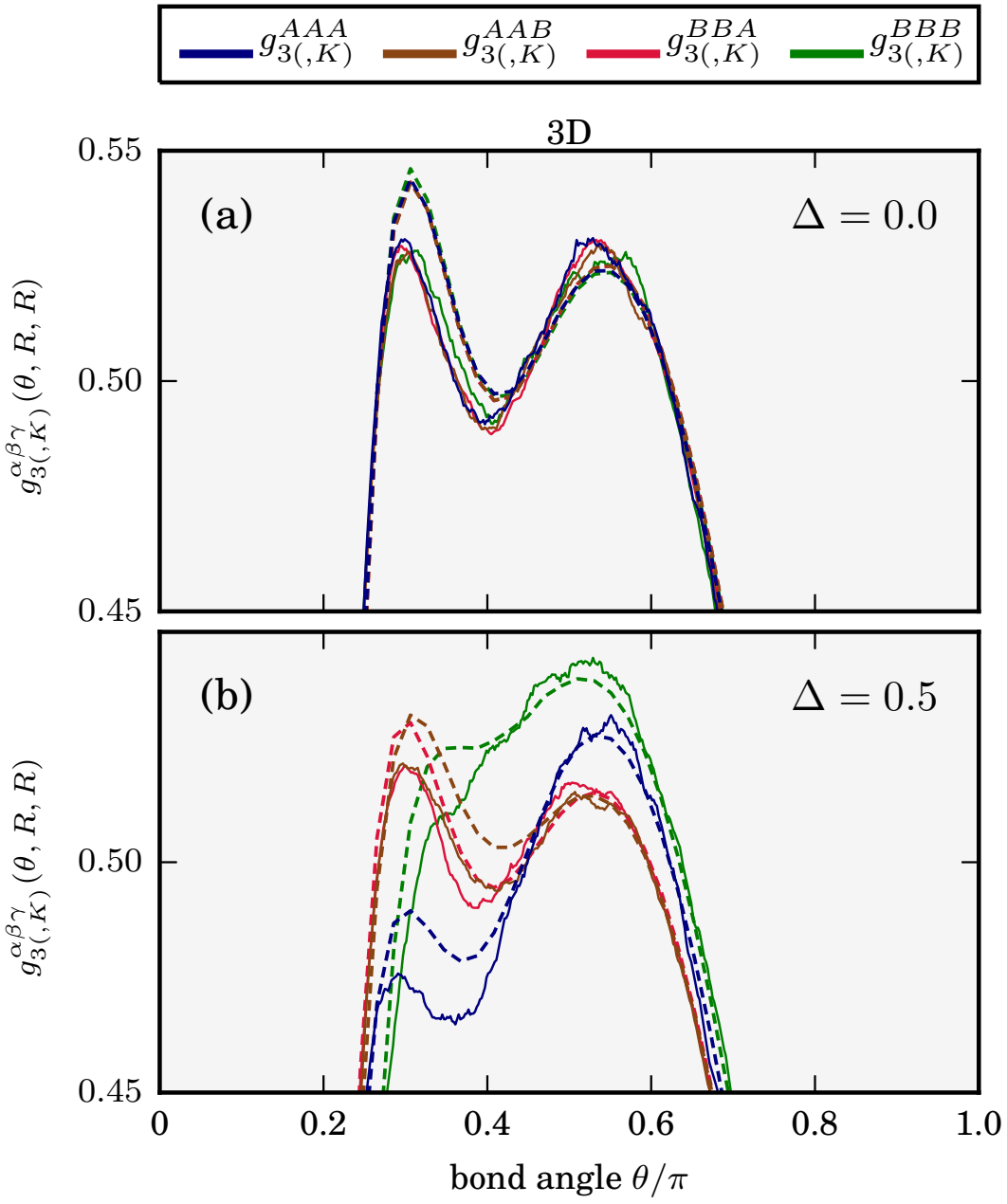

Figure 3.5: *3D bond angle distribution function $g_3^{\alpha\beta\gamma}(\theta, R, R)$ computed directly from our computer simulation (solid curves) and Kirkwood approximations, $g_{3,K}^{\alpha\beta\gamma}(\theta, R, R)$, of the bond angle distribution functions (dashed curves). The functions $g_{3,K}^{\alpha\beta\gamma}(\theta, R, R)$ are computed on basis of Eq.* (3.15)*, using the pair correlation functions $g^{\alpha\beta}(r)$ from the simulations as input. Simulation parameters are the same as for Fig. 3.1.*

Smoluchowski theory with Kirkwood closure exhibit the lowest level of accuracy (*c.f.*, Figs. 3.1,3.4 and 3.5).

3.5 Conclusions

We have studied 2D and 3D systems of Brownian particles with reciprocal and nonreciprocal particle interactions. A microscopic theory based on the many-body Smoluchowski equation with the Kirkwood superposition approximation as a closure predicts the particle pair-correlation functions with good accuracy. Nonreciprocal interactions have distinct influence of the pair-correlations, as revealed by the differences between the correlation functions for systems with reciprocal and nonreciprocal forces. Our predictions for the pair- and triplet-correlation functions can be tested experimentally with binary mixtures of diffusiophoretic microswimmers.

Future theory could improve the closure beyond the Kirkwood superposition principle. Possible candidates for future development are dynamical density functional theory [152–156] or mode coupling theory [157] for nonequilibrium systems, which still need to be generalized to systems with nonreciprocal interactions. Furthermore, the effect of different nonreciprocity classes (constant versus r-dependent Δ) on the structural correlations should be carefully explored.

CHAPTER 4

EMERGING ACTIVITY IN BILAYERED DISPERSIONS WITH WAKE-MEDIATED INTERACTIONS

In the previous chapters, it is shown that effective forces between mesoscopic particles often become nonreciprocal when the interactions are mediated by a nonequilibrium environment. Such situations can be realized in various soft matter systems – most notably in colloidal dispersions [22–27] and complex plasmas [14–17], where microparticles are embedded, respectively, in a liquid solvent or a dilute weakly ionized gas. In particular, the action-reaction symmetry in these systems is broken when the surrounding fluid moves with respect to the particles [1, 10–13], or when the interaction of molecules with the particle surface is out of equilibrium [22, 23, 26, 27].

Studies of nonreciprocal interactions have gained increased interest in recent time. When the dynamics of individual particles is undamped or weakly damped Newtonian [1], which is typical for complex plasmas, one can observe a remarkable state of *detailed dynamic equilibrium* with different species having different temperatures. For Brownian dynamics, it has recently been shown that mixtures of diffusiophoretic colloids experience effective nonreciprocal forces which stimulate the formation of stable aggregates (so-called active molecules) [27] and trigger collective oscillatory motion [28].

In this chapter we consider a layered (quasi two-dimensional) system of charged Brownian particles exposed to a perpendicular electric field gradient. The electric field causes a micro-ion flow, which generates wakes below the particles while the solvent itself is at rest. The particles are kept within their layer by additional fields, such as gravity or laser-optical fields. The resulting interparticle interactions are mediated by flow generated wakes, and therefore the actio-reactio symmetry is broken

At the time of writing this thesis, this chapter is submitted in a very similar form by Jörg Bartnick, Andreas Kaiser, Hartmut Löwen and Alexei V. Ivlev, see Reference [3].

(see Chapter 2). Such a generic nonreciprocal system can be experimentally realized both in strongly damped complex plasmas and colloidal dispersions, and has the advantage that the strength of nonreciprocity can be tuned by the external field. Under quite general conditions posed on the mutual reciprocal and nonreciprocal forces, we observe here a continuous transition from inactive (stacked) pairs to active units, indicating the emergence of active fluids. Different from ordinary active particle systems [158–160], these active units can break and become passive again. Using analytical theory and simulation, we explore the full density regime up to freezing and find an unusual melting upon densification, along with a reentrant freezing and an enormous diffusivity in the concentrated fluid.

4.1 Model

The motion of a particle i at position $\mathbf{r}_i$ is governed by the fully damped Langevin equation [91]

$$\dot{\mathbf{r}}_i = \sum_j \boldsymbol{L}_{ij} \left(\mathbf{F}_j + \boldsymbol{\xi}_j\right) + \frac{1}{2} k_\mathrm{B} T \sum_j \frac{\partial \boldsymbol{L}_{ij}}{\partial \mathbf{r}_j}, \tag{4.1}$$

where $\boldsymbol{L}_{ij}$ is the mobility matrix and $\boldsymbol{\xi}_i$ is a random force. The total force $\mathbf{F}_i$ on particle i is given by $\mathbf{F}_i = \sum_j \mathbf{F}_{ij}$, where $\mathbf{F}_{ij}$ is the pair-interaction force exerted by a particle i on the particle j. The random force $\boldsymbol{\xi}_i$ is Gaussian distributed with zero mean, $\langle \boldsymbol{\xi}_i(t) \rangle = 0$, and variance $\langle \boldsymbol{\xi}_i(t) \boldsymbol{\xi}_j(t') \rangle = 2\, \boldsymbol{L}_{ij}^{-1}\, k_\mathrm{B} T \delta(t - t')$, where T is the thermostat temperature, k_B the Boltzmann constant, $\delta(t)$ the Dirac delta function and $\boldsymbol{L}^{-1}$ the inverse of the $\boldsymbol{L}$. In this chapter, we include hydrodynamic interactions in the zero-temperature limit, and neglect them at finite temperatures. The latter approach is justified, when the suspension is highly dilute, but still strongly interacting. Then, each mobility matrix reduces to $\boldsymbol{L}_{ij} = \delta_{ij} \boldsymbol{I} / \gamma_i$, where $\boldsymbol{I}$ is the unit matrix and γ_i is a friction coefficient. In the zero-temperature limit, we consider the mobility matrix to be approximated by the Oseen tensor [91]

$$\boldsymbol{L}_O(\mathbf{r}) = \frac{3 R_H}{4 \gamma_i r} (\boldsymbol{I} + \hat{\mathbf{r}} \hat{\mathbf{r}}), \tag{4.2}$$

where R_H is the hydrodynamic radius, $r = |\mathbf{r}|$ and $\hat{\mathbf{r}} = \mathbf{r}/r$. Thus, we have $\boldsymbol{L}_{ij} \approx \boldsymbol{L}_O(\mathbf{r}_i - \mathbf{r}_j)$ for $i \neq j$ and $\boldsymbol{L}_{ii} = \boldsymbol{I}/\gamma_i$.

We consider a typical situation when interactions between particles are isotropic. In this case the mutual forces between particles i and j are radial, i.e., $\mathbf{F}_{ij} = F_{ij} \mathbf{n}_{ij}$ with $\mathbf{n}_{ij}$ being the unit vector from i to j, and F_{ij} only depends on the absolute distance $r_{ij} = |\mathbf{r}_i - \mathbf{r}_j|$. Furthermore, we introduce species A and B and attribute particles to the same species if their pair interactions are reciprocal, i.e., $F_\mathrm{AA}(r) = F_\mathrm{BB}(r) = -d\varphi_\mathrm{r}(r)/dr$. A generic form for the forces between different species,

$$F_\mathrm{AB,BA}(r) = -d\varphi_\mathrm{r}(r)/dr \pm d\varphi_\mathrm{n}(r)/dr, \tag{4.3}$$

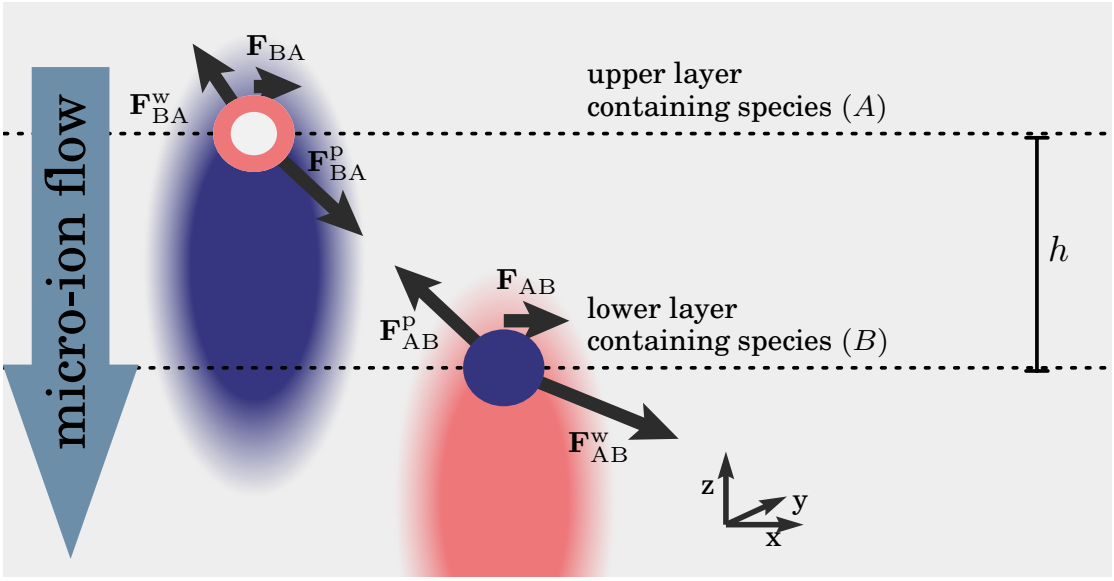

Figure 4.1: *Schematic sketch of nonreciprocal wake-mediated interactions. The particle species A and B are confined in the upper and lower layers, respectively. While the direct interparticle forces are reciprocal,* $\mathbf{F}^{\mathrm{p}}_{\mathrm{BA}} + \mathbf{F}^{\mathrm{p}}_{\mathrm{AB}} = \mathbf{0}$*, the particle-wake forces are nonreciprocal,* $\mathbf{F}^{\mathrm{w}}_{\mathrm{BA}} + \mathbf{F}^{\mathrm{w}}_{\mathrm{AB}} \neq \mathbf{0}$ *such that for the total forces* $\mathbf{F}_{\mathrm{AB}} \neq -\mathbf{F}_{\mathrm{BA}}$.

is a superposition of the reciprocal (r) and nonreciprocal (n) components, determined by the respective potentials $\varphi_{\mathrm{r,n}}$. The latter are related to the potential φ_{ij} generated by the particle i at the location of the particle j via $\varphi_{\mathrm{r,n}} = \frac{1}{2}(\varphi_{ji} \pm \varphi_{ij})$. Thus, the pair interactions are reciprocal if $\varphi_{ij} = \varphi_{ji}$, and are nonreciprocal otherwise.

In Chapter 2, we introduced an important class of a constant nonreciprocity, where $\varphi_{\mathrm{r}}(r)$ and $\varphi_{\mathrm{n}}(r)$ are similar functions, i.e., when the nonreciprocity $\varphi_{\mathrm{n}}(r)/\varphi_{\mathrm{r}}(r) \equiv \Delta = \mathrm{const}$. For undamped or weakly damped Newtonian dynamics with $\Delta = \mathrm{const}$, the equations of motion can be equivalently transformed into a reciprocal form by a simultaneous proper renormalization of the interaction forces and masses, i.e., such dynamics can in fact always be described by a (pseudo) Hamiltonian. It is noteworthy that for the Brownian dynamics with nonreciprocal interactions one can employ a similar approach: By performing the same renormalization for the interactions, Eq. (2.2) and (2.3), and introducing the renormalized damping coefficients $\tilde{\gamma}_{\mathrm{A,B}} = \gamma_{\mathrm{A,B}}/(1 \mp \Delta)$, we readily transform Eq. (4.1) to the form where the interactions are reciprocal, while the solvent temperatures for the species A and B are different and equal to $\widetilde{T}_{\mathrm{A,B}} = T/(1 \mp \Delta)$. Interestingly, such a "hetero-Brownian" model has been recently introduced in a different context, to describe DNA dynamics [161, 162], and was also proposed for colloidal pairs under external forcing [163].

In this chapter we consider the so-called wake-mediated interactions, representing a generic class of nonreciprocal interactions occurring when particles are embedded in a flowing medium. Such interactions can be induced in two-dimensional complex

plasmas [10, 14, 17], or between colloidal particles [11–13] under flow. Such situations can be modeled with a binary mixture of point-like particles with effective charges $Q_{\rm A}$ and $Q_{\rm B}$, confined in a horizontal xy-plane in two layers with a height difference h, as sketched in Fig. 4.1. The point-like approximation is justified as long as the distance between the particles stays larger than their diameter. Due to an externally imposed micro-ion flow, parallel to the vertical z-axis, each particle induces a wake, while the fluid remains at rest. The wake's excess charge $q_i \propto -Q_i$ is considered as a point-like effective charge at the distance δ downstream from the particle.

The particle's total force is the combination of the direct particle interaction and the particle-wake interaction. Following Refs. [104, 131], we assume that both forces are described by a model Yukawa potential with the same effective screening length λ. Let us introduce the three-dimensional particle coordinates $\mathbf{R}_i$ and the corresponding coordinates $\mathbf{r}_i$ in the horizontal plane. Then the force $\mathbf{F}_{ij} = -\partial\varphi_{ij}/\partial\mathbf{r}_j$ exerted in the horizontal plane by the particle i on the particle j is determined by the potential $\varphi_{ij} = Q_iQ_jY(R_{ij}) + q_iQ_jY(R^{\rm w}_{ij})$, where $Y(R) = R^{-1}e^{-R/\lambda}$ is the (unity charge) Yukawa potential which depends on the distance $R_{ij} = |\mathbf{R}_i - \mathbf{R}_j|$ between the particles as well as on the distance $R^{\rm w}_{ij} = |\mathbf{R}_i - \mathbf{R}_j - \delta\mathbf{n}_z|$ between the particle j and the wake center of the particle i. For particles in the same layer, A or B, we have $R^{\rm w}_{ij} = R^{\rm w}_{ji}$; therefore, $\varphi_{\rm n} = 0$ (since $q_iQ_j = q_jQ_i$), and hence the forces are reciprocal. For the AB interactions the symmetry is broken, $R^{\rm w}_{ij} \neq R^{\rm w}_{ji}$, and the forces are nonreciprocal.

The analysis below shows that for fully damped systems with wake-mediated interactions a rich variety of self-organization phenomena occurs, provided the species A and B are oppositely charged, or the screening lengths for the direct interactions and for the particle-wake interactions are different. While the latter case is typical for complex plasmas [15], in colloidal dispersions the former situation can be realized [164]. Therefore, in this chapter we focus on a system of the oppositely charged particles, and assume for simplicity that the charges have the same magnitude, i.e., $Q_{\rm A} = -Q_{\rm B} \equiv Q$, the same friction coefficients $\gamma_{\rm A} = \gamma_{\rm B} \equiv \gamma$, and that the height difference is $h = \lambda$. A natural measure of nonreciprocity in this case is the relative wake charge, $\tilde{q} = -q_i/Q_i > 0$.

4.2 Stability analysis and self-organization

In order to illustrate a tendency of particles with nonreciprocal interactions to self-organize themselves with increasing $\tilde{q}$, and to identify the characteristic building blocks of this complex process, let us consider the formation of small clusters in the absence of hydrodynamic interactions. Then, the equilibrium configurations for a cluster of N particles are determined from the force balance in the *horizontal* plane, $\sum_j^N \mathbf{F}_{ji}(r_{ij}) = \mathbf{F}$, where the net force $\mathbf{F}$ is a constant horizontal vector for $\forall i \in [1, N]$. We apply the standard stability analysis of the derived configurations in the zero-temperature limit. This corresponds to the eigenvalue problem $\det\left(\partial\mathbf{F}_{ij}/\partial\mathbf{r}_j|_{\rm eq} - \gamma\lambda\mathbb{1}\right) = 0$, where $\ldots|_{\rm eq}$ denotes the $(2N \times 2N)$ dynamical matrix calculated for the equilibrium configurations.

4.2.1 Active and inactive doublets

A pair of particles of different species form an equilibrium *doublet* with the horizontal separation r_D when $F_{\rm AB}(r_D) = -F_{\rm BA}(r_D) \equiv F$; the doublet is stable if $d\left[F_{\rm AB}(r) + F_{\rm BA}(r)\right]/dr|_{r=r_D} < 0$. From Eq. (4.3) we conclude that the stability condition is only fulfilled when the reciprocal component of the force is equal to zero, $d\varphi_{\rm r}(r)/dr|_{r=r_D} = 0$.

For a vertical pair $r_D = 0$ – we call it *an inactive doublet* – two regimes can be distinguished: (i) When $dF_{ij}(r)/dr|_{r=0} < 0$ for both particles, they return to the equilibrium after a small perturbation. Below we demonstrate that this case, sketched in Fig. 4.2(a), is observed for a "weak" nonreciprocity, when the relative wake charge is smaller than a certain critical value, $\tilde{q} < \tilde{q}_{\rm cr1}$ (i.e., this always occurs for reciprocal interactions). (ii) When $dF_{ij}(r)/dr|_{r=0} > 0$ for one of the particles, the restoring forces are pointed in the same direction, as shown in Fig. 4.2(b). The equilibrium in this case, corresponding to $\tilde{q}_{\rm cr1} < \tilde{q} < \tilde{q}_{\rm cr2}$, would only be restored in the zero-temperature limit; in the presence of an infinitesimal thermal noise the doublet should break apart.

Under the general condition

$$d\varphi_{\rm r}(r)/dr|_{r=r_D} = 0 \;\text{ and }\; d\varphi_{\rm n}(r)/dr|_{r=r_D} \neq 0, \tag{4.4}$$

satisfied for $r_D > 0$, a pair emerges which is self-propelled in the direction $\mathbf{n}_{\rm AB}$ with the velocity $v_D = -\left[d\varphi_{\rm n}(r)/dr|_{r=r_D}\right]/\gamma$. Such clusters will be referred to as *active doublets* and occur when $\tilde{q} > \tilde{q}_{\rm cr2}$. Note that for a constant nonreciprocity, $\Delta = {\rm const}$, stable doublets are always at rest, since $\varphi_{\rm n}(r) = \varphi_{\rm r}(r)/\Delta$ and therefore the nonreciprocal force is equal to zero at $r = r_D$ [1].

Figures 4.2(d) and (e) illustrate the results of the stability analysis in the horizontal plane, performed in the zero-temperature limit. In the present example, two particles of different species are stacked on top of each other (i.e., they form an inactive doublet) when the relative wake charge is smaller than $\tilde{q}_{\rm cr2} \simeq 0.74$. For larger $\tilde{q}$, the separation r_D continuously increases and an active doublet moves along its symmetry axis, with the velocity v_D which varies non-monotonically with $\tilde{q}$. Thus, in dilute systems (with infinitesimal number density) one can expect the formation of multiple individual doublets. Hydrodynamic interactions do not influence the pair separation r_D, but cause an increase in the velocity.

Now, we study the effect of hydrodynamic interactions on a doublet in the dilute limit. We consider two particles of species A and B, which are confined at different heights. The position of the particles, projected on the xy-plane, shall be called $\mathbf{r}_{\rm A}$ and $\mathbf{r}_{\rm B}$, respectively. The position of the particles, projected on the horizontal xy-plane, shall be called $\mathbf{r}_{\rm A}$ and $\mathbf{r}_{\rm B}$, respectively. The general requirement for stable clusters is the equality of the velocities

$$\dot{\mathbf{r}}_{\rm A} = \dot{\mathbf{r}}_{\rm B}\,. \tag{4.5}$$

[1] Given the vertical separation of particles within an active unit, we refrain from the term active molecules used in Ref. [27]

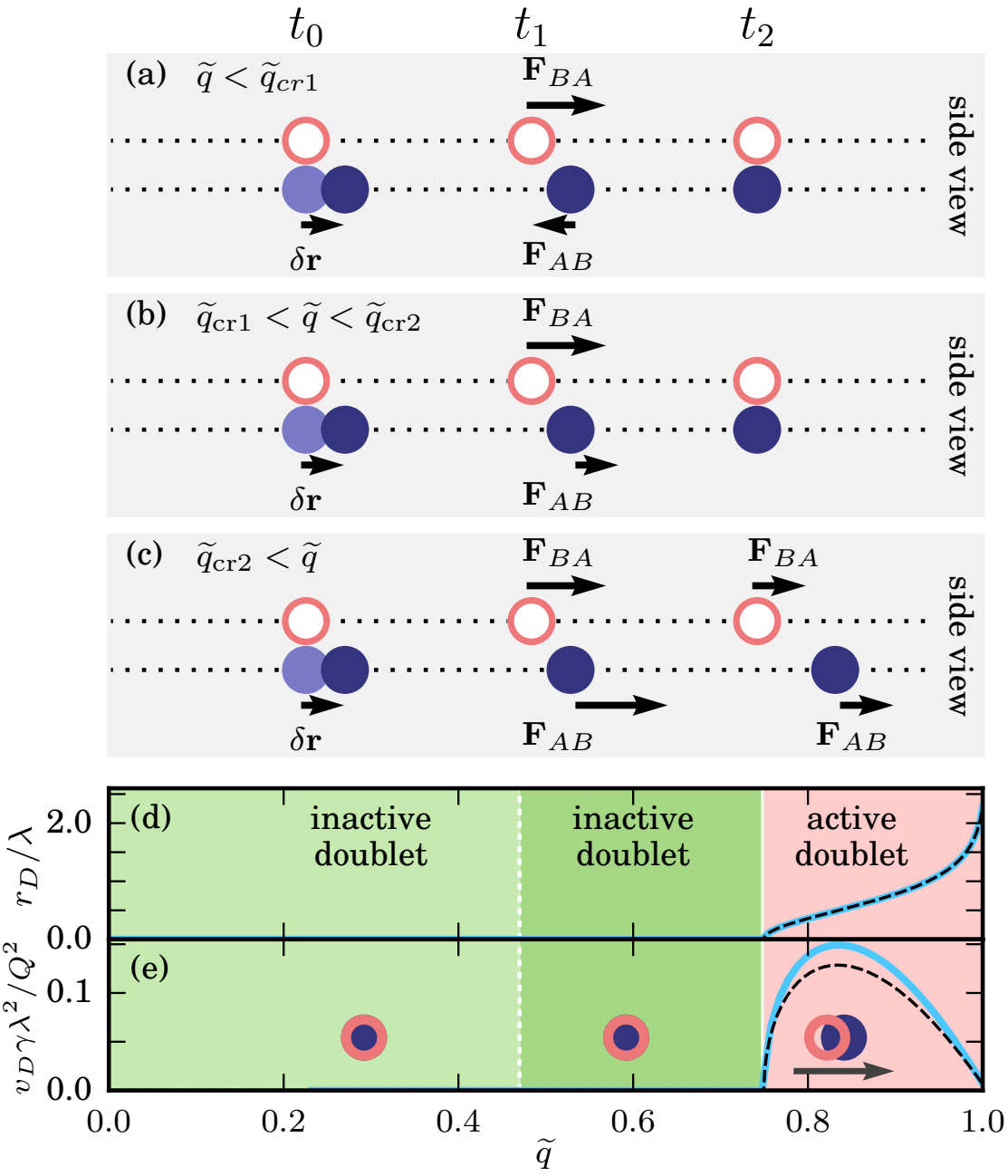

Figure 4.2: *Stable configurations of two-particle clusters, depending on the relative wake charge $\tilde{q}$. (a-c) Sketches illustrate three distinct regimes (side view): For $\tilde{q} < \tilde{q}_{\mathrm{cr1}}$, particles form a stable vertical pair, an inactive doublet, since the restoring forces $\mathbf{F}_{\mathrm{AB}}$ and $\mathbf{F}_{\mathrm{BA}}$ exerted by a small perturbation pull the particles back; for $\tilde{q}_{\mathrm{cr1}} < \tilde{q} < \tilde{q}_{\mathrm{cr2}}$, the vertical pair remains stable only in the zero-temperature limit assumed here, since $\mathbf{F}_{\mathrm{AB}}$ and $\mathbf{F}_{\mathrm{BA}}$ are pointed in the same direction; for $\tilde{q} > \tilde{q}_{\mathrm{cr2}}$, the particles form an active doublet with a finite horizontal separation, moving along the force $\mathbf{F}_{\mathrm{AB}} = \mathbf{F}_{\mathrm{BA}}$. (d,e) Equilibrium horizontal separation of the doublet, r_D (normalized by λ) and the corresponding doublet velocity v_D (normalized by $Q^2/\lambda^2\gamma$), the shading indicates the stability regimes illustrated in (a-c). The results are for the wake length $\delta = 0.2\lambda$, $h = \lambda$ and $R_H = 0$ (black dashed line) as well as $R_H = 0.2\lambda$ (blue solid line).*

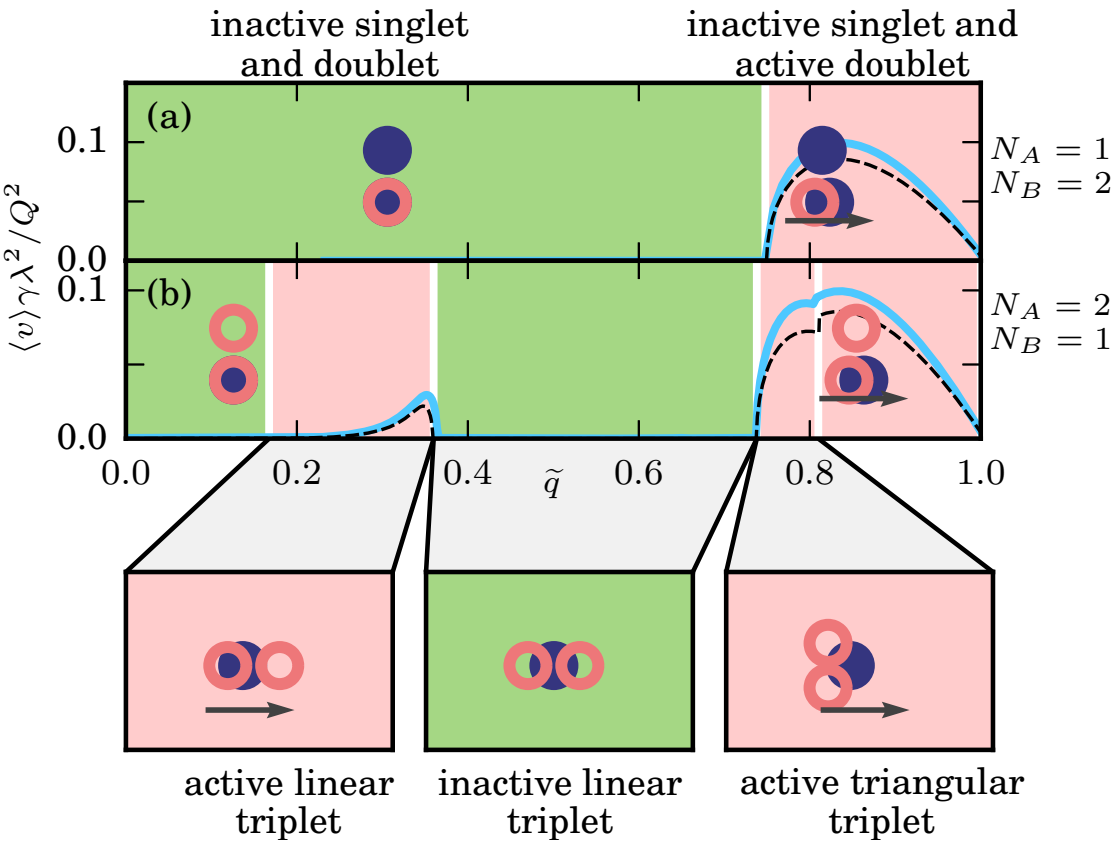

Figure 4.3: *Stable configurations and velocities of three-particle clusters in the zero-temperature limit. The two possible combinations of the species A and B are shown. The figure legend is the same as in Fig. 4.2.*

The equation of motion of the A particle can be written as

$$\dot{\mathbf{r}}_{\mathrm{A}} = \frac{1}{\gamma}\mathbf{F}_{\mathrm{A}}(\mathbf{r}_{\mathrm{A}} - \mathbf{r}_{\mathrm{B}}) + \left[\frac{3R_H}{4\gamma\tilde{r}}\left(1 + \frac{r^2}{\tilde{r}^2}\right)\right]\mathbf{F}_{\mathrm{B}}(\mathbf{r}_{\mathrm{B}} - \mathbf{r}_{\mathrm{A}})\,, \tag{4.6}$$

with the friction coefficient γ and $\tilde{r} = \sqrt{r^2 + h^2}$ where h is the vertical distance between the particles and $r = |\mathbf{r}_{\mathrm{A}} - \mathbf{r}_{\mathrm{B}}|$; the respective equation for the B particle, is obtained by $\mathrm{A} \leftrightarrow \mathrm{B}$ permutation. Equation (4.6) is only fulfilled if $F_{\mathrm{AB}}(r_D) = -F_{\mathrm{BA}}(r_D)$, as in the case without hydrodynamic interactions. Thus for a finite hydrodynamic radius, Eqs. (4.4) remain valid. Figure 4.2 shows the result for a doublet with and without hydrodynamic interactions. The doublet distance r_D remains unchanged, while the doublet velocity is slightly increased.

4.2.2 Active and inactive triplets

In a similar manner, one can straightforwardly generalize the analysis for larger clusters. For three particles, there is a variety of possible *triplet* configurations. To start with, let us consider a cluster composed of one particle B and two particles A with negligible hydrodynamic interactions. We work in the frame of reference of the first (B) particle, i.e., the coordinates of the second and third (A) particles are $\mathbf{r}_{2,3}$. In this case, the general equilibrium condition, $\sum_j^N \mathbf{F}_{ji}(r_{ij}) = \mathbf{F}$, can be identically transformed to the following two equations for the particle coordinates (plus one equation for the net force $\mathbf{F}$):

$$\tilde{F}(r_2)\mathbf{n}_2 + \tilde{F}(r_3)\mathbf{n}_3 = \mathbf{0}, \tag{4.7a}$$

$$2F_{\mathrm{AA}}(r_{23})\mathbf{n}_{32} - F_{\mathrm{BA}}(r_3)\mathbf{n}_3 + F_{\mathrm{BA}}(r_2)\mathbf{n}_2 = \mathbf{0}, \tag{4.7b}$$

with $\tilde{F}(r) \equiv F_{\mathrm{BA}}(r) + 2F_{\mathrm{AB}}(r)$. In the reverse case, where clusters are composed of one A and two B particles, the labels are simply to be swapped.

Using Eq. (4.7a), one can distinguish two principal cases: (i) $\tilde{F}(r_{2,3}) \neq 0$, then solutions exist only for $\mathbf{r}_2 \parallel \mathbf{r}_3$; (ii) $\tilde{F}(r_2) = \tilde{F}(r_3) = 0$, then solutions are possible for non-collinear $\mathbf{r}_2$ and $\mathbf{r}_3$.

(i) If $\tilde{F}(r)$ is a monotonic function, the only solution is $\mathbf{r}_2 = -\mathbf{r}_3$; from Eq. (4.7b) we obtain $F_{\mathrm{AA}}(2r) = F_{\mathrm{BA}}(r)$, which yields $r_2 = r_3 \equiv r$. Due to symmetry, $F = 0$ and hence we call such configurations *inactive linear triplets*. However, if $\tilde{F}(r)$ is a non-monotonic function, also solutions with $r_2 \neq r_3$ are possible – in this case Eqs. (4.7) are reduced to $\tilde{F}(r_2) = \tilde{F}(r_3)$ and $2F_{\mathrm{AA}}(r_2 + r_3) = F_{\mathrm{BA}}(r_2) + F_{\mathrm{BA}}(r_3)$. Such asymmetric clusters usually imply a non-vanishing net force, $F \neq 0$, which generates a directed propulsion. We call these configurations *active linear triplets*.

(ii) If $F_{\mathrm{BA}}(r)$ is monotonic, solutions for $\mathbf{r}_{2,3}$ are limited to triangles with $r_2 = r_3 \equiv r$ and the apex angle θ, obtained from $F(r) = 0$ and $F_{\mathrm{AA}}(2r\sin\frac{1}{2}\theta)/\sin\frac{1}{2}\theta = F_{\mathrm{BA}}(r)$. Such configurations are called *active triangular triplets*. Finally, if $F_{\mathrm{BA}}(r)$ is a non-monotonic function, triangular triplets with $r_2 \neq r_3$ are possible.

As for the doublets, we apply the standard stability analysis of the derived configurations in the zero-temperature limit.

If the number of particles B is twice as high as the number of A particles, the dependence on $\tilde{q}$ remains the same as in Fig. 4.2. The "excess" particle B simply remains an *inactive singlet* [see Fig. 4.3(a)]. On the contrary, in the situation with two particles A for one particle B various active and inactive structures emerge, as presented in Fig. 4.3(b): An inactive doublet and an inactive singlet are formed when $\tilde{q} < 0.17$, while for $\tilde{q} \in (0.17, 0.36)$ they merge into an *active linear triplet*, where the position of particle B is slightly shifted from the center (which determines the propagation direction along the symmetry axis). The linear triplet becomes inactive at $\tilde{q} \in (0.36, 0.74)$. The further increase of the wake charge, $\tilde{q} \in (0.74, 0.81)$, causes particle B to shift perpendicular to the symmetry axis, leading to an *active triangular triplet*. For even larger values of

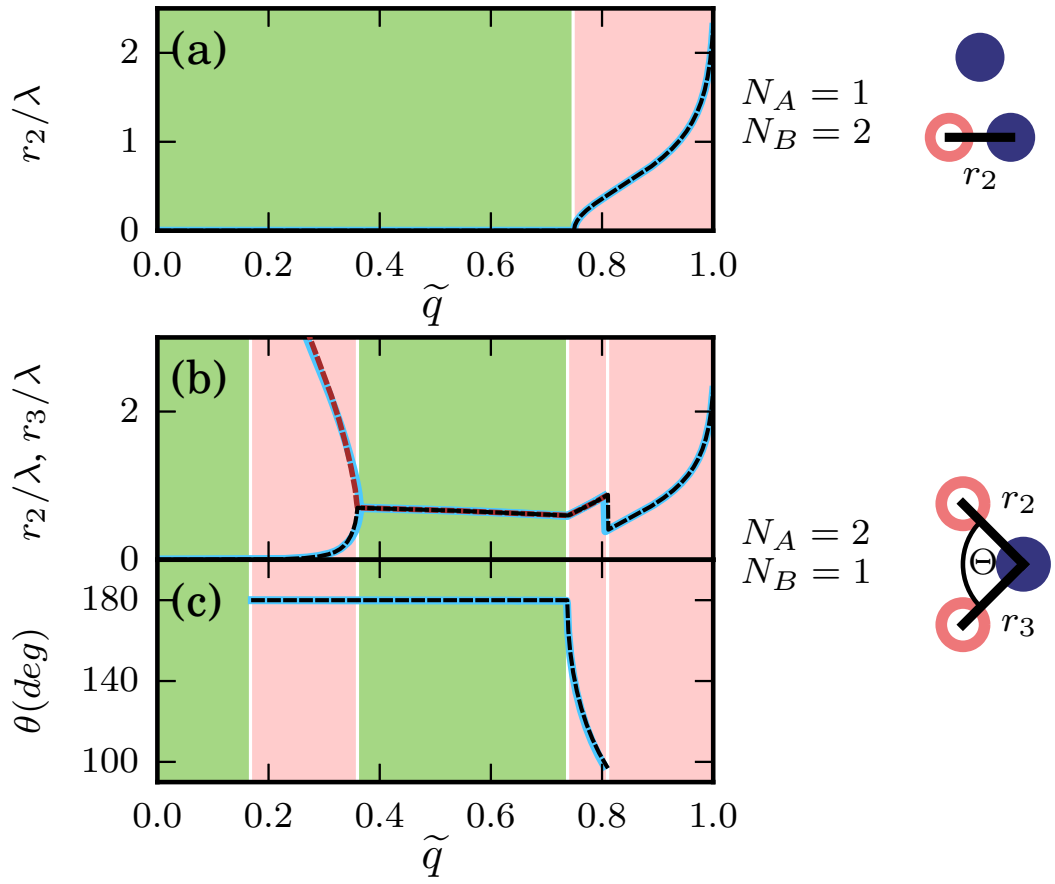

Figure 4.4: *Equilibrium horizontal separation in the doublet and triplet configurations shown in Fig. 4.2.*

$\tilde{q}$, the triplet breaks apart and an active doublet and an inactive singlet emerge. In a similar manner, one can straightforwardly generalize the analysis for larger clusters or investigate, e.g., the rotation activity.

Figure 4.4(a) shows the horizontal separation r_1 for the case of $(N_A = 1, N_B = 2)$, where a passive singlet and a doublet form. In the reverse situation $(N_A = 2, N_B = 1)$, we characterize the emerging triplets by their individual bond distances r_2, r_3 [Fig. 4.4(b)] and the respective apex angle θ [Fig. 4.4(c)]. Activity is a result of symmetry breaking, therefore active units are found if $r_2 \neq r_3$ or $\theta < 180°$.

If hydrodynamic interactions are taken into account, the general equilibrium condition becomes

$$\dot{\mathbf{r}}_i = \dot{\mathbf{r}} \quad \forall \quad i \in \{1, \ldots, N\} \ . \tag{4.8}$$

Generally, the triplet coordinates derived above do not fulfill this equilibrium condition. This is in contrast with the doublets, where the inclusion of hydrodynamic interactions only induces a rescaling of the velocity. For three particles, we solve Eq. (4.1) numerically and show the results in Figs. 4.2 and 4.4. However, the resulting changes to the positions

are minor, as shown in Fig. 4.4. Similar to doublets, the inclusion of hydrodynamic interactions merely causes a slight increase of the velocity, see again Fig. 4.2.

4.2.3 Stability analysis for finite densities

For a finite number density ϕ in systems without hydrodynamic interactions, we analyze the stability of crystalline structures in the zero-temperature limit. The time-dependent coordinate of the ith-particle is presented as a sum of its equilibrium lattice position and a displacement, $\mathbf{r}_i(t) = \mathbf{r}_{\mathrm{eq},i} + \mathbf{u}_i(t)$. The interaction force, Eq. (4.3), is then expanded to the first order in $\mathbf{u}_i$ and substituted in Eq. (4.1). Using $\mathbf{u}_i \propto \exp(i\mathbf{k}\cdot\mathbf{r}_{\mathrm{eq},i} + \omega t)$, the dispersion relations $\omega(\mathbf{k})$ are derived as eigenvalues of the resulting dynamical matrix [104]. We examine a vertically stacked hexagonal lattice and an *interdigitated hexagonal* lattice, the stability requires Re $\omega(\mathbf{k}) < 0$ for all $\mathbf{k}$ from the first Brillouin zone of the lattice.

4.2.4 Diffusion of a doublet under thermal noise

Now, let us study the case of finite temperature in the absence of hydrodynamic interactions. For a single stacked doublet, where $r_D = 0$, we compute the mean-squared displacement starting from Eq. (4.1). We compute the Taylor expansion of the forces at a given $\tilde{q}$ around the equilibrium positions. Then, $\mathbf{F}_{\mathrm{BA}}(\tilde{q}, t) \approx C_{\mathrm{A}}(\tilde{q})\,[\mathbf{r}_{\mathrm{A}}(t) - \mathbf{r}_{\mathrm{B}}(t)]$ and $\mathbf{F}_{\mathrm{AB}}(\tilde{q}, t) \approx C_{\mathrm{B}}(\tilde{q})\,[\mathbf{r}_{\mathrm{B}}(t) - \mathbf{r}_{\mathrm{A}}(t)]$, where $C_{\mathrm{A}}(\tilde{q})$ and $C_{\mathrm{B}}(\tilde{q})$ are the prefactors of the linear order terms in the expansion. We define $\boldsymbol{A}(\tilde{q})$ as a matrix containing these prefactors, such that Eq. (4.1) can be written as a matrix equation

$$\gamma \frac{\partial \mathbf{X}(t)}{\partial t} = \boldsymbol{A}(\tilde{q})\mathbf{X}(t) + \mathbf{T}(t), \tag{4.9}$$

where $\mathbf{X}(t) = (\mathbf{r}_{\mathrm{A}}(t),\ \mathbf{r}_{\mathrm{B}}(t))$ is the super vector of the particle positions and $\mathbf{T}(t) = (\boldsymbol{\xi}_1(t),\ \boldsymbol{\xi}_2(t))$ the vector with the random forces acting on the particles. For simplicity, we set the friction coefficient γ independent of the particle index. Using variation of constants, this differential equation is solved by the integration over a matrix exponential:

$$\mathbf{X}(t) = \frac{1}{\gamma}\int_0^t \mathrm{d}\tau\ \exp\left[\boldsymbol{A}(\tilde{q})(t-\tau)/\gamma\right]\ \mathbf{T}(\tau),$$

with $\langle \mathbf{T}(t)\rangle = 0$ and $\langle \mathbf{T}_i(t)\mathbf{T}_j(t')\rangle = 2\gamma k_B T \delta_{ij}\delta(t-t')$, leading to $\langle \mathbf{X}(t)\rangle = 0$. Via computing the the mean squared displacement, we determine the diffusion ratio to

$$\frac{D_L(\tilde{q})}{D_S} = \frac{C_{\mathrm{A}}^2(\tilde{q}) + C_{\mathrm{B}}^2(\tilde{q})}{\left[C_{\mathrm{A}}(\tilde{q}) + C_{\mathrm{B}}(\tilde{q})\right]^2}\,. \tag{4.10}$$

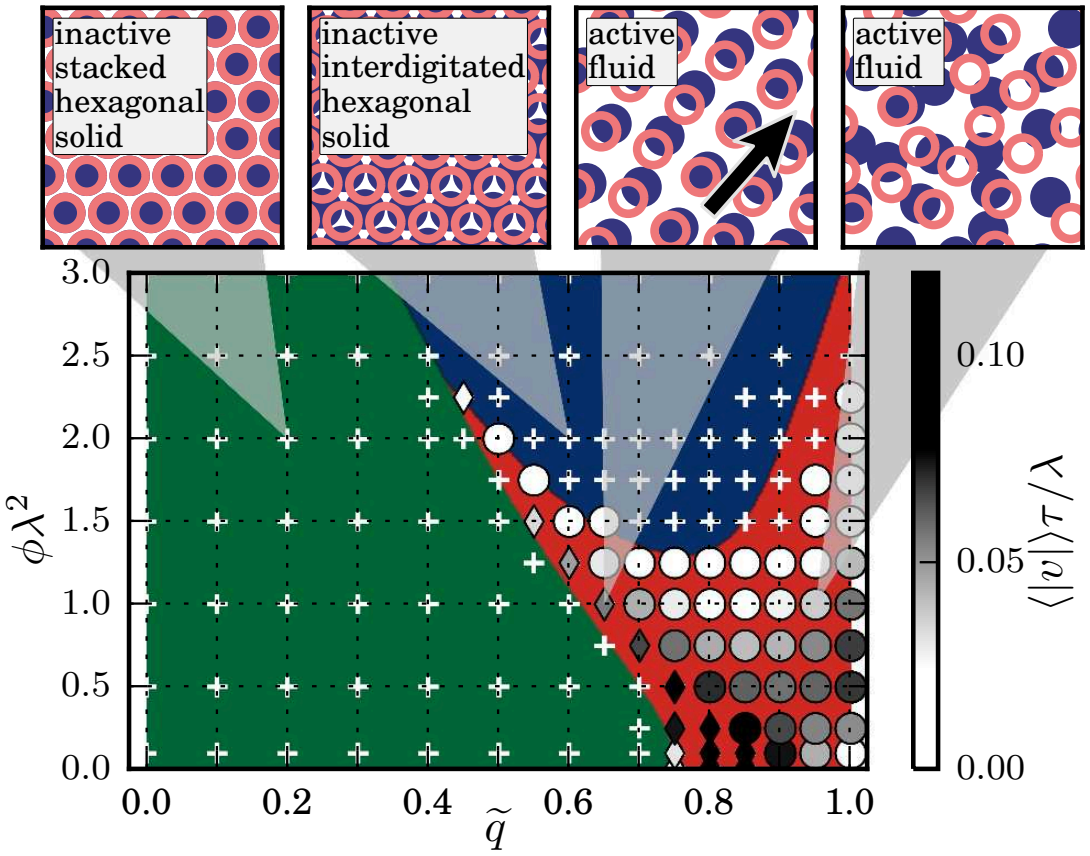

Figure 4.5: *State diagram in the zero-temperature limit, plotted in the plane of the number density ϕ and relative wake charge $\tilde{q}$. Color coding depicts results obtained from the stability analysis, symbols show numerical results. Inactive systems (+) can be either stacked hexagonal solid (green background) or interdigitated hexagonal solid (blue background). For active fluid regimes (◯, red background), the average particle velocities are indicated by a grey scale. Diamonds (♢) are used instead of circles if active doublets emerge whose decay time τ_D exceeds a threshold of $10^3\tau$. The states are illustrated by typical snapshots.*

The result of Eq. (4.10) is shown in Fig. 4.9 and in Fig. 4.10 as a black dashed line. As long as the approximation of the forces remains justified, this result is valid independent of the finite temperature.

4.3 Numerical simulations

The above analytical results are complemented with a numerical analysis [148]. We solve the equation of motion, Eq. (4.1), using a forward time-step algorithm in a Brownian dynamics simulation for three distinct cases: neglecting hydrodynamics we consider (i) the zero-temperature limit and (ii) finite temperatures as well as (iii) the zero-temperature limit taking hydrodynamic interactions into account. We use a 2D rectangular simulation box with periodic boundary conditions and the edge ratio $L_y/L_x = \sqrt{3}/2$. The particles are initialized on a distorted stacked hexagonal lattice with a fixed number density $\phi = N/(L_x L_y)$.

In the case (i) and (ii), we use $N = 2 \times 2500$ particles. The respective edge lengths of the simulation domain are varying from $(L_x, L_y) \simeq (240\lambda, 210\lambda)$ at low densities to $(L_x, L_y) \simeq (43\lambda, 38\lambda)$ at $\phi\lambda^2 = 3$. In the case (iii), we use $N = 2 \times 576$ particles, and the simulation domain is between $(L_x, L_y) \simeq (115\lambda, 100\lambda)$ at low densities and $(L_x, L_y) \simeq (28\lambda, 24\lambda)$ at high densities. For all cases, the wake length is $\delta = 0.2\lambda$, the height between the layers is $h = \lambda$, the time t is measured in units of $\tau = \gamma\lambda^3/Q^2$ and the distance r in units of λ. We set the time step to $\delta t = 0.005\tau$ in the cases (i) and (ii) and to $\delta t = 0.0025\tau$ in case (iii), which ensures proper resolution of the particle dynamics. After initialization, the system is given time of $10^4\tau$ to relax into a steady state. Statistics is gathered for multiple simulations runs with independent initializations and the simulation time of 2500τ. By measuring the displacement of individual particles within the time step, a particle velocity is calculated as $\mathbf{v}_i(t) = [\mathbf{r}_i(t + \delta t) - \mathbf{r}_i(t)]/\delta t$.

4.3.1 Emerging states

Figure 4.5 presents the state diagram of the emerging activity, where we compare the theoretical results against simulations in the zero-temperature limit. The state diagram is plotted in the plane spanned by number density ϕ and relative wake charge $\tilde{q}$. We identify three distinct domains: Toward the reciprocal limit $\tilde{q} = 0$, the particles form a bilayered *stacked hexagonal crystal* (green); for larger $\tilde{q}$, at increased density the system goes into an *interdigitated hexagonal solid* (blue); for even larger $\tilde{q}$, at low densities we find an *active regime* where the crystal melts (red). In addition, we show the results obtained from the numerical simulations. Here, we differentiate between *inactive solids* (+) and *active fluids* (◯). The mobile units of the fluid are active doublets, that behave similar to (deformable) active Brownian particles [165–167]. The active regime in the simulations is defined for the average particle velocity $\langle|\mathbf{v}|\rangle$ above a threshold of $10^{-2}\lambda/\tau$. One can see that the emerging state diagram exhibits a reentrant behavior both with ϕ and $\tilde{q}$.

Notably, for intermediate $\tilde{q}$, there is an anomalous "water-like" melting upon an increase in ϕ followed by reentrant freezing.

4.3.2 Characteristics of active fluids

We introduce the averaged velocity $\langle \mathbf{v} \rangle = \langle [\mathbf{r}_i(t+\delta t) - \mathbf{r}_i(t)]/\delta t \rangle$, Fig. 4.6(a), as well as an alignment parameter $c = |\langle \mathbf{v} \rangle| / \langle |\mathbf{v}| \rangle$, Fig. 4.6(b): $c = 1$ for a perfect nematic order and $c = 0$ in a totally disordered case. Furthermore, to quantify the stability of doublets we define $N_D(t)$, the average number of particle pairs that remain nearest neighbors over the time interval t. Generally, it is well described by an exponential decay, $N_D(t) \propto e^{-t/\tau_D}$, with a doublet decay time τ_D. By an exponential fit $N_D(t) \propto e^{-t/\tau_D}$, we can obtain the doublet decay time τ_D, shown in Fig. 4.6(c) and (f). If no doublet splits during the simulation time of 2500τ, then τ_D is set to infinity. Long-living active clusters are marked by a diamond in Fig. 4.5. The existence of a finite decay time τ_D reveals a qualitative difference of our system to a system of permanently active particles [52, 159, 160, 168].

Figure 4.6(a) demonstrates that at low densities ($\phi\lambda^2 = 0.1$), the average velocity $\langle |\mathbf{v}| \rangle$ is well reproduced by the velocity of a single active doublet, v_D, calculated analytically. Above the threshold value of $\tilde{q}_{\mathrm{cr2}} = 0.74$, the distance r_D increases [see Fig. 4.2(d)]. For this reason, the average velocity first increases with $\tilde{q}$, but then it starts falling off due to decreasing interaction strength of a doublet [see also Fig. 4.2(e)]. As the activity sets in, long-living doublets are formed throughout the system and their mutual collisions lead to the velocity alignment [see Fig. 4.5], since the angle of reflection α_r after their mutual collision is always smaller the the incidence angle α_i, as shown in Fig. 4.7. With increasing the number density ϕ the onset of activity shifts towards smaller $\tilde{q}$, whereby the average velocity vs. wake charge becomes a non-monotonic function, leading to a reentrant effect for $\phi\lambda^2 > 1.25$, where an inactive interdigitated hexagonal solid emerges [see also Fig. 4.5].

The effects of hydrodynamic interactions are shown in Fig. 4.8. Similar to the analysis of doublets and triplets, the general velocity is increased. The onset of activity is practically unchanged, even for the dense colloidal fluid. In contrast to the case without hydrodynamic interactions, larger number density leads to higher velocity than the dilute colloidal fluids. The overall-alignment is increased, while the pair stability is practically unchanged. In the region of large $\tilde{q}$, we observe high alignment, but low pair-stability and low velocity, since the instable pairs are dragged with the background fluid.

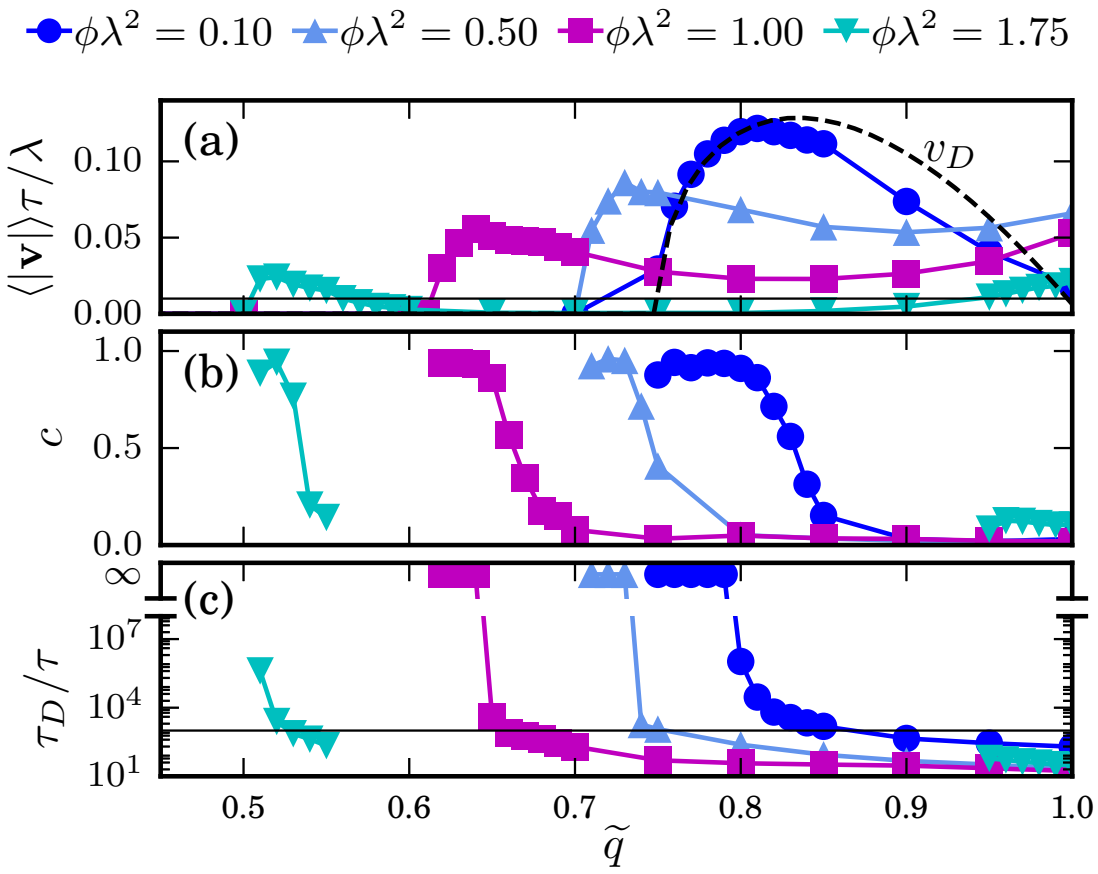

Figure 4.6: *Characteristics of active fluids where hydrodynamic interactions are neglected: (a) average particle velocity $\langle|\mathbf{v}|\rangle$, (b) alignment parameter c, and (c) decay time of doublets τ_D, plotted versus the relative wake charge $\tilde{q}$ for several values of the number density ϕ. The dashed line in panel (a) shows the velocity of a single active doublet v_D in the dilute case ($\phi\lambda^2 \ll 1$), the horizontal lines in panels (a) and (c) indicate the threshold values of the velocity ($10^{-2}\lambda/\tau$) and decay time ($10^3\tau$), respectively.*

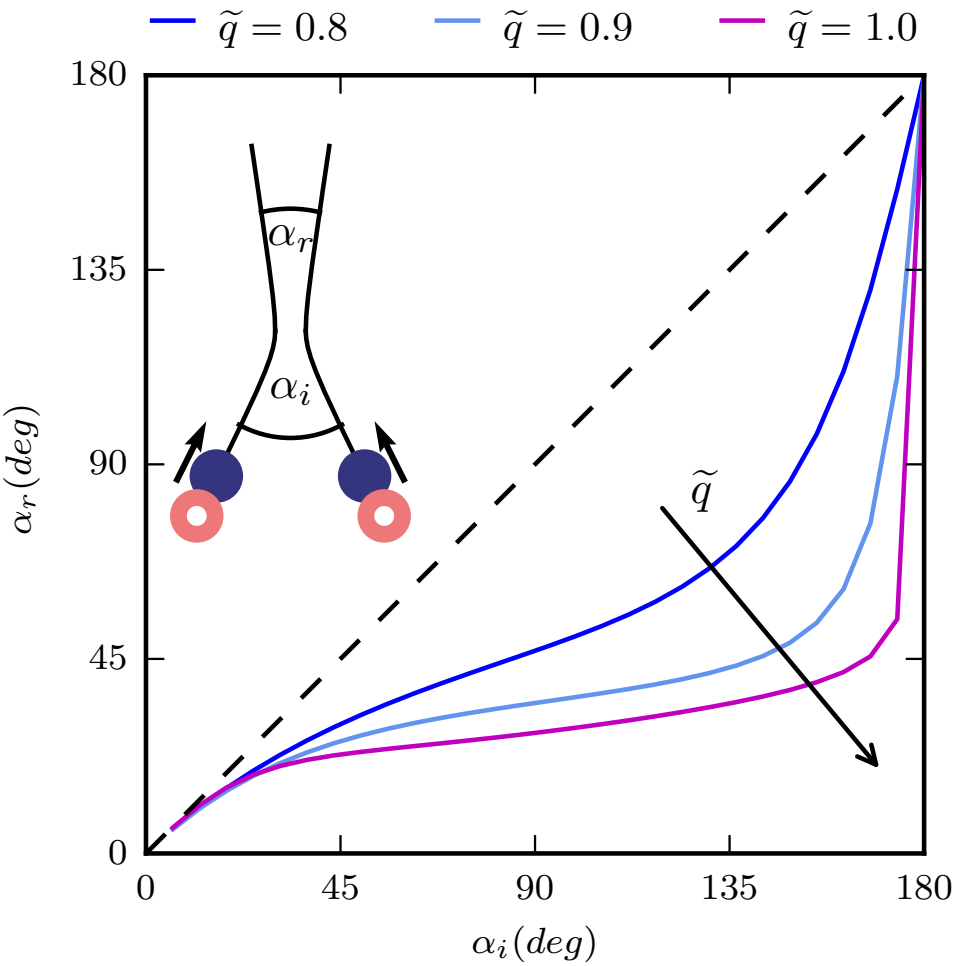

Figure 4.7: *Angle of reflection α_r versus the incidence angle α_i for a collision of two active doublets, plotted for different values of the relative wake charge $\tilde{q}$. The symmetric scattering, $\alpha_r = \alpha_i$, is indicated by the dashed line.*

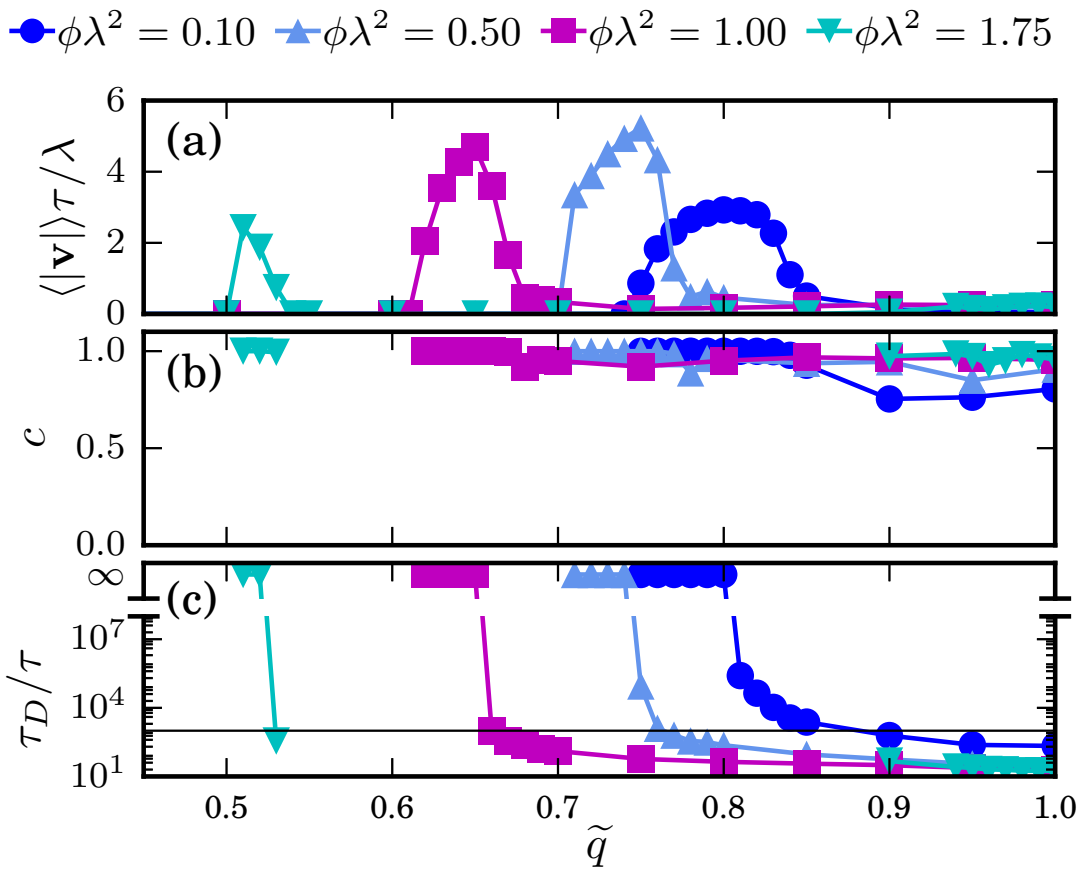

Figure 4.8: *Characteristics of active fluids with finite hydrodynamic radius $R_H = 0.2\lambda$: (a) average particle velocity $\langle|\mathbf{v}|\rangle$, (b) alignment parameter c, and (c) decay time of doublets τ_D, plotted versus the relative wake charge $\tilde{q}$ for several values of the number density ϕ. The horizontal line in panel (c) indicates the threshold values of the decay time ($10^3\tau$).*

4.3.3 Finite Temperatures

Finally, we study the impact of finite temperature in the many-body simulations on the characteristics of an active fluid, see Figs. 4.12 and 4.13. The temperature "smears out" the velocity profile and the previously defined velocity threshold value to detect an active fluid becomes obsolete. Instead for finite temperatures, the diffusion coefficient ratio is the appropriate quantity to identify an active fluid, $D_L/D_S > 1$. The alignment rapidly decreases, since the direction of propagation as well as the actual orientation of the doublet are affected by the additional random forces. However stable active units can still be found for a broad regime of relative wake charges $\tilde{q}$, see again Figs. 4.12 and 4.13. In Fig. 4.10 we compare those analytical results of Eq. (4.10) to numerical results obtained for number density $\phi\lambda^2 = 0.01$. The onset of activity defined by $D_L/D_S > 1$ is hardly affected by the given temperature. With increasing temperature, the diffusion ratio itself goes to one, see Fig. 4.10.

Finally, we study the dynamics for finite temperatures. Results for the time-dependent diffusion coefficient $D(t) = \frac{1}{4t}\langle|\mathbf{r}(t) - \mathbf{r}(0)|^2\rangle$ are summarized in Fig. 4.9 for a finite temperature $T = 10^{-3}\, Q^2/(k_{\mathrm{B}}\lambda)$. There is diffusion at long times, as characterized by the long-time diffusion coefficient $D_L = \lim_{t\to\infty} D(t)$. The latter is naturally normalized by the short-time coefficient $D_S = \lim_{t\to 0} D(t) = k_B T/\gamma$. For intermediate times there is either a sub-diffusive regime due to particle caging, or a ballistic regime arising from the emerging activity [169,170]. The diffusion ratio of the particles is also shown in Fig. 4.11. As discussed above (see Fig. 4.2), in dilute systems the activity at finite temperatures is expected to set in at $\tilde{q} > \tilde{q}_{\mathrm{cr1}}(\simeq 0.45)$. From Fig. 4.9 we see that for $\phi\lambda^2 = 0.01$ the transition to active fluids, $D_L/D_S > 1$, indeed occurs near this value. The long-time diffusion increases over several orders of magnitude as a function of nonreciprocity $\tilde{q}$. Even in dense colloidal fluids (at $\phi\lambda^2 = 1.75$) the ratio D_L/D_S exceeds 5, implying that there is an enormous diffusivity relative to the case of infinite dilution. As revealed by the snapshots in Fig. 4.5, this is mainly due to significant local alignment in the fluid, which allows for an efficient traveling of active doublets.

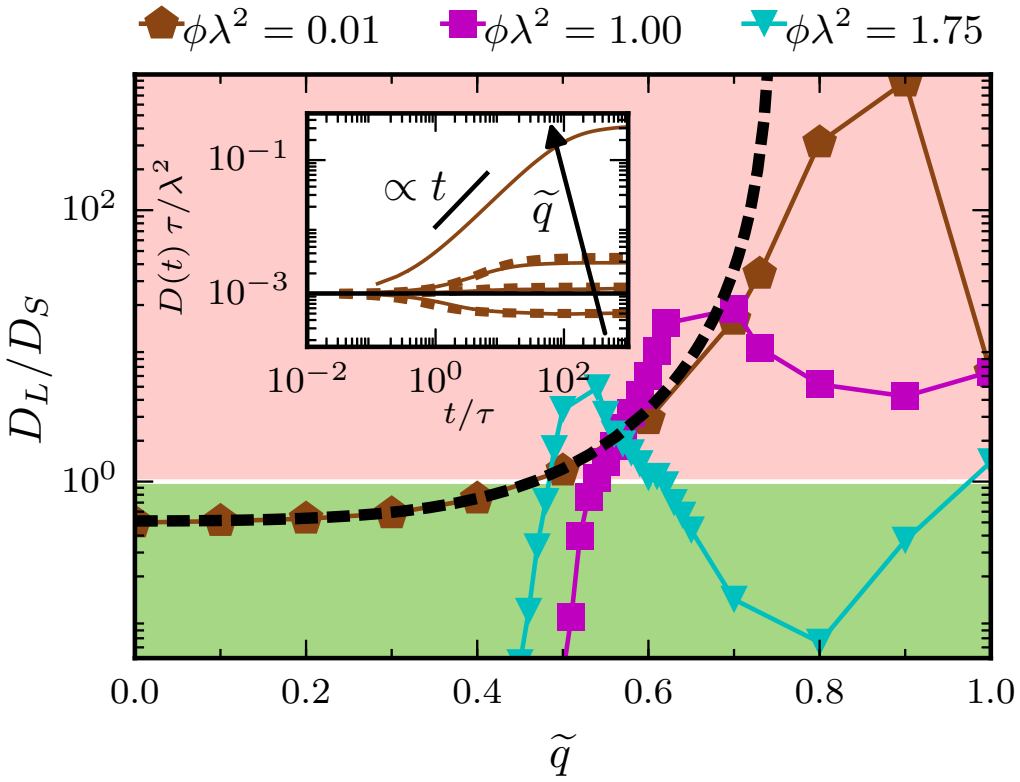

Figure 4.9: *Ratio of the long-time to short-time diffusion coefficients, D_L/D_S, obtained from the time dependent diffusion coefficient $D(t)$ for a finite temperature $T = 10^{-3}\,Q^2/(k_B\lambda)$. The shading indicates a transition between active fluids ($D_L/D_S > 1$) and solids ($D_L/D_S < 1$). The inset depicts the normalized $D(t)$ for $\phi\lambda^2 = 0.01$ and $\tilde{q} \in \{0, 0.5, 0.6, 0.8\}$, demonstrating the transition from subdiffusive to ballistic intermediate behavior with increasing $\tilde{q}$. The dashed lines represent the analytical solution for the diffusion of a single doublet, the solid lines and symbols show numerical results for finite density.*

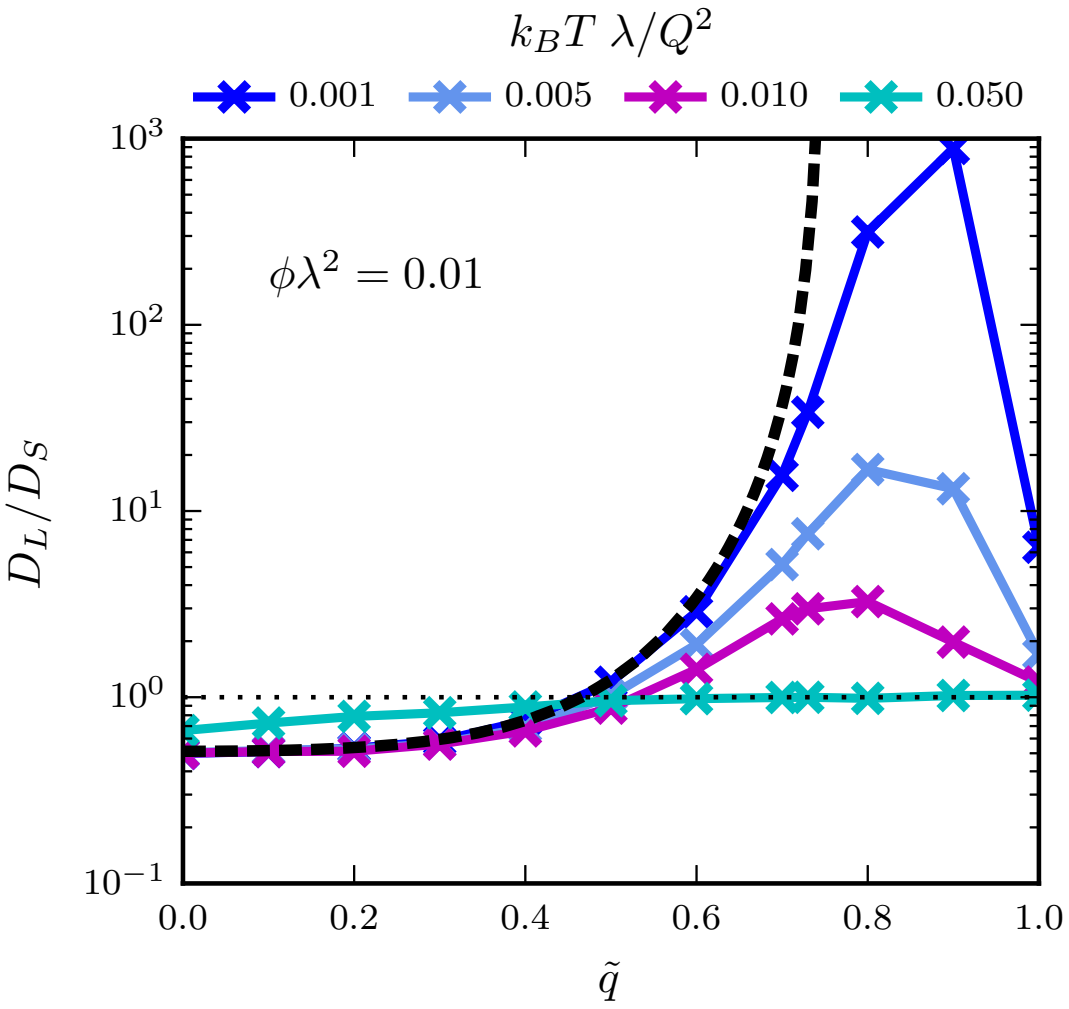

Figure 4.10: *Ratio of the long-time to short-time diffusion coefficients, D_L/D_S, obtained from the time dependent diffusion coefficient $D(t)$ for given finite temperatures and number density $\phi\lambda^2 = 0.01$. The horizontal dotted line indicated the transition between active fluids ($D_L/D_S > 1$) and solids ($D_L/D_S < 1$). The dashed line represent analytical solution, the solid lines and symbols show numerical results.*

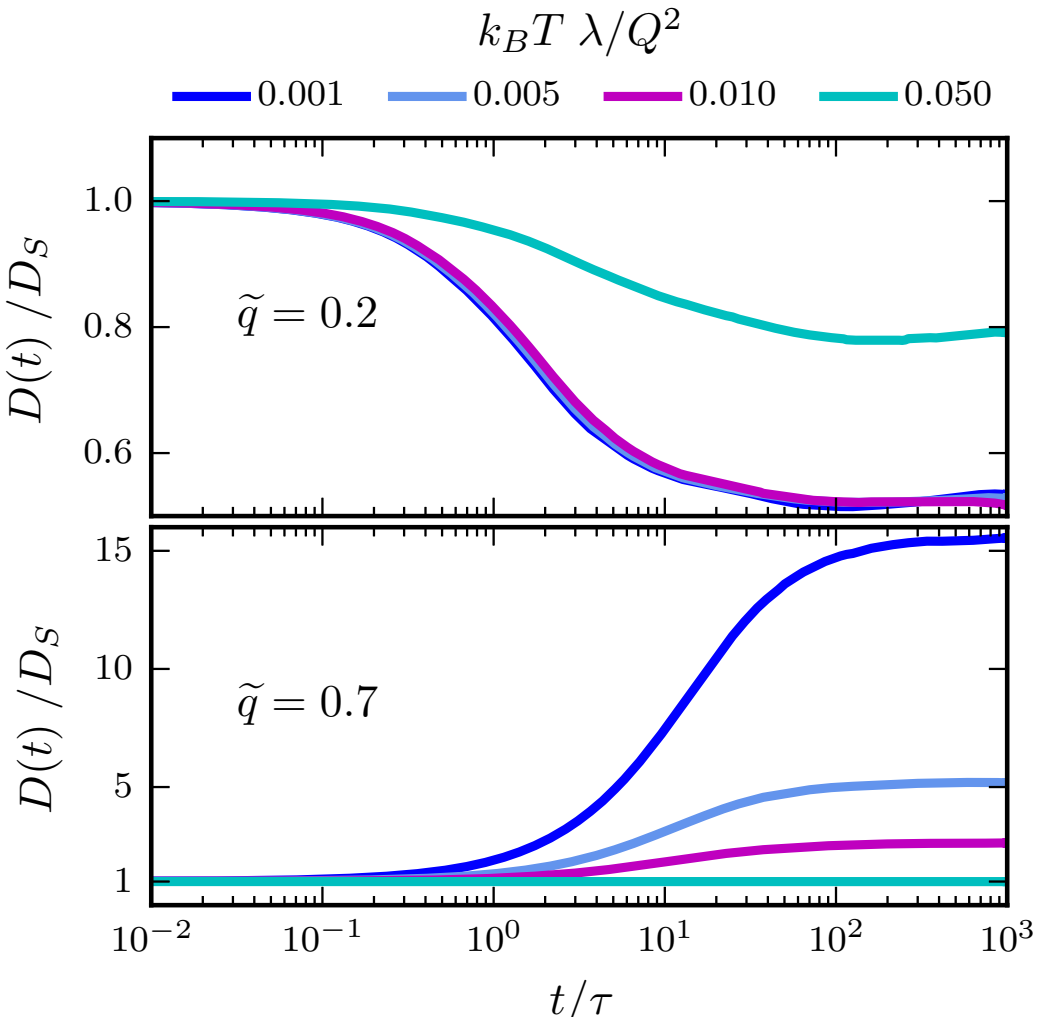

Figure 4.11: *Temporal evolution of $D(t)$ normalized by D_S for two chosen relative wake charges $\tilde{q} = 0.2$ and $\tilde{q} = 0.7$ with $\phi\lambda^2 = 0.01$ and varied finite temperature.*

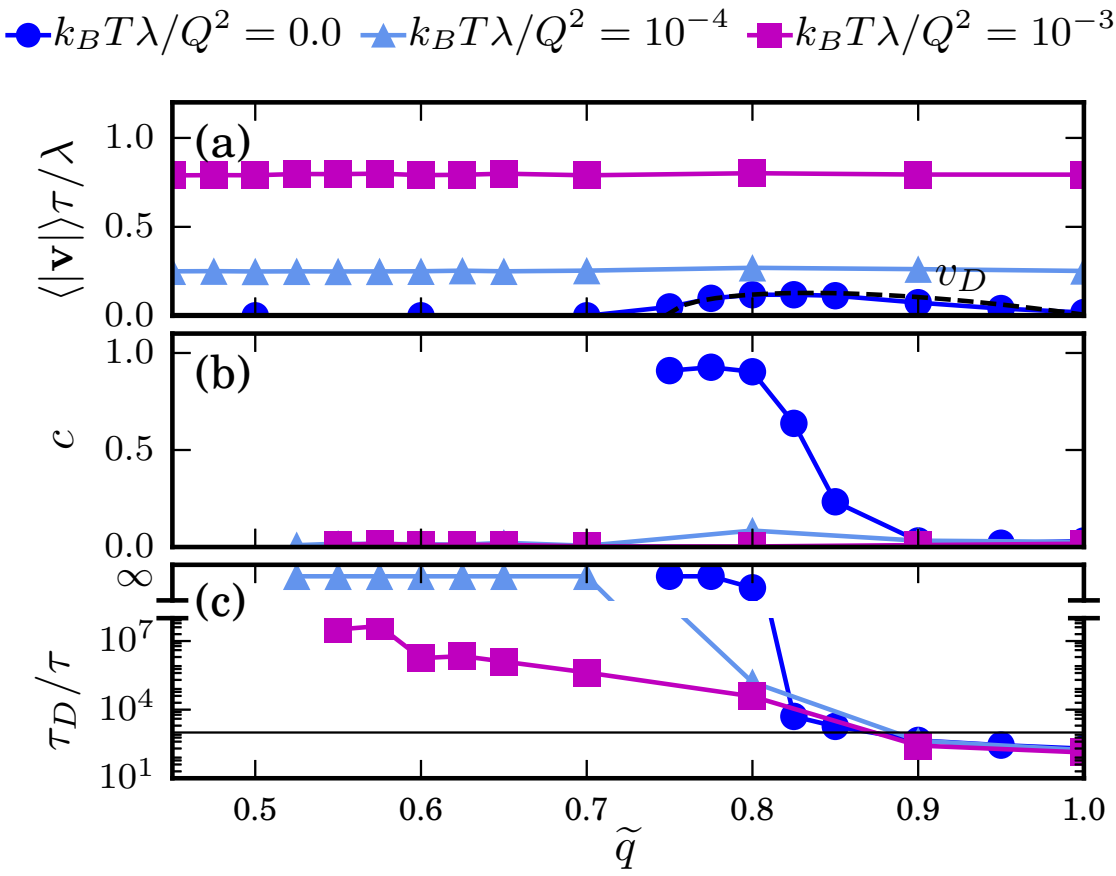

Figure 4.12: *Characteristics of active fluids for given finite temperatures at number density $\phi\lambda^2 = 0.1$: (a) average particle velocity $\langle v\rangle$, (b) alignment parameter c, and (c) decay time of doublets τ_D, plotted versus the relative wake charge $\tilde{q}$ if the respective criterion for an active fluid is fulfilled. The dashed line in panel (a) shows the velocity of a single doublet v_D in the dilute case at zero-temperature.*

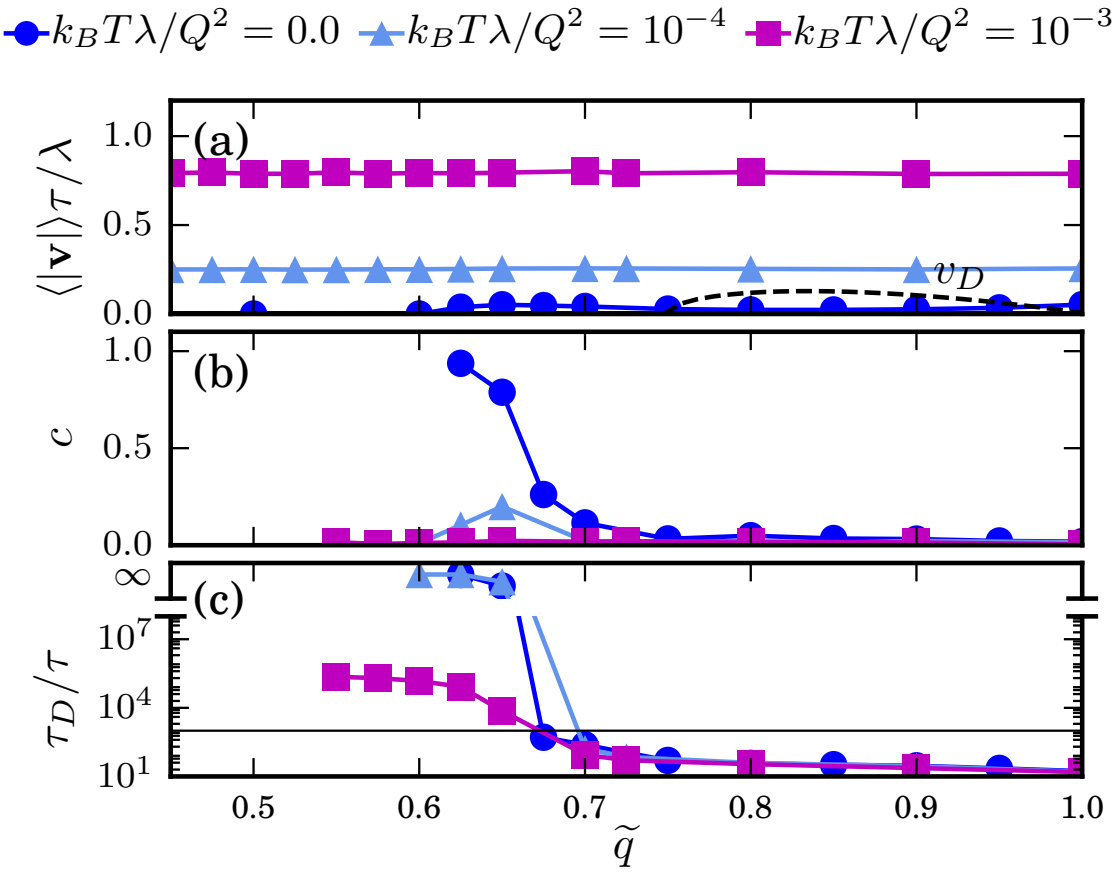

Figure 4.13: *Characteristics of active fluids for given finite temperatures at number density $\phi\lambda^2 = 1.0$: (a) average particle velocity $\langle v \rangle$, (b) alignment parameter c, and (c) decay time of doublets τ_D, plotted versus the relative wake charge $\tilde{q}$ if the respective criterion for an active fluid is fulfilled. The dashed line in panel (a) shows the velocity of a single doublet v_D in the dilute case at zero-temperature.*

4.4 Conclusion

In conclusion, we have shown that in two-dimensional systems with wake-mediated interactions a rich variety of self-organization phenomena occur. In the zero-temperature limit, the nonreciprocal forces exerted by wakes generate a complex diagram of steady states. Hydrodynamic interactions do not qualitatively change our results. In particular, we showed the formation of active units – bound particle pairs, having interesting similarities with permanently active Brownian particles – and the realization of unusual melting scenarios. At finite temperatures we identified regimes of anomalously high diffusion. The ability of particles with the wake-mediated interactions to form active units, the unusual melting and the unique diffusive behavior make such systems interesting for many fields of research.

CHAPTER 5

CONCLUSION

In this thesis, we explored the statistical mechanics of systems, where the reciprocity of particle interactions can be broken. Nonreciprocal interactions are of fundamental importance for many different experimental systems, and are attracting increasing attention. The majority of results presented in this thesis are generic, and independent of the specific realization of the nonreciprocity. For the broad class of systems with constant nonreciprocity and Newtonian dynamics, we showed the existence of the remarkable state of detailed dynamic equilibrium, where the different reciprocal sub-ensembles obtain distinct steady-state temperatures. There, the temperature ratio is uniquely determined by the nonreciprocity. For the systems where the nonreciprocity parameter depends on the inter-particle distance, we predicted a temperature growth that converges to universal asymptotes. In numerical simulations, we studied systems with different initial temperatures and varying number density, and we observed a good agreement with the theoretical predictions. Additionally, our analysis was confirmed by experiments carried out in two-dimensional complex plasmas with wake-mediated interactions.

We extended our study to the strong-damping regime, where the kinetic temperature of particles is imposed by an external heat bath. Based on diffusiophoresis in colloidal dispersions, we proposed a model that leads to Yukawa-like pair nonreciprocal interactions. Based on the Smoluchowski equation, we developed a microscopic theory for the pair-correlation functions and tested it against detailed Brownian dynamics simulation results in 2D and 3D. Using the Kirkwood approximation as a closure, the theory allowed for the prediction of the pair distribution functions. Within this theory no explicit restrictions to the species dependent particle interactions were made and it compares to the simulation results with good accuracy. We show that for nonreciprocal interactions, the reciprocal sub-ensembles exhibit distinct structural correlations. Via the triplet angle distribution function, we studied the quality of the Kirkwood approximation explicitly. We computed the triplet angle distribution function, once directly from simulation data and also via the pair distribution function and Kirkwood approximation. We compared

reciprocal and nonreciprocal interactions, and showed that for nonreciprocal interactions, the Kirkwood-approximation is less accurate.

Eventually, we studied a quasi-two-dimensional bilayered system with nonreciprocal, wake-mediated interactions by theory and simulations. This system shows the fascinating ability of spontaneous activity and self-organization. The particles can form an active doublets, where these individual units can break and become passive again. We observed interesting phase transitions and re-entrant phenomenons, e.g. where an increase in the number density leads to a melting of a crystal. For broad regions in the active regime of the phase diagram there is a strong alignment, which is enhanced by hydrodynamic interactions. Also, we analyzed the effect of finite temperature on such a system, where the activity of the system emerges as an increase in the relative diffusion.

The results presented in Chapter 2 have already motivated a different group to study the redistribution of kinetic energies in detail [171] and we expect that field of nonreciprocal interactions will grow in importance. There are many problems yet unexplored, like the extension of mode coupling theory or dynamical density functional theory to nonreciprocal interactions. Also, we expect that a two-temperature steady state can exhibit very interesting melting phenomena. The Yukawa-like interactions, introduced in Chapter 3, exhibit a nonreciprocity dependent demixing transition that should be carefully investigated. In conclusion, nonreciprocal effective particle interactions provide a multitude of promising research studies for the future.

DANKSAGUNG

An dieser Stelle möchte ich die Chance nutzen, und mich bei denjenigen bedanken, durch die diese Arbeit zu dem geworden ist, was sie ist. Hartmut Löwen hat mich während der letzten drei Jahre als Erstgutachter und Betreuer wissenschaftlich begleitet und unterstützt. Für die Möglichkeiten die er mir gegeben hat, und für sein persönliches Engagement, gilt ihm mein ganz besonderer Dank. Ebenfalls bedanke ich mich bei meinem Zweitgutachter Alexei Ivlev, der mich auf das Thema der nichtreziproken Kräfte hingewiesen hat, und mir mit seinem Rat immer zur Seite stand.

Außerdem möchte ich meine Ko-Autoren Andreas Kaiser und Marco Heinen nennen und ihnen herzlich danken. Marco und Andreas haben sich oft für jeden kleinen Fortschritt Zeit genommen. Ihre Unterstützung war für meine Arbeit von besonderer Bedeutung. Mein Dank gilt auch meinem Mentor Andreas Menzel, meinen Büro-Kollegen Giorgio Pessot und Arnab Saha, und Joachim Wenk, dem Computeradministrator des Instituts. Bei ihnen und meinen Kollegen und Freunden vom Institut für theoretische Physik bedanke ich mich herzlich für die gemeinsame Zeit und die vielen gewinnbringenden Gespräche.

Ohne meine Familie, insbesondere meine Eltern und Geschwister, wäre ich nie an den Punkt gekommen überhaupt eine Doktorarbeit anzufangen. Meinem Vater, der mir viele interessante Impulse für meine Arbeit gegeben hat sei besonderer Dank. Der größte Dank gilt meiner Frau Daniela Rena, die mir während der Anfertigung dieser Arbeit zur Seite stand und mir den Rücken frei gehalten hat. Danke!

BIBLIOGRAPHY

[1] A. V. Ivlev, J. Bartnick, M. Heinen, C.-R. Du, V. Nosenko, and H. Löwen. Statistical Mechanics where Newton's Third Law is Broken. Phys. Rev. X **5**, 011035 (2015).

[2] J. Bartnick, M.Heinen, A. Ivlev, and H. Löwen, Structural correlations in binary colloidal mixtures with nonreciprocal interactions, *arXiv:1510.01870* [cond-mat.soft] (2015).

[3] J. Bartnick, A. Kaiser, H. Löwen, and A. Ivlev, Emerging activity in bilayered dispersions with wake-mediated interactions, *arXiv:1507.08962* [cond-mat.stat-mech] (2015).

[4] I. Newton. Philosophiae naturalis principia mathematica, (1687).

[5] J. N. Israelachvili. *Intermolecular and Surface Forces* (Elsevier, Amsterdam, 1992).

[6] M. Dijkstra, R. van Roij, and R. Evans. Effective interactions, structure, and isothermal compressibility of colloidal suspensions. J. Chem. Phys. **113**, 4799 (2000).

[7] M. Praprotnik, L. D. Site, and K. Kremer. Multiscale Simulation of Soft Matter: From Scale Bridging to Adaptive Resolution. Annu. Rev. Phys. Chem. **59**, 545 (2008).

[8] B. M. Mognetti, P. Virnau, L. Yelash, W. Paul, K. Binder, M. Müller, and L. G. MacDowell. Coarse-grained models for fluids and their mixtures: Comparison of Monte Carlo studies of their phase behavior with perturbation theory and experiment. J. Chem. Phys. **130**, 044101 (2009).

[9] P. Bolhuis, A. A. Louis, J.-P. Hansen, and E. J. Meijer. Accurate effective pair potentials for polymer solutions. J. Chem. Phys. **114**, 4296 (2001).

[10] A. Melzer, V. A. Schweigert, I. V. Schweigert, A. Homann, S. Peters, and A. Piel. Structure and stability of the plasma crystal. Phys. Rev. E **54**, R46 (1996).

[11] A. S. Khair and J. F. Brady. On the motion of two particles translating with equal velocities through a colloidal dispersion. Proc. R. Soc. A **463**, 223 (2007).

[12] C. Mejía-Monasterio and G. Oshanin. Bias- and bath-mediated pairing of particles driven through a quiescent medium. Soft Matter **7**, 993 (2011).

[13] J. Dzubiella, H. Löwen, and C. N. Likos. Depletion Forces in Nonequilibrium. Phys. Rev. Lett. **91**, 248301 (2003).

[14] G. E. Morfill and A. V. Ivlev. Complex plasmas: An interdisciplinary research field. Rev. Mod. Phys. **81**, 1353 (2009).

[15] A. V. Ivlev, H. Löwen, G. E. Morfill, and P. C. Royall. *Complex Plasmas and Colloidal Dispersions: Particle-resolved Studies of Classical Liquids and Solids* (World Scientific, 2012).

[16] M. Bonitz, C. Henning, and D. Block. Complex plasmas: a laboratory for strong correlations. Reports Prog. Phys. **73**, 066501 (2010).

[17] M. Chaudhuri, A. V. Ivlev, S. A. Khrapak, H. M. Thomas, and G. E. Morfill. Complex plasma – the plasma state of soft matter. Soft Matter **7**, 1287 (2011).

[18] V. N. Tsytovich. Dust plasma crystals, drops, and clouds. Physics-Uspekhi **40**, 53 (1997).

[19] S. Khrapak, A. V. Ivlev, and G. E. Morfill. Interaction potential of microparticles in a plasma: Role of collisions with plasma particles. Phys. Rev. E **64**, 046403 (2001).

[20] V. A. Schweigert, I. V. Schweigert, A. Melzer, A. Homann, and A. Piel. Alignment and instability of dust crystals in plasmas. Phys. Rev. E **54**, 4155 (1996).

[21] I. Sriram and E. M. Furst. Out-of-equilibrium forces between colloids. Soft Matter **8**, 3335 (2012).

[22] K. Hayashi and S.-i. Sasa. The law of action and reaction for the effective force in a non-equilibrium colloidal system. J. Phys. Cond. Matter **18**, 2825 (2006).

[23] P. R. Buenzli and R. Soto. Violation of the action-reaction principle and self-forces induced by nonequilibrium fluctuations. Phys. Rev. E **78**, 020102 (2008).

[24] K. Dholakia and P. Zemánek. Colloquium: Gripped by light: Optical binding. Rev. Mod. Phys. **82**, 1767 (2010).

[25] E. R. Shanblatt and D. G. Grier. Extended and knotted optical traps in three dimensions. Opt. Express **19**, 5833 (2011).

[26] B. Sabass and U. Seifert. Efficiency of Surface-Driven Motion: Nanoswimmers Beat Microswimmers. Phys. Rev. Lett. **105**, 218103 (2010).

[27] R. Soto and R. Golestanian. Self-Assembly of Catalytically Active Colloidal Molecules: Tailoring Activity Through Surface Chemistry. Phys. Rev. Lett. **112**, 68301 (2014).

[28] R. Soto and R. Golestanian. Self-assembly of active colloidal molecules with dynamic function. Phys. Rev. E **91**, 52304 (2015).

[29] A. Sengupta, T. Kruppa, and H. Löwen. Chemotactic predator-prey dynamics. Phys. Rev. E **83**, 031914 (2011).

[30] M. Kollmann, L. Løvdok, K. Bartholomé, J. Timmer, and V. Sourjik. Design principles of a bacterial signalling network. Nature **438**, 504 (2005).

[31] U. B. Kaupp, N. D. Kashikar, and I. Weyand. Mechanisms of sperm chemotaxis. Annu. Rev. Physiol. **70**, 93 (2008).

[32] D. Helbing and P. Molnár. Social force model for pedestrian dynamics. Phys. Rev. E **51**, 4282 (1995).

[33] D. Helbing, I. Farkas, and T. Vicsek. Simulating dynamical features of escape panic. Nature **407**, 487 (2000).

[34] W. C. K. Poon. The physics of a model colloid–polymer mixture. J. Phys. Cond. Matter **14**, R859 (2002).

[35] G. Kahl and H. Löwen. Classical density functional theory: an ideal tool to study heterogeneous crystal nucleation. J. Phys. Cond. Matter **21**, 464101 (2009).

[36] T. Palberg. Crystallization kinetics of colloidal model suspensions: recent achievements and new perspectives. J. Phys. Cond. Matter **26**, 333101 (2014).

[37] P. Pusey, in *Liquids, freezing and the glass transition*, edited by J. P. Hansen, D. Levesque, and J. Zinn-Justin (Elsevier, Amsterdam, 1991).

[38] M. Marechal, U. Zimmermann, and H. Löwen. Freezing of parallel hard cubes with rounded edges. J. Chem. Phys. **136**, 144506 (2012).

[39] P. Bolhuis and D. Frenkel. Tracing the phase boundaries of hard spherocylinders. J. Chem. Phys. **106**, 666 (1997).

[40] J. Bialké, T. Speck, and H. Löwen. Crystallization in a Dense Suspension of Self-Propelled Particles. Phys. Rev. Lett. **108**, 168301 (2012).

[41] E. Allahyarov, K. Sandomirski, S. U. Egelhaaf, and H. Löwen. Crystallization seeds favour crystallization only during initial growth. Nat. Commun. **6**, 7110 (2015).

[42] C. A. Murray and D. G. Grier. Video Microscopy of Monodisperse Colloidal Systems. Annu. Rev. Phys. Chem. **47**, 421 (1996).

[43] J. Zhu and P. M. Chaikin. Crystallization of hard-sphere colloids in microgravity. Nature **387**, 1996 (1997).

[44] H. Löwen. Melting, freezing and colloidal suspensions. Phys. Rep. **237**, 249 (1994).

[45] M. Heinen, S. K. Schnyder, J. F. Brady, and H. Löwen. Classical Liquids in Fractal Dimension. Phys. Rev. Lett. **115**, 097801 (2015).

[46] A. M. Menzel. Tuned, driven, and active soft matter. Phys. Rep. **554**, 1 (2015).

[47] H. N. W. Lekkerkerker, W. C. K. Poon, P. Pusey, A. Stroobants, and P. Warren. Phase Behaviour of Colloid + Polymer Mixtures. Europhys. Lett. **20**, 559 (1992).

[48] M. Adams, Z. Dogic, S. L. Keller, and S. Fraden. Entropically driven microphase transitions in mixtures of colloidal rods and spheres. Nature **393**, 349 (1998).

[49] A. Stradner, H. Sedgwick, F. Cardinaux, W. C. K. Poon, S. U. Egelhaaf, and P. Schurtenberger. Equilibrium cluster formation in concentrated protein solutions and colloids. Nature **432**, 492 (2004).

[50] H. Löwen. Possibilities of phase separation in colloidal suspensions. Phys. A. **235**, 129 (1997).

[51] J. Stenhammar, R. Wittkowski, D. Marenduzzo, and M. E. Cates. Activity-Induced Phase Separation and Self-Assembly in Mixtures of Active and Passive Particles. Phys. Rev. Lett. **114**, 018301 (2015).

[52] Y. Fily and M. C. Marchetti. Athermal Phase Separation of Self-Propelled Particles with No Alignment. Phys. Rev. Lett. **108**, 235702 (2012).

[53] R. Wittkowski, A. Tiribocchi, J. Stenhammar, R. J. Allen, D. Marenduzzo, and M. E. Cates. Scalar ϕ4 field theory for active-particle phase separation. Nat. Commun. **5**, 4351 (2014).

[54] G. L. Hunter and E. R. Weeks. The physics of the colloidal glass transition. Rep. Prog. Phys. **75**, 066501 (2012).

[55] P. C. Royall, D. G. A. L. Aarts, and H. Tanaka. Bridging length scales in colloidal liquids and interfaces from near-critical divergence to single particles. Nat. Phys. **3**, 636 (2007).

[56] P. J. Lu, E. Zaccarelli, F. Ciulla, A. B. Schofield, F. Sciortino, and D. A. Weitz. Gelation of particles with short-range attraction. Nature **453**, 499 (2008).

[57] A. Yazdi, M. Heinen, A. V. Ivlev, H. Löwen, and M. Sperl. Glass transition of charged particles in two-dimensional confinement. Phys. Rev. E **91**, 052301 (2015).

[58] M. Doi. *Soft Matter Physics* (OUP Oxford, 2013).

[59] N. J. Wagner and J. F. Brady. Shear thickening in colloidal dispersions. Phys. Today **62**, 27 (2009).

[60] H. Hamaker. The London – van der Waals attraction between spherical particles. Physica **4**, 1058 (1937).

[61] E. J. W. Verwey and J. T. G. Overbeek. *Theory of the Stability of Lyophobic Colloids* (Elsevier, Amsterdam, 1948).

[62] I. S. Aranson. Active colloids. Physics-Uspekhi **56**, 79 (2013).

[63] J. Buhl, D. J. T. Sumpter, I. D. Couzin, J. J. Hale, E. Despland, E. R. Miller, and S. J. Simpson. From disorder to order in marching locusts. Science **312**, 1402 (2006).

[64] M. Ballerini, N. Cabibbo, R. Candelier, A. Cavagna, E. Cisbani, I. Giardina, V. Lecomte, A. Orlandi, G. Parisi, A. Procaccini, M. Viale, and V. Zdravkovic. Interaction ruling animal collective behavior depends on topological rather than metric distance: evidence from a field study. Proc. Natl. Acad. Sci. U. S. A. **105**, 1232 (2008).

[65] Y. Katz, K. Tunstrøm, C. C. Ioannou, C. Huepe, and I. D. Couzin. Inferring the structure and dynamics of interactions in schooling fish. Proc. Natl. Acad. Sci. U. S. A. **108**, 18720 (2011).

[66] A. John, A. Schadschneider, D. Chowdhury, and K. Nishinari. Trafficlike Collective Movement of Ants on Trails: Absence of a Jammed Phase. Phys. Rev. Lett. **102**, 108001 (2009).

[67] J. L. Silverberg, M. Bierbaum, J. P. Sethna, and I. Cohen. Collective Motion of Humans in Mosh and Circle Pits at Heavy Metal Concerts. Phys. Rev. Lett. **110**, 228701 (2013).

[68] J. Zhang, W. Klingsch, A. Schadschneider, and A. Seyfried. Ordering in bidirectional pedestrian flows and its influence on the fundamental diagram. J. Stat. Mech. Theory Exp. **2012**, P02002 (2012).

[69] T. Vicsek, A. Czirók, E. Ben-Jacob, I. Cohen, and O. Shochet. Novel Type of Phase Transition in a System of Self-Driven Particles. Phys. Rev. Lett. **75**, 1226 (1995).

[70] B. Sabass and U. Seifert. Dynamics and efficiency of a self-propelled, diffusiophoretic swimmer. J. Chem. Phys. **136**, 064508 (2012).

[71] S. Thakur and R. Kapral. Dynamics of self-propelled nanomotors in chemically active media. J. Chem. Phys. **135**, 024509 (2011).

[72] R. Golestanian, T. B. Liverpool, and A. Ajdari. Propulsion of a Molecular Machine by Asymmetric Distribution of Reaction Products. Phys. Rev. Lett. **94**, 220801 (2005).

[73] R. Golestanian. Anomalous Diffusion of Symmetric and Asymmetric Active Colloids. Phys. Rev. Lett. **102**, 188305 (2009).

[74] I. Langmuir. Oscillations in Ionized Gases. Proc. Natl. Acad. Sci. U. S. A. **14**, 627 (1928).

[75] W. Baumjohann and R. A. Treumann. *Basic Space Plasma Physics* (Imperial College Press, London, 1996).

[76] B. A. Smith, L. Soderblom, R. Batson, P. Bridges, J. Inge, H. Masursky, E. Shoemaker, R. Beebe, J. Boyce, G. Briggs, A. Bunker, S. A. Collins, C. J. Hansen, T. V. Johnson, J. L. Mitchell, R. J. Terrile, A. F. Cook, J. Cuzzi, J. B. Pollack, G. E. Danielson, A. P. Ingersoll, M. E. Davies, G. E. Hunt, D. Morrison, T. Owen, C. Sagan, J. Veverka, R. Strom, and V. E. Suomi. A new look at the saturn system: the voyager 2 images. Science **215**, 504 (1982).

[77] J. H. Chu and L. I. Direct observation of Coulomb crystals and liquids in strongly coupled rf dusty plasmas. Phys. Rev. Lett. **72**, 4009 (1994).

[78] Y. Hayashi and K. Tachibana. Observation of Coulomb-Crystal Formation from Carbon Particles Grown in a Methane Plasma. Jpn. J. Appl. Phys. **33**, L804 (1994).

[79] H. M. Thomas, G. E. Morfill, V. Demmel, J. Goree, B. Feuerbacher, and D. Möhlmann. Plasma Crystal: Coulomb Crystallization in a Dusty Plasma. Phys. Rev. Lett. **73**, 652 (1994).

[80] P. K. Shukla and A. A. Mamun. *Introduction to Dusty Plasma Physics* (IOP Publishing, Bristol, 2001).

[81] M. A. Lieberman and A. J. Lichtenberg. *Principles of Plasma Discharges and Materials Processing* (John Wiley & Sons, 1994).

[82] J. E. Allen. Probe theory - the orbital motion approach. Phys. Scr. **45**, 497 (1992).

[83] H. M. Mott-Smith and I. Langmuir. The Theory of Collectors in Gaseous Discharges. Phys. Rev. **28**, 727 (1926).

[84] Y. P. Raizer. *Gas Discharge Physics* (Springer Berlin Heidelberg, 1991).

[85] J. K. Olthoff and K. E. Greenberg. The Gaseous Electronics Conference RF Reference Cell - An Introduction. J. Res. Natl. Inst. Stand. Technol. **100**, 327 (1995).

[86] M. Lax. Classical Noise IV: Langevin Methods. Rev. Mod. Phys. **38**, 541 (1966).

[87] P. Langevin. Sur la théorie du mouvement brownien. C. R. Acad. Sci. **146**, 530 (1908).

[88] N. N. Bogolyubov and D. P. Sankovich. N.N. Bogolyubov and statistical mechanics. Russ. Math. Surv. **49**, 19 (1994).

[89] J. K. G. Dhont. *An introduction to the dynamics of colloids* (Elsevier, 2003).

[90] A. R. E. Sinclair, S. Mduma, and J. S. Brashares. Patterns of predation in a diverse predator-prey system. Nature **425**, 288 (2003).

[91] M. Doi and S. F. Edwards. *The Theory of Polymer Dynamics* (Clarendon Press, 1986).

[92] L. D. Landau and E. M. Lifshitz. *Fluid Mechanics, Volume 6* (Elsevier Science, 1959).

[93] A. Reinmüller, E. C. Oğuz, R. Messina, H. Löwen, H. J. Schöpe, and T. Palberg. Colloidal crystallization in the quasi-two-dimensional induced by electrolyte gradients. J. Chem. Phys. **136**, 164505 (2012).

[94] J. L. Anderson. Colloid Transport by Interfacial Forces. Annu. Rev. Fluid Mech. **21**, 61 (1989).

[95] F. Jülicher and J. Prost. Generic theory of colloidal transport. Eur. Phys. J. E **29**, 27 (2009).

[96] B. Abécassis, C. Cottin-Bizonne, C. Ybert, A. Ajdari, and L. Bocquet. Boosting migration of large particles by solute contrasts. Nat. Mater. **7**, 785 (2008).

[97] J. Palacci, B. Abécassis, C. Cottin-Bizonne, C. Ybert, and L. Bocquet. Colloidal Motility and Pattern Formation under Rectified Diffusiophoresis. Phys. Rev. Lett. **104**, 138302 (2010).

[98] R. Golestanian, T. B. Liverpool, and A. Ajdari. Designing phoretic micro- and nano-swimmers. New J. Phys. **9**, 126 (2007).

[99] G. Rückner and R. Kapral. Chemically Powered Nanodimers. Phys. Rev. Lett. **98**, 150603 (2007).

[100] M. N. Popescu, M. Tasinkevych, and S. Dietrich. Pulling and pushing a cargo with a catalytically active carrier. EPL **95**, 28004 (2011).

[101] S. Michelin, E. Lauga, and D. Bartolo. Spontaneous autophoretic motion of isotropic particles. Phys. Fluids **25**, 061701 (2013).

[102] L. D. Site. Some fundamental problems for an energy-conserving adaptive-resolution molecular dynamics scheme. Phys. Rev. E **76**, 047701 (2007).

[103] V. E. Fortov, A. V. Ivlev, S. A. Khrapak, A. G. Khrapak, and G. E. Morfill. Complex (dusty) plasmas: Current status, open issues, perspectives. Phys. Rep. **421**, 1 (2005).

[104] L. Couëdel, V. Nosenko, A. V. Ivlev, S. K. Zhdanov, H. M. Thomas, and G. E. Morfill. Direct Observation of Mode-Coupling Instability in Two-Dimensional Plasma Crystals. Phys. Rev. Lett. **104**, 195001 (2010).

[105] L. D. Landau and E. M. Lifshitz. *Mechanics* (Pergamon, Oxford, 1976).

[106] E. M. Lifshitz and L. P. Pitaevskii. *Physical Kinetics* (Pergamon, Oxford, 1981).

[107] L. Spitzer. *Physics of Fully Ionized Gases* (Dover, New York, 2006).

[108] N. G. van Kampen. *Stochastic Processes in Physics and Chemistry* (Elsevier, Amsterdam, 1981).

[109] W. C. Swope, H. C. Andersen, P. H. Berens, and K. R. Wilson. A computer-simulation method for the calculation of equilibrium-constants for the formation of physical clusters of molecules – application to small water clusters. J. Chem. Phys. **76**, 637 (1982).

[110] J. C. Pamies, A. Cacciuto, and D. Frenkel. Phase diagram of Hertzian spheres. J. Chem. Phys. **131**, 044514 (2009).

[111] L. Berthier, A. J. Moreno, and G. Szamel. Increasing the density melts ultrasoft colloidal glasses. Phys. Rev. E **82**, 060501(R) (2010).

[112] H. M. Thomas and G. E. Morfill. Melting dynamics of a plasma crystal. Nature **379**, 806 (1996).

[113] P. Hartmann, Z. Donkó, G. J. Kalman, S. Kyrkos, K. I. Golden, and M. Rosenberg. Collective Dynamics of Complex Plasma Bilayers. Phys. Rev. Lett. **103**, 245002 (2009).

[114] V. Nosenko, G. E. Morfill, and P. Rosakis. Direct Experimental Measurement of the Speed-Stress Relation for Dislocations in a Plasma Crystal. Phys. Rev. Lett. **106**, 155002 (2011).

[115] C.-R. Du, V. Nosenko, S. K. Zhdanov, H. M. Thomas, and G. E. Morfill. Interaction of two-dimensional plasma crystals with upstream charged particles. Eur. Lett. **99**, 55001 (2012).

[116] V. Steinberg, R. Sütterlin, A. V. Ivlev, and G. Morfill. Vertical Pairing of Identical Particles Suspended in the Plasma Sheath. Phys. Rev. Lett. **86**, 4540 (2001).

[117] Y. Feng, J. Goree, and B. Liu. Errors in particle tracking velocimetry with high-speed cameras. Rev. Sci. Instrum. **82**, 053707 (2011).

[118] J. D. Williams, H. M. Thomas, L. Couëdel, A. V. Ivlev, S. K. Zhdanov, V. Nosenko, H. M. Thomas, and G. E. Morfill. Kinetics of the melting front in two-dimensional plasma crystals: Complementary analysis with the particle image and particle tracking velocimetries. Phys. Rev. E **86**, 046401 (2012).

[119] M. Lampe, G. Joyce, G. Ganguli, and V. Gavrishchaka. Interactions between dust grains in a dusty plasma. Phys. Plasmas **7**, 3851 (2000).

[120] S. V. Vladimirov, S. A. Maiorov, and O. Ishihara. Molecular dynamics simulation of plasma flow around two stationary dust grains. Phys. Plasmas **10**, 3867 (2003).

[121] R. Kompaneets, U. Konopka, A. V. Ivlev, V. N. Tsytovich, and G. Morfill. Potential around a charged dust particle in a collisional sheath. Phys. Plasmas **14**, 052108 (2007).

[122] S. Nunomura, T. Misawa, N. Ohno, and S. Takamura. Instability of Dust Particles in a Coulomb Crystal due to Delayed Charging. Phys. Rev. Lett. **83**, 1970 (1999).

[123] O. S. Vaulina, S. A. Khrapak, A. P. Nefedov, and O. F. Petrov. Charge-fluctuation-induced heating of dust particles in a plasma. Phys. Rev. E **60**, 5959 (1999).

[124] M. Y. Pustylnik, N. Ohno, S. Takamura, and R. Smirnov. Modification of the damping rate of the oscillations of a dust particle levitating in a plasma due to the delayed charging effect. Phys. Rev. E **74**, 046402 (2006).

[125] I. Theurkauff, C. Cottin-Bizonne, J. Palacci, C. Ybert, and L. Bocquet. Dynamic Clustering in Active Colloidal Suspensions with Chemical Signaling. Phys. Rev. Lett. **108**, 268303 (2012).

[126] J. Palacci, S. Sacanna, A. P. Steinberg, D. J. Pine, and P. M. Chaikin. Living Crystals of Light-Activated Colloidal Surfers. Science **339**, 936 (2013).

[127] I. Buttinoni, J. Bialké, F. Kümmel, H. Löwen, C. Bechinger, and T. Speck. Dynamical Clustering and Phase Separation in Suspensions of Self-Propelled Colloidal Particles. Phys. Rev. Lett. **110**, 238301 (2013).

[128] T. Brotto, J. B. Caussin, E. Lauga, and D. Bartolo. Hydrodynamics of Confined Active Fluids. Phys. Rev. Lett. **110**, 038101 (2013).

[129] S. Ebbens, D. A. Gregory, G. Dunderdale, J. R. Howse, Y. Ibrahim, T. B. Liverpool, and R. Golestanian. Electrokinetic effects in catalytic platinum-insulator Janus swimmers. Eur. Lett. **106**, 58003 (2014).

[130] S. Alabrudzinski, M. L. Ekiel-Jezewska, D. Chehata-Gomez, and T. A. Kowalewski. Particle clusters settling under gravity in a viscous fluid. Phys. Fluids **21**, 73302 (2009).

[131] A. V. Ivlev and G. E. Morfill. Anisotropic dust lattice modes. Phys. Rev. E **63**, 016409 (2000).

[132] I. V. Schweigert, V. A. Schweigert, A. Melzer, and A. Piel. Melting of dust plasma crystals with defects. Phys. Rev. E **62**, 1238 (2000).

[133] K. Qiao, J. Kong, E. V. Oeveren, L. S. Matthews, and T. W. Hyde. Mode couplings and resonance instabilities in dust clusters. Phys. Rev. E **88**, 043103 (2013).

[134] K. Qiao, J. Kong, J. Carmona-Reyes, L. S. Matthews, and T. W. Hyde. Mode coupling and resonance instabilities in quasi-two-dimensional dust clusters in complex plasmas. Phys. Rev. E **90**, 033109 (2014).

[135] A. Melzer, V. A. Schweigert, and A. Piel. Transition from Attractive to Repulsive Forces between Dust Molecules in a Plasma Sheath. Phys. Rev. Lett. **83**, 3194 (1999).

[136] R. Grima. Strong-Coupling Dynamics of a Multicellular Chemotactic System. Phys. Rev. Lett. **95**, 128103 (2005).

[137] R. Grima. Phase transitions and superuniversality in the dynamics of a self-driven particle. Phys. Rev. E **74**, 011125 (2006).

[138] P. de Buyl, A. S. Mikhailov, and R. Kapral. Self-propulsion through symmetry breaking. Europhys. Lett. **103**, 60009 (2013).

[139] Y. Tsori and P.-G. de Gennes. Self-trapping of a single bacterium in its own chemoattractant. Europhys. Lett. **66**, 599 (2004).

[140] J. F. Brady. Particle motion driven by solute gradients with application to autonomous motion: continuum and colloidal perspectives. J. Fluid Mech. **667**, 216 (2011).

[141] F. Westermeier, B. Fischer, W. Roseker, G. Grübel, G. Nägele, and M. Heinen. Structure and short-time dynamics in concentrated suspensions of charged colloids. J. Chem. Phys. **137**, 114504 (2012).

[142] M. Heinen, E. Allahyarov, and H. Löwen. Highly asymmetric electrolytes in the primitive model: hypernetted chain solution in arbitrary spatial dimensions. J. Comput. Chem. **35**, 275 (2014).

[143] J.-P. Hansen and I. R. McDonald. *Theory of Simple Liquids* (Academic Press, 2006).

[144] M. Kohl, A. V. Ivlev, P. Brandt, G. E. Morfill, and H. Löwen. Microscopic theory for anisotropic pair correlations in driven binary mixtures. J. Phys. Cond. Matter **24**, 464115 (2012).

[145] J. G. Kirkwood. Statistical mechanics of fluid mixtures. J. Chem. Phys. **3**, 300 (1935).

[146] A. J. S. Hamilton. Uncorrelated modes of the non-linear power spectrum. Mon. Not. R. Astron. Soc. **312**, 257 (2000).

[147] J. D. Talman. Numerical Fourier and Bessel Transforms in Logarithmic Variables. J. Comput. Phys. **29**, 35 (1978).

[148] P. H. Colberg and F. Höfling. Highly accelerated simulations of glassy dynamics using GPUs: Caveats on limited floating-point precision. Comput. Phys. Commun. **182**, 1120 (2011).

[149] J.-L. Barrat, J.-P. Hansen, and G. Pastore. Factorization of the Triplet Direct Correlation Function in Dense Fluids. Phys. Rev. Lett. **58**, 2075 (1987).

[150] J.-L. Barrat, J.-P. Hansen, and G. Pastore. On the equilibrium structure of dense fluids. Mol. Phys. **63**, 747 (1988).

[151] H. Löwen. Structure and Brownian dynamics of the two-dimensional Yukawa fluid. J. Phys. Cond. Matter **4**, 10105 (1992).

[152] U. M. B. Marconi and P. Tarazona. Dynamic density functional theory of fluids. J. Chem. Phys. **110**, 8032 (1999).

[153] A. J. Archer and R. Evans. Dynamical density functional theory and its application to spinodal decomposition. J. Chem. Phys. **121**, 4246 (2004).

[154] M. Rex, H. H. Wensink, and H. Löwen. Dynamical density functional theory for anisotropic colloidal particles. Phys. Rev. E **76**, 021403 (2007).

[155] P. Español and H. Löwen. Derivation of dynamical density functional theory using the projection operator technique. J. Chem. Phys. **131**, 244101 (2009).

[156] H. H. Wensink and H. Löwen. Aggregation of self-propelled colloidal rods near confining walls. Phys. Rev. E **78**, 031409 (2008).

[157] G. Szamel, E. Flenner, and L. Berthier. Glassy dynamics of athermal self-propelled particles: Computer simulations and a nonequilibrium microscopic theory. Phys. Rev. E **91**, 062304 (2015).

[158] P. Romanczuk, M. Bär, W. Ebeling, B. Linder, and L. Schimansky-Geier. Active Brownian particles: From individual to collective stochastic dynamics. Eur. Phys. J. Spec. Top. **202**, 1 (2012).

[159] J. Elgeti, R. G. Winkler, and G. Gompper. Physics of microswimmers – single particle motion and collective behavior: a review. Rep. Prog. Phys. **78**, 56601 (2015).

[160] I. Buttinoni, G. Volpe, F. Kümmel, G. Volpe, and C. Bechinger. Active Brownian motion tunable by light. J. Phys. Condens. Matter **24**, 284129 (2012).

[161] A. Awazu. Segregation and phase inversion of strongly and weakly fluctuating Brownian particle mixtures and a chain of such particle mixtures in spherical containers. Phys. Rev. E **90**, 042308 (2014).

[162] N. Ganai, S. Sengupta, and G. I. Menon. Chromosome positioning from activity-based segregation. Nucleic Acids Res. **42**, 4145 (2014).

[163] A. Bérut, A. Petrosyan, and S. Ciliberto. Energy flow between two hydrodynamically coupled particles kept at different effective temperatures. Europhys. Lett. **107**, 60004 (2014).

[164] M. E. Leunissen, C. G. Christova, A.-P. Hynninen, C. P. Royall, A. I. Campbell, A. Imhof, M. Dijkstra, R. van Roij, and A. van Blaaderen. Ionic colloidal crystals of oppositely charged particles. Nature **437**, 235 (2005).

[165] A. M. Menzel and T. Ohta. Soft deformable self-propelled particles. Europhys. Lett. **99**, 58001 (2012).

[166] F. Alarcón and I. Pagonabarraga. Spontaneous aggregation and global polar ordering in squirmer suspensions. J. Mol. Liq. **185**, 56 (2013).

[167] M. Hennes, K. Wolff, and H. Stark. Self-Induced Polar Order of Active Brownian Particles in a Harmonic Trap. Phys. Rev. Lett. **112**, 238104 (2014).

[168] C. Reichhardt and C. J. O. Reichhardt. Active microrheology in active matter systems: Mobility, intermittency, and avalanches. Phys. Rev. E **91**, 32313 (2015).

[169] J. R. Howse, R. A. L. Jones, A. J. Ryan, T. Gough, R. Vafabakhsh, and R. Golestanian. Self-Motile Colloidal Particles: From Directed Propulsion to Random Walk. Phys. Rev. Lett. **99**, 048102 (2007).

[170] X. Zheng, B. ten Hagen, A. Kaiser, M. Wu, H. Cui, Z. Silber-Li, and H. Löwen. Non-Gaussian statistics for the motion of self-propelled Janus particles: Experiment versus theory. Phys. Rev. E **88**, 032304 (2013).

[171] O. S. Vaulina, I. I. Lisina, and E. A. Lisin. Kinetic energy in a system of particles with a nonreciprocal interaction. EPL **111**, 50003 (2015).

Eidesstattliche Versicherung

Ich versichere an Eides Statt, dass die Dissertation von mir selbständig und ohne unzulässige fremde Hilfe unter Beachtung der „Grundsätze zur Sicherung guter wissenschaftlicher Praxis an der Heinrich-Heine-Universität Düsseldorf“ erstellt worden ist.

Düsseldorf, 2. November 2015